Characterization of SPECC1L function in cell adhesion and migration in craniofacial morphogenesis

By

Nathan Wilson

B.Sc., Rockhurst University, 2010

Submitted to the graduate degree program in Anatomy and Cell Biology and the Graduate Faculty of the University of Kansas in partial fulfillment of the requirements for the degree of Doctor of Philosophy.

_____

Dr. Irfan Saadi, Ph.D. (Chair)

_____

Dr. András Czirók, Ph.D.

_____

Dr. William Kinsey, Ph.D.

_____

Dr. Paul Trainor, Ph.D.

_____

Dr. Pamela Tran, Ph.D.

_____

Dr. Jinxi Wang, M.D., Ph.D.

Date Defended: 19 April 2017

The dissertation committee for Nathan Wilson certifies that this is the approved version of the following dissertation:

Characterization of SPECC1L function in cell adhesion and migration in craniofacial morphogenesis

_____

Dr. Irfan Saadi, Ph.D. (Chair)

Date approved: 12 May 2017

Abstract

Orofacial clefts are frequent congenital malformations, which can result from reduced contribution of cranial neural crest cells (CNCCs) to the developing cranium. Upon delamination from embryonic neural folds, CNCCs migrate to pharyngeal arches, which give rise to mid-facial structures. Previously, mutations in the cytoskeletal gene *SPECC1L* were implicated in rare, severe atypical facial clefting. Overexpression of a patient isolated SPECC1L mutation showed disrupted association with acetylated microtubules. We show a similar disruption upon overexpression of *SPECC1L* variants isolated from patients with less severe syndromic cleft lip and palate. Severe *Specc1l* deficiency in homozygous mouse mutants is embryonic lethal, showing a reduction in pan-AKT levels and arrested CNCC delamination from the neural folds. Staining of adherens junction (AJ) proteins is increased in mutant neural folds, consistent with impaired CNCC delamination, a process requiring AJ dissolution. *In vitro*, AJ changes induced by *SPECC1L*-kd are rescued by activating PI3K-AKT signaling. We also looked at cell migration properties of SPECC1L-deficient cells *in vitro*. Collective cell migration is a cooperative process fundamental to embryonic development. Wound-repair assays using primary mouse embryonic palatal mesenchyme (MEPM), derived from CNCCs, with moderate *Specc1l* deficiency show impaired collective migration with reduced correlation lengths. These data indicate SPECC1L as a novel modulator of AJs and PI3K-AKT signaling in CNCC delamination and migration of CNCC-derived cells in craniofacial development.

Acknowledgements

So many people have contributed to both the completion of this project, as well as my progress in completing this degree, that I struggle to adequately list their names, let alone describe their contributions – there are many. First and foremost are my parents, who created every possible educational opportunity, for all of us. I also wish to prominently acknowledge and thank the members of my committee – Dr. András Czirók, Dr. William Kinsey, Dr. Irfan Saadi, Dr. Paul Trainor, Dr. Pamela Tran and Dr. Jinxi Wang, who have offered me invaluable guidance and feedback. I deeply appreciate the time each of them has dedicated to my progress. Each has contributed, in a specific way, to help me move forward and complete this project, as well as to each of their individual contributions towards my scientific training.

Importantly, I also need to acknowledge our collaborators, which includes two members of my committee. I wish to acknowledge and thank deeply Dr. Paul Trainor and Dr. Kristin Watt, for collaborating with us, as well as the group of Drs. András Czirók, Brenda Rongish and Charles Little, who have each offered me guidance and shared their expertise, facilities and other resources with me, throughout this project. Also, I enjoy acknowledging here the profound efforts of Edina Kósa, Dona-Gréta Isai and Mike Fila throughout that collaboration. Their hard work made many difficult things possible, and for that I will always be thankful. There are collaborators I wish to acknowledge, whom I have not yet met, such as Dr. Paul Kruszka and his colleagues, at Children's Hospital of Philadelphia, as well as Dr. Bryan Bjork and his, at Midwestern University.

The staff of the Anatomy and Cell Biology department deserve my heartiest acknowledgments, as my progress as a student would not be possible without their efforts. I wish to thank and acknowledge the efforts of our previous graduate education director, Dr. Peggy Petroff, and especially the current director, Dr. Julie Christianson, for guiding me throughout this

process. Also, I wish to thank and acknowledge both our departmental chair, Dr. Dale Abrahamson, and our Dean of Graduate studies, Dr. Mike Werle, for their invaluable guidance throughout this stage in my education, as that guidance was ultimately both invaluable and warmly offered.

This project was made possible through the tireless contributions of the many fine core facilities we all rely upon. I wish to acknowledge the guidance and support offered by Pat St. John and Barbara Fegley, in the Electron microscopy core, as well as Richard Hastings, in the Flow cytometry core and Jing Huang, in the histology core. Also, I wish to acknowledge Stan Fernald and Phil Shafer, of the Integrative imaging core, for their assistance with all things aesthetic.

Many friends have also helped me along this path, including Dr. Pratik Home, who has always loaned me his ear and given his me wise advice, along with a lot of laughs. Also, my friend John Schupp, who often loaned me his dining room table, mainly for the purposes of writing, yet also for dining and stimulating conversation. I couldn't have done this without with either of them.

I have also had the honor of making many good friends, throughout this journey. I should begin by acknowledging Adam Olm-Shipman and Dr. Syed Rafi, whom I met shortly after the founding of Dr. Saadi's lab. Later, I also had the honor of working with Diana Acevedo, an effective and amazing lab manager.

I also acknowledge Dr. Kanagaraj Palaniyandi, a friend and colleague, with whom working together was a great pleasure. We have also enjoyed the company of hard-working, visiting summer students I wish to acknowledge – Kelly Stumpff, Guerin Smith, Abby Stork, Lauren Hipp and Shahnawaz Yousuf. They all contributed much and made the journey quite a bit more fun and warm, from my perspective.

Lastly, I acknowledge my mentor and our current lab members. I offer my heartfelt thanks and best wishes to Everett Hall, my friend and lab mate. His enthusiasm, hard work, humor and friendship have made the latter part of this journey most enjoyable for me, for which I am very thankful all around. I predict and hope for all the best things in his future. Luke Wenger and Jeremy Goering are much more recent lab members and friends, but no less deserving of acknowledgment, as their efforts are moving the project I soon leave in exciting new directions.

To my most valued and esteemed mentor, Dr. Irfan Saadi, no words can adequately express the gratitude in my heart, for not just the effort he has taken in educating me and helping me to become a scientist, but also his great friendship. Further, I need to acknowledge and thank him for the grand sum of time he has spent helping me investigate, shape and complete the project described in this document. He will always have my endless gratitude, as he has been both the mentor I needed and wanted.

Last, and most importantly, I lovingly acknowledge my wife Lina Yu, who has always supported me throughout the good and also the challenging times, and who contributed the hierarchical edge bundling analysis included in this appendix of this document. She will defend her doctoral dissertation a few weeks after me, and thus I am very proud of her and excited for our future together. She is the light of my life, and I am the most fortunate man alive to share these challenges, opportunities and joys with her.

Dedication

I dedicate this work to four generations. The first and eldest are my beautiful grandparents. Together, they taught me many things but specifically the vital elements of persistence, scholarship and how to best appreciate the fruits which blossom from them, in time. Next and foremost, my parents, who created every opportunity I had in my childhood. They made everything possible for all of us and made it look easy. As l look backward and forward, I know that it was not easy, but they made it seem so – loving and always nurturing.

I equally dedicate this work to the love of my life, my wife Lina. She always makes my heart and eyes shine bright, and lifts me when I need love, support and every other wonderful thing that she brings. Last, but always first in my mind, I dedicate this work to the next generation – my three nieces, Lilly, Olivia and Sage, our daughter Toni and the child we will welcome soon, to accompany her throughout her life and ours.

Table of Contents

List of figures

List of tables

List of abbreviations:

AJ	Adherens junction
C/Ctrl	Control
CCD	Coiled coil domain
CCM	Collective cell migration
CCR	Cell circularity ratio
CDH	Congenital diaphragmatic hernia
CHD	Calponin homology domain
CKR	Chemokine receptor
CLO	Cleft lip only
CLP	Cleft lip and palate
CME	Clathrin-mediated endocytosis
CNC	Cranial neural crest
CNCC	Cranial neural crest cells
CP	Cleft palate
CPO	Cleft palate only
Cre	Cre recombinase
CT	Computed tomography
C2	C2 protein domain, involved in membrane targeting
DTM	*Specc1l* genetrap construct/allele
E	Embryonic development day
ECM	Extracellular matrix
EMT	Epithelial-mesenchymal transition
ENU	*N*-ethyl-*N*-nitrosourea-induced mutagenesis
EPI	Epithelium
FNP	Frontonasal prominence
GFP	Green fluorescent protein
GPCR	G protein-coupled receptor
GTP	Guanosine-5'-triphosphate
HEK-293	Human embryonic kidney-derived cell line
H1299	Human non-small cell lung carcinoma-derived cell line
IGG	Immunoglobulin G
ITG	Integrin
KD	Knockdown
LacZ	Gene encoding β-galactosidase
LNP	Lateral nasal prominence
MDCK	Madin-Darby Canine Kidney Epithelium-derived cell line
MdP	Mandibular prominence
MEE	Medial-edge epithelium
MEPM	Mouse embryonic palatal mesenchyme
MNP	Median nasal prominence
MRI	Magnetic resonance imaging
MSC	Mesenchymal stem cell
MT	Microtubule
MxP	Maxillary prominence

List of abbreviations (continued):

NPB	Neural plate border
NC	Neural crest
NE	Neural ectoderm
NF	Neural fold
NG	Neural groove
NP	Neural plate
NS	Nasal septum
NT	Neural tube
ObFC	Oblique facial cleft
PA	Pharyngeal arch
PM	Paraxial mesoderm
PCR	Polymerase chain reaction
PH	Pleckstrin homology domain
PI	Phosphatidyl inositol
PIP_2	Phosphatidylinositol 4,5-bisphosphate / PtdIns(4,5)P_2
PIP_3	Phosphatidylinositol (3,4,5)-trisphosphate / PtdIns(3,4,5)P_3
PIV	Particle image velocimetry
PM	Plasma membrane
PP	Primary palate
PS	Palatal shelf
PTM	Post-translational modification
qRT-PCR	Quantitative real-time polymerase chain reaction
R	Rhombomere
RBD	Ras-binding domain
RFP	Red fluorescent protein
ROSA	Reverse-orientation splice acceptor
RRH	*Specc1l* genetrap construct/allele
RTK	Receptor tyrosine kinase
SH2	Sarc homology 2 protein domain
SH3	Sarc homology 3 protein domain
SNP	Single nucleotide polymorphism
SNV	Single nucleotide variant
T	Tongue
T(*n*)	Timepoint *n*
TEM	Transmission electron microscopy
TJ	Tight junction
U2OS	Human bone osteosarcoma epithelium-derived cell line
WES	Whole exome sequencing
Wnt1-GFP	*Wnt1*transcription-dependent green fluorescent protein
Wort	Wortmannin
WT	Wild type
X-gal	5-bromo-4-chloro-3-indolyl-β-D-galactopyranoside
Y2H	Yeast two-hybrid screen
Δ300	*Specc1l* allele harboring zinc finger nuclease-induced deletion

List of protein symbols and names:

ADAM10-19	Disintegrin and metalloproteinase domain-containing protein 10
AKT	RAC-alpha serine/threonine-protein kinase
AMOTL2	Angiomotin-like protein 2
APC	Adenomatous polyposis coli
AP2	Adaptor protein 2
AP2α	Transcription factor AP-2-alpha
ARRB2	Beta-arrestin-2
BAD	Bcl2-associated agonist of cell death
BAX	Bcl2 -associated protein
BCL-XL	B-cell lymphoma-extra large
BCL2	B-cell lymphoma 2
BIM	Bcl2-like protein 11
BMP4	Bone morphogenetic protein 4
CAP350	Centrosome-associated protein 350
CCDC8	Coiled-coil domain-containing protein 8
c-MYC	Myc proto-oncogene
CDC42	Cell division control protein 42 homolog
CD44	Cluster of differentiation 44
CFL1	Cofilin 1
CYCLIN D1	G1/S-specific cyclin-D1
DAB2	Disabled homolog 2
DLX5	Distal-less homeobox 5
E-Cadherin	Epithelial cadherin / Cadherin 1
ECM29	Proteasome-associated protein ECM29
EFNB1	Ephrin-B1
EGF	Epidermal growth factor
FAK	Focal adhesion kinase
FCHO1/2	F-BAR domain only protein 1/2
FGF	Fibroblast growth factor
FOXD3	Forkhead box protein D3
FOXO1/3A	Forkhead box protein O1/3A
GAB1/2	GRB2-associated-binding protein 1/2
GBX2	Gastrulation brain homeobox 2
GHRL3	Grainyhead like transcription factor 3
GLI1	GLI Family Zinc Finger 1
GPC3	Glypican-3
GP135	Podocalyxin
GSK-3	Glycogen synthase kinase 3
HERC2	HECT And RLD Domain Containing E3 Ubiquitin Protein Ligase 2
HIPK2	Homeodomain-interacting protein kinase 2
HRB	HIV virus Rev-binding protein
HSP90	Heat shock protein 90
ID2/3	Inhibitor of differentiation 2/3
IκB	Nuclear factor of kappa light polypeptide gene enhancer in B-cells inhibitor

List of protein symbols and names (continued):

ILK	Integrin linked kinase
IRS1	Insulin receptor substrate 1
IRF6	Interferon regulatory factor 6
JAK1	Janus kinase 1
KI67	Proliferation marker protein KI67
KIF4A/5C	Kinesin 4A/5C
MAPRE1	Microtubule-associated protein RP/EB family member 1
MCL-1	Induced myeloid leukemia cell differentiation protein Mcl-1
MDM2	Mouse double minute 2
MERLIN	Neurofibromin
MID1	E3 ubiquitin-protein ligase Midline-1
MIP1	Mps1 interacting protein-1
MMP2-9	Matrix metallopeptidase 2-9
MPS1	Mono-polar spindle 1
MSX1/2	Msh homeobox 1/2
mTORC1/2	Master target of Rapamycin complex 1/2
MYH9	Myosin heavy chain 9
MYO3A/5C	Myosin 3A/5C
MYT1	Myelin transcription factor 1
N-Cadherin	Neuronal Cadherin
NOXA	Phorbol-12-myristate-13-acetate-induced protein 1
PAXA	Paxillin A
PAX3/7	Paired box 3/7
PDGF	Platelet-derived growth factor
PDGFRα	Platelet-derived growth factor receptor α
PDK1	3-Phosphoinositide Dependent Protein Kinase 1
PFKB2	Fructose-1-phosphate kinase 2
PHLPP	PH domain lnd Leucine rich repeat protein phosphatase
PIAS1	Protein inhibitor of activated STAT 1
PIPK1	Phosphatidyl Inositol phosphate kinase 1
PI3K	Phosphatidylinositol-4,5-bisphosphate 3-kinase
PI4K	Phosphatidyl Inositol phosphate kinase 1
PP2A	Protein phosphatase 2 A
PRK2	Protein kinase N2
PTCH	Patched
PTEN	Phosphatase and Tensin homolog
P21 CIP	Cyclin-dependent kinase inhibitor 1A
P27 KIP	Cyclin-dependent kinase inhibitor 1B
P53	Tumor protein P53
P70 S6K	Ribosomal protein S6 kinase
RAC1	Ras-related C3 botulinum toxin substrate 1
RAPTOR	Regulatory-associated protein of mTOR
RAS	Ras GTPase
RHOA	Ras homolog gene family, member A

List of protein symbols and names (continued):

RHOGAP22	Rho GTPase Activating Protein 22
RICTOR	Rapamycin-insensitive companion of MTOR
SACM1L	SAC1 mutations 1-like
SAC1	Suppressor of Actin
SDF1	Stromal cell-derived factor 1
SENP1	SUMO1/Sentrin specific peptidase 1
SHH	Sonic hedgehog
SHIP	SH2 domain containing inositol 5-phosphatases
SNAIL-1	Snail family transcriptional repressor 1 (SNAIL)
SNAIL-2	Snail family transcriptional repressor 2 (SLUG)
SNAIL-3	Snail family transcriptional repressor 3 (TWIST)
SNX9	Sorting Nexin 9
SMARCA4	Transcription activator BRG1
SOX9/10	SRY (Sex determining region Y)-box 9/10
SPAST	Spastin
SPECC1L	Sperm antigen with Calponin homology and coiled-coil domains 1-like
SSH1L	Slingshot protein phosphatase 1
STAT1	Signal transducer and activator of transcription 1
SUMO1	Small Ubiquitin-like modifier 1
S6K	40S ribosomal protein S6K
TBX1	T-box transcription factor TBX1
TGF-β	Transforming growth factor beta
TGFBR1/2	Transforming growth factor beta receptor 1/2
TLR2/4	Toll-like receptor 2/4
TSC1/2	Tuberous Sclerosis 1/2
UBE2I	Ubiquitin conjugating enzyme E2 I
USP10/15	Ubiquitin specific peptidase 10/15
VE-Cadherin	Vascular-Endothelial Cadherin
VEGF	Vascular-Endothelial growth factor
WEE1	G2 checkpoint kinase WEE1
WNT1/5A	Wingless-related integration site family member 1/5A
XIAP	X-linked inhibitor of apoptosis
ZEB1	Zinc finger E-box Binding homeobox 1
ZIC1	Zinc finger protein ZIC1
14-3-3	Tyrosine 3-Monooxygenase

CHAPTER ONE:

GENERAL INTRODUCTION

Chapter One: General introduction

1.1 The neural crest

A key developmental process which distinguishes vertebrates from invertebrates is the contribution made by the neural crest to the cranium, heart and gut (Bronner, 2012). The neural crest constitutes a multipotent group of cell populations, which are similar in their shared multipotency, migratory infiltration of and contribution to a variety of developing embryonic tissues, throughout development. While the cranial neural crest cells (CNCCs) contribute to the developing cranial skeleton, the vagal neural crest contributes to the heart and the trunk neural crest to the gut. CNCCs are specified within and delaminate from the neural folds, subsequently migrating into the first pharyngeal arch to contribute to the bones of the maxilla and mandible.

1.1.1 Emergence of the neural crest from the neuroectoderm: Specification

The establishment of neural crest identity begins in the neural plate border (NPB), which lies at the interface of the developing neural plate and non-neural ectoderm. This process begins prior to neural tube closure, during gastrulation, and the NPB eventually becomes a morphologically distinct population as neurulation completes (Bronner, 2012). These induction and specification processes require initiating extracellular signaling and subsequent activation of NC gene networks, along with other layers of transcriptional regulation (Bronner, 2012).

Initially, the NPB arises from the ectoderm covering the embryo, upon gastrulation (Figure 1.1). This emerging structure shows gene expression relevant to establishing border identity, such as Msx1/2 and Pax3/7. In time the NPB elevates, giving rise to the paired neural folds, which will

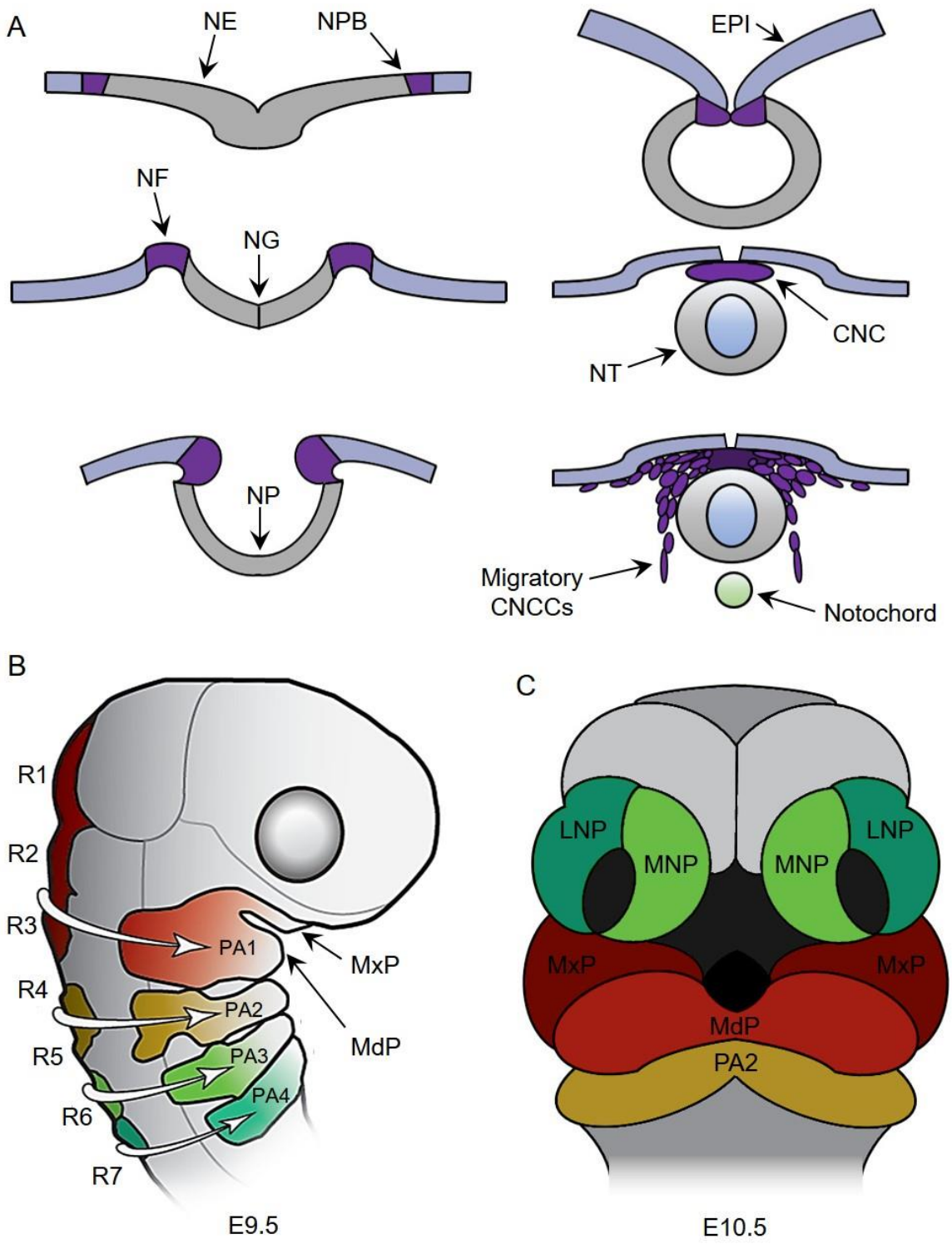
A
NE
NPB
NF
NG
NP
EPI
CNC
NT
Migratory
CNCCs
Notochord
B
R1
R2
R3
R4
R5
R6
R7
PA1
PA2
PA3
PA4
MxP
MdP
E9.5
C
LNP
MNP
MNP
LNP
MxP
MxP
MdP
PA2
E10.5

Figure 1.1. The delamination and migration of the cranial neural crest are required for craniofacial development. (**A**) The cranial neural crest (CNC) originate within the neural plate border (NPB, arrow), at the boundary of the neuroectoderm (NE, arrow). Subsequent development of NE involves invagination around the neural groove (NG, arrow), with CNC-precursors in the raised neural folds (NF, arrow). The forming neural plate (NP, arrow) brings the paired NFs into contact, allowing the fusion of the overlying epithelium (EPI, arrow) and the formation of the neural tube (NT, arrow), positioned dorsally to the Notochord (arrow). Subsequently, the cranial neural crest (CNC, arrow) are specificed, which in turn delaminate and migrate throughout the developing cranium (Migratory CNCCs, arrow). (**B**) At E9.5, CNCCs migrate ventrally, away from their rhombomere of origin (R1 through R7, arrows), to infiltrate primitive tissues, pharyngeal arches (PA1 through PA4, arrows). CNCCs originating from the three most rostral rhombomeres infiltrate PA1, contribing to the maxillary prominences (MxP, arrow) and the mandibular prominence (MdP). **C**) At E10.5, the developing face is comprised of facial prominences, including the lateral nasal prominences (LNPs), medial nasal prominences (LNPs), paired maxillary prominences (MxP) and a mandibular prominence (MdP), rostral to the second pharyngeal arch (PA2).

in time fuse at the dorsal midline to form the neural tube (Smith, 1987). Induction of NC in the NPB is initiated by signaling factors secreted by the surrounding non-neural ectoderm and non-neural plate, such as Bone morphogenetic proteins (BMPs), Fibroblast growth factors (FGF) as well as Wnts. Although the NPB also contacts the paraxial mesoderm (PM), the extent, if any, of pro-induction signaling originating from it is not fully understood. However, there are some indications that the PM may contribute, as a *Xenopus* study showed that removal of the PM resulted in reduced expression of *Snail2*. Upon reintroduction of the PM, ectodermal explant expression was restored, resulting in melanocyte production (Bonstein et al., 1998).

Generally, CNCC specification is known to require four overlapping signaling inputs. The non-neural ectoderm is known to secrete BMPs and Wnt, while the paraxial mesoderm provides these signals, along with FGF. Lastly, Notch/Delta secretion by the overlying ectoderm (Cornell & Eisen, 2005). These inputs work synergistically to initiate expression of the genes known as NPB specifiers, including numerous transcription factors, such as Zic1, Pax3/7, Dlx5, Msx1/2, Gbx2 and AP2 (Li et al., 2009). The products of these NPB specifiers in turn initiate expression of the CNCC specifier genes associated with lineage emergence. These include specifying transcription factors, such as Snail1/2, which promotes EMT (Cheung et al., 2005), Id3 and c-Myb (Bronner, 2012). Twist, c-Myc, Sox 9 and Sox10 participate in EMT and other aspects of CNCC maintenance (Taylor & LaBonne, 2005, Honoré et al., 2003).

1.1.2 Delamination: A neural crest EMT required for migration

Neural crest exit from the neural tube is a rapid process, taking perhaps less than an hour (Ahlstrom, 2009). This process requires temporally sensitive activation and inactivation of

multiple gene regulatory networks, as well as a temporally sensitive repression or activation of specific cadherins, which is primarily seen in the initial repression of E-cadherin expression, a vital event in the early loss of epithelial characteristics (Duband, 2015). Indeed, ectopic cadherin expression interrupts CNCC delamination (Acloque et al., 2009).

Among the transcriptional regulators fine-tuned to generate an environment friendly for EMT, Snail, Zeb and Twist show specific temporal expression patterns (Duband, 2015). The transcription factor Snail is a regulator of gene expression enabling EMT, including repression of E-cadherin expression (Cano et al., 2000). Similarly, Zinc Finger E-Box Binding Homeobox 1 (Zeb1) and Snail-3 (Twist) also reduces E-cadherin expression, by binding and repressing its promoter region (Sanchez-Tillo et al., 2010).

The exit of CNCCs from the neural folds is provoked by bone morphogenetic protein 4 (BMP-4) activation of SMAD signaling, as well as contributory Wnt signaling, upregulating Snail-1/2 in the premigratory population, priming the cell for loss of epithelial characteristics (Sakai, 2005). A related transcription factor, c-Myb, activates expression of Snail-2, in the premigratory status (Betancur, 2005). Snail-1/2 activity increases throughout the specification phase, reaching a plateau in delamination (Duband, 2015). Upon successful delamination, Snail-1/2 activity is repressed by ubiquitination and degradation, allowing a migration-specific pattern of expression. Critical to CNCC functions is the transcriptional activator AP2 alpha, whose disruption causes severe cranial dysmorphology in mouse (Schorle et al., 1996), as well as the transcriptional repressor Sox10, which maintains CNCC multipotency during migration (Kim et al., 2003).

1.1.3 Migration dynamics and associated matrix substrates

Migratory CNCC, the population which contributes to the development of the maxilla and mandible, express distinct proteins and interact with each other and their microenvironment in specific ways distinct from the other subpopulations, such as the vagal and trunk neural crest (McKeown 2013). One such example lies in the selectivity of CNC chemotaxis throughout migration. While CNC have shown *in vitro* and *in vivo* sensitivities to chemoattractants such as platelet-derived growth factor (PDGF) and vascular endothelial-derived growth factor (VEGF) (McKeown et al., 2013). However, other NC subpopulations show sensitivities to other factors, such as fibroblast growth factor (FGF) and stromal cell-derived factor 1 (SDF1) (McKeown et al., 2013). This is one example of NC-environment interactions, which drive and regulate migration.

Another example can be found in the selective expression of matrix metalloproteinases (MMPs), which cleave the extracellular domains of surface proteins as well as some molecules which contribute to the extracellular matrix (ECM) (McKeown et al., 2013). Unlike vagal NC, which primarily employs MMPs such as MMP2 and ADAM17/19 or trunk NC which express MMP8, CNCs employ ADAM10, 12 and 18 (McKeown et al., 2013). Such difference has functional relevance, given the discovery of regulatory factors in the environments of CNC migration. One example is the discovery of so-called neural crest exclusion zones, which potentially exclude CNC migration through the expression of uncleavable MMP substrates (Kulesa et al., 2015). Evidence exists for MMP-substrate pairing as a guiding migratory factor, as work done with chick embryo shows that ADAM10 cleavage of cell adhesion protein CD44 allows CNC migration into the developing cornea (Huh et al., 2007).

Recently others have described mechanisms affecting both cell-matrix and cell-cell interactions synergistically, in CNC migration. Blocking the activity of matrix metalloproteinase 9 (MMP9) interrupted delamination and migration of CNC. These defects were due to blocking the ability of MMP9 to cleave N-cadherin during EMT and the basement membrane protein laminin, in migration (Monsonego-Ornan et al., 2009). Rodent models of CNC migration have shown subpopulation specificity of other cell adhesion proteins, such as cadherins and integrins. CNC show specific expression of Cadherins 6,11 and 19, while vagal-enteric NC also express multiple protocadherins, which can interact with host kinases such as Fyn, thus regulating distinct aspects of cell behavior (Gumbiner, 2005).

However, cell-cell specific interactions also guide NC migration. Throughout their journey, CNC typically remains in contact with each other, a movement described as 'chain migration' (Kulesa et al., 2015). CNC maintain cohesion throughout migration through shared gap junctions, tight junctions and other cell adhesions (Kulesa et al., 2015). Interestingly, work exploring the impact of reducing the population size of migratory CNC showed that individual cells compensated for the loss, clustering together to maintain cohesion and increasing their rate of intra-migratory proliferation (Kulesa et al., 2015). This result, when considered with other work showing that migratory CNC share cytoplasm via gap junctions, paints a larger picture of intracellular cooperation throughout this developmental process (Kulesa et al., 2015).

Taking a broader view of migration, two patterns emerge. An early, primary migration along the ventrolateral pathway provides the CNC contributing to the cartilage, bone, musculature and innervation of the frontonasal skeleton. This process is later joined by a dorsolateral migration proximal to the ectoderm, which infiltrates the dermis, generating melanocytes (Erickson & Goins, 1995). The structures which they each contribute to will now be described.

1.1.4 Ultimate structural contributions of the neural crest

The cranial skeleton of vertebrates is patterned by CNCCs (Gendron-Maguire et al., 1993). The cartilage, bone and nervous tissues generated are produced by CNCC proliferation throughout and after migration, generating craniofacial mesenchyme, which is multipotent (Calloni et al., 2007). This distinguishes CNC from trunk neural crest, which do not differentiate into bone or cartilage (Santagati 2003). The CNC originate from two separate populations, emerging from the hindbrain and midbrain. The posterior mesencephalic CNC population invades the pharyngeal arches to contribute to the maxilla, mandible and other structures. The more rostral diencephalic populations contribute to the frontonasal aspects of the cranial skeleton (Santagati & Rijli, 2003).

Hindbrain tissue identity varies along the anteroposterior axis, with adjacent compartments, known as rhombomeres differing in gene expression as well as the migratory pathways their distinct CNC populations will adopt, upon delamination (Santagati & Rijli, 2003). Thus, the first pharyngeal arch (PA1), the anlagen of the maxilla, mandible, incus, malleus and Meckel's cartilage, are colonized by CNC originating in the most anterior rhombomeres 1-3 (R1-3). CNC originating from posterior from posterior R3 through anterior R5 colonize the PA2, which gives rise to the stapes and hyoid bone, which is also contributed to by the CNC originating from posterior R5 and R6. These migratory streams also contribute to PA3. Finally, R7 colonization of PA4 generates supporting hyoid and epiglottic cartilage (Piotrowski et al., 1996).

The terminal identities of the tissues derived from each rhombomere are determined in part by the initial identity of the rhombomere itself (Hunt & Gulisano, 1991). Each rhombomere has an intrinsic identity determined by the variable expression of a set of paralogous homeotic transcription factors of the Hox family. The developmental destiny of each CNC population is

predetermined by the individual and synergistic expression patterns of the four members of the mammalian HOX cluster (Hunt & Gulisano, 1991). In this way, the more evolutionarily ancient patterns of hindbrain development are projected upon the more ventral and initially primitive pharyngeal arch sequence.

1.1.5 Variations in neural crest migratory patterns

Upon delamination, distinct anteroposterior neural crest populations begin their migratory invasion of the developing embryo. Broadly, these four populations are either cranial, trunk, vagal or cardiac. Cranial neural crest cells undergo dorsolateral migration, giving rise to the mesenchyme of the craniofacial prominences, bone, connective and neural tissue, as well as melanocytes. The trunk neural crest give also give rise to melanocytes, as well as the vertebral cartilage and dorsal root ganglia. Vagal neural crest contributes the enteric ganglia of the developing gut (Le Dourain & Teillet, 1973). The Cardiac neural crest gives rise to the large cardiac arteries and septum of the developing heart (Le Lievre & Dourain, 1975).

These distinct populations show different migratory qualities (Scarpa & Mayor, 2016). As the neural crest engage in a form of collective behavior known as collective cell migration (CCM), which involves the formation of streams of migrating cells, which transiently contact each other. These species -specific migration patterns are dynamic, with respect to the anterior-posterior axis, and show a reduction in width and size, proceeding from the head to the trunk, where single-cell wide streams are seen (Szabó & Mayor, 2016).

Collective migration of neural crest sub-populations is often categorized as being either chain-like or streaming migration or as migration of a sheet of cells (Schumacher et al., 2017).

These morphologies are generated by a combination of factors, including cell-cell cohesion and cell density (Schumacher et al., 2017). Chain migration (Figure 1.2) features continuous contact between neighbors or along trails generated by previous migration. Sheet migration requires a high cellular density, while streaming migration involves less persistent cell-cell contacts and frequent rearrangements (Schumacher et al., 2017).

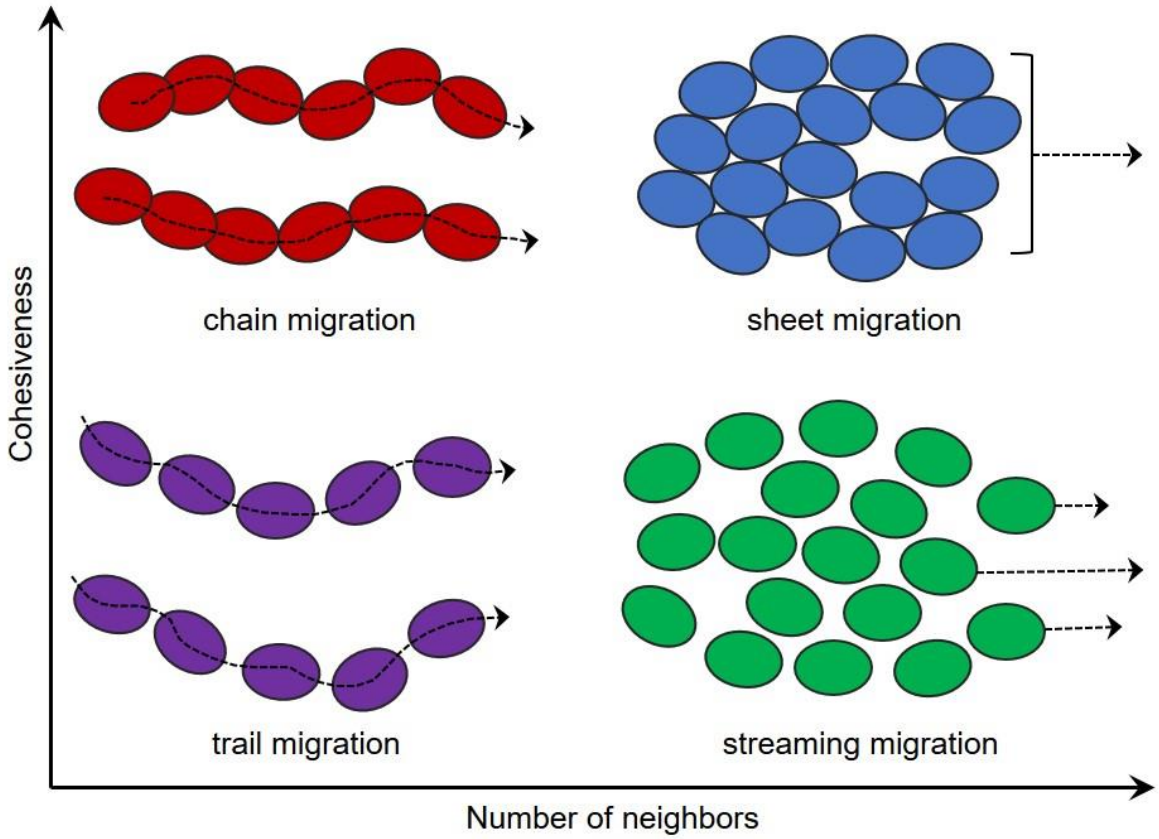

(Adapted from Schumacher, 2017)

Figure 1.2 Categories of collective cell migration and their relationships with density and cohesiveness. Cohesiveness and density affect the morphology of collective cell migration. Chain migration features continuous contact between neighbors (top left) or along trails generated by previous migrants (bottom left). Sheet migration involves the highest number of nearest neighbors (top right). Streaming migration involves less persistent cell-cell contacts and frequent rearrangements (bottom right).

1.1.6 Defining the unique properties of the neural crest

The cells of the neural crest are unique to vertebrate development and serve unique roles within it. An additional unique property of the neural crest is their anatomic origin. Upon gastrulation and the subsequent emergence of the three primary germ layers, the dorsal, neuroectodermal component of embryonic ectoderm gives rise to the neural plate. Upon receiving inductive signaling from the proximal epidermis, the region surrounding the neural plate, the neural plate border, gives rise to the neural crest.

A fundamental property of the neural crest is their ability to reacquire multipotency, after having already differentiated into the ectodermal lineage. This reacquisition of multipotency is a prerequisite for their unique roles in vertebrate development, as the distinct populations within the neural crest ultimately differentiate a second time. This secondary differentiation contributes to a diversity of cell lineages throughout the developing body, including cartilage and bone of the craniofacial skeleton, melanocytes and smooth muscle, as well as neurons and glia though out the trunk.

Prior to this contribution, cells of the neural crest show an additional property, the ability to collectively migrate, maintaining cell-cell adhesions throughout their various migratory paths. This collective behavior is necessary for their contribution to embryonic development, as well as a being a distinct process separate from the directed individual migration of cells seen in other lineages, throughout embryogenesis.

1.2 A synopsis of mammalian palatogenesis

The developing pharynx is initially flanked by five distinct tissue outgrowths, which will grow because of the proliferation of NC-derived mesenchyme (Ashique et al., 2002) and integrate with each other at multiple interfaces, which is disturbed in facial clefting (Tessier, 1976). Mammalian palatogenesis is similarly a unification of developing tissues, in the paired palatal shelves required for normal maxillary development.

Development of the mammalian mouth initially involves five facial prominences surrounding it, the frontonasal prominence (FNP), which must integrate with bilateral maxillary prominences (MxP). Similarly, paired mandibular prominences (MdP) also fuse, caudal to the maxilla, establishing the equivalent template for mandibular development (Figure 1.3). The interface of the paired MxPs and FNP form the upper lip and philtrum (Jiang et al., 2006). Defective integration of these prominences is one origin of cleft lip (Zaghloul & Brugmann, 2011).

Subsequent palatogenesis originates from paired outgrowths of the now integrated MxPs and FNP. These outgrowths, palatal shelves, must ultimately grow vertically, undergo elevation rostral to the developing tongue, enlarge to complete the void between them, achieve apposition at the frontal midline of the body (Figure 1.4) and, all within a very specific developmental window which shows little variation in timing for a given species, with disruptions of any of these processes potentially causing cleft palate (Bush & Jiang, 2012).

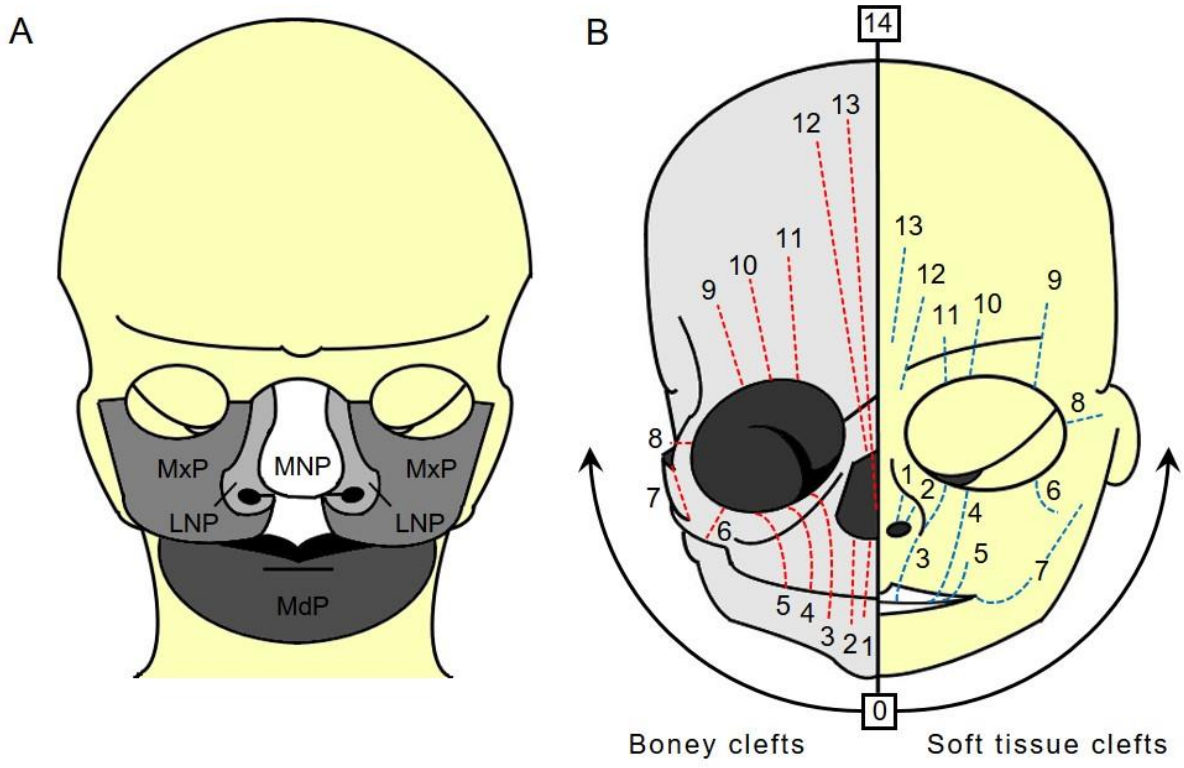

(Adapted from Tessier, 1976)

Figure 1.3. Orofacial clefts can result from unfused facial prominences. (**A**) Embryonic tissue contributions to the developed neonatal face. Proper facial formation requires the fusion of maxillary and mandibular prominences, with the maxillary prominences (MxP) fusing with both the mandibular prominence (MdP) and the later nasal prominences (LNP). The median nasal prominence (MNP) fuse with both the LNPs and MxPs. (**B**) Failed fusion of facial prominences can cause orofacial clefting involving either bone (left) or soft tissue (right). Facial clefting is categorized by position and tissue affected, as first described by Dr. Paul Tessier.

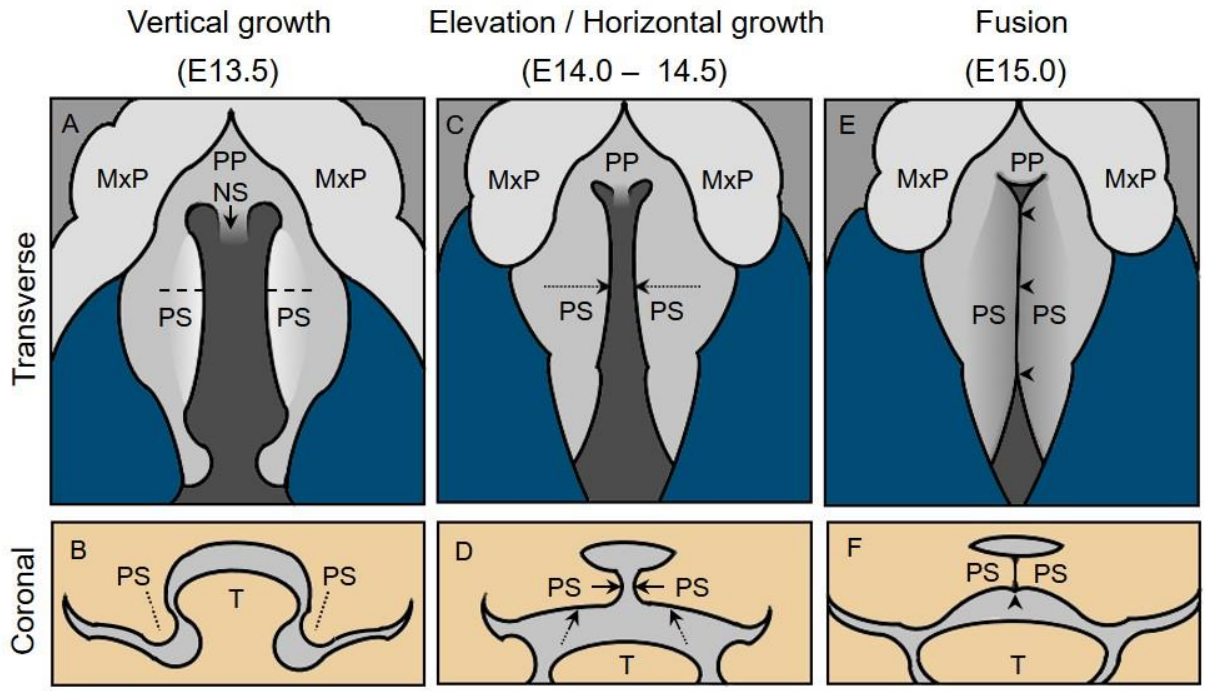

(Adapted from Bush, 2012)

Figure 1.4. Palatogenesis requires the growth, elevation and fusion of palatal shelves. During mouse embryogenesis, paired oral structures, the palatal shelves (PS), undergo vertical outgrowth at E13.5 (hashed line), closing the void that extends dorsally from the region containing the maxillary prominences (MxP), the primary palate (PP) and the nasal septum (NS), as seen in transverse view of the maxilla **(A)**. **(B)** A coronal view of the same process shows vertical outgrowth of PS (hashed line), anterior to the developing tongue (T). Beginning during E14.0, PS elevation (**C**, **D**, hashed arrows) is followed by horizontal growth (**D**, solid arrows). Subsequently, upon convergence, PS fusion along the midline completes palate formation, at E15.0 (**E**, **F**, arrowheads).

1.2.1 Proliferation within the palatal shelves yields outgrowth

The palatal shelves themselves offer a seemingly simple architecture involving only two broad cellular lineages, a polarized epithelium shrouding an enlarging mass of proliferating mesenchyme derived largely from the cranial neural crest (Ito et al., 2003). Interactions between these two cellular lineages are required for palatal shelf outgrowth (Bush & Jiang, 2012). Such outgrowth requires regulation of the cell cycle, ensuring optimal levels of mitosis in outgrowth. Epithelial secretion of patched (Ptch), the sonic hedgehog (Shh) receptor is a major driver of mesenchymal proliferation, along with Fibroblast growth factor (Fgf) signaling (Lan et al., 2009), with interactions between these pathways likely (Bush & Jiang, 2012).

1.2.2 Models of palatal shelf elevation

Elevation of the palatal shelves is a rapid process, which occurs in mouse at approximately E14.0, taking under an hour (Bush & Jiang, 2012). This rapidity is also the cause of palatal shelf elevation being the least understood element of palatogenesis, due to the challenges it presents in observing or attempting its recapitulation *in vitro*. Multiple models have been proposed to explain such a rapid tissue reorientation, which include hydrostatic interactions with palatal shelf ECM (Goudy et al., 2010) and mechanical force resulting from proliferation (Bush & Jiang, 2012), none of which have conclusively answered this question. Interestingly, one of the only genetic models of delayed palatal shelf elevation is *Zfhx1a* (*Zeb1*). *Zeb1* mutant mice consistently show elevation delay, without other features associated with defective palatogenesis (Kurima et al., 2011). This transcription factor plays a prominent role in EMT, suppressing transcription of epithelial cadherin, along with other genes (Batlle et al., 2000), suggesting a role for cell adhesion in

elevation. Collective cell migration, involving coordinated movements of cell streams, is potentially relevant to palatal shelf development. Deficiency of one of the few known proteins which coordinates collective migration, the tumor suppressor Merlin, shows cleft palate in mouse (Gritli-Linde 2008).

1.2.3 Signaling induced upon apposition and adhesion of the palatal shelves

Upon palatal shelf apposition, adhesion of palatal shelves proceeds anterior and posterior to the site of first contact (Bush & Jiang, 2012). As this joining first involves contact between two seemingly identical, bilateral epithelia, an exploration of epithelial cell-cell interactions is important. Medial-edge epithelium (MEE) interactions between palatal shelves have been shown to be essentially temporally sensitive (Jin et al., 2008). Thus, qualities intrinsic to each palatal shelf epithelia are likely guiding factors in adhesion.

Interestingly, mouse mutants of the transcription factor Irf6 have cleft palate, due to abnormal adhesion between the palatal shelves and other oral structures, such as the tongue (Ingraham et al., 2006). However, *Irf6* expression is activated by another transcription factor, p63, disruption of which also causes clefting (Thomason et al., 2010). Both factors are expressed in the periderm, a thin epithelium overlying the continuous epithelium underneath. The periderm is a transient tissue, which is thought to serve a function in preventing the palatal shelves from fusing with other oral structures during outgrowth and elevation (Richardson et al., 2014). Ultimately, the cells of the periderm undergo apoptosis, in MEE, upon the medial apposition of the palatal shelves (Polakowska et al., 1994).

1.2.4 Palatal shelf fusion and the completion of the palate

The fusion of the now apposed palatal shelves first requires removal of the periderm from the MEE, allowing adhesion and subsequently the abolition of the underlying MEE (Tudela et al., 2002). Palatal shelf adhesion involves TGF-β signaling, with disruption yielding failed adhesion and persistent MEE (Kaartinen 1995, Proetzel 1995). Failed MEE removal, which is required for the integration of the apposed mesenchyme, is a cause of cleft palate (Proetzel 1995). Proper fusion at E15.5 begins at the central meeting point and a subsequent wave of ventral and dorsal adhesion (Alexander et al., 2011). This is followed by the anterior fusion with the primary palate (Bush & Jiang, 2012).

1.3 Neurocristopathies: Pathologies of the neural crest

The disruption of any process involved in embryonic development has pathogenic potential. The neural crest is no exception, as a spectrum of diverse pathologies of the neural crest, collectively termed neurocristopathies, has been described (Bolande, 1974). Neurocristopathies are as varied as are the derivatives of the neural crest. Broadly, neurocristopathies affect craniofacial development, as seen in Waardenburg syndrome (Waardenburg, 1951), cardiac morphogenesis, as seen in Velo-cardio-facial syndrome (Shprintzen et al., 1981), or intestinal innervation, specifically Hirschprung's disease (Amiel & Lyonnet, 2001). Often, the symptoms of neurocristopathies can overlap between two syndromes in the same patient, complicating our understanding of the pathogenetic mechanism responsible.

1.3.1 Neurocristopathies feature orofacial clefting:

A common feature of multiple neurocristopathies is orofacial clefting, as frequently seen in common syndromes such as Van der Woude syndrome, Pierre Robin sequence, Velo-cardio facial syndrome and Median facial dysplasia (Venkatesh et al., 2009). Clefting can occur as cleft lip only (CLO), cleft palate only (CPO) or cleft lip and palate (CLP) (Sun et al., 2015). Patients afflicted by Waardenburg syndrome, which primarily involves mild craniofacial abnormalities such as broad nasal root and pigmentation defects. The primary pathogenesis of Waardenburg syndrome, which can also involve CP (Yoshida et al., 2016), is due to heterozygous mutations in *Pax3*, a transcription factor involved in NC specification. Pax3 activates expression of *AP2 alpha*, a critical transcription factor in CNCC specification (Plouhinec et al., 2014).

DiGeorge syndrome patient frequently present CP (Narges et al., 2016). The pathogenesis of DiGeorge syndrome (also known as 22q11.2 deletion syndrome) is a microdeletion of variable length, in the q11.2 locus of chromosome 22. Work has focused upon the transcription factor Tbx1, which functions in the differentiation of post-migratory NC. Indeed, an ENU mutagenesis – derived mouse model of *Tbx1* disruption shows a range of phenotypes like DiGeorge (Barrett et al., 1981). Finally, the symptoms of Goldenhar syndrome include CP and infrequently lateral facial clefts (Chauhan et al., 2015). Its genetic etiology is unknown.

1.4 SPECC1L: A novel cytoskeletal protein with a role in craniofacial morphogenesis

1.4.1 The discovery of *SPECC1L* mutations in patients with atypical clefts

The cytoskeletal crosslinking protein encoded by the gene Sperm antigen with calponin homology and coiled-coil domains 1 like (*SPECC1L*) was first identified as disrupted by a balanced chromosomal translocation involving chromosomes 1 and 22 of a female neonate born with severe, atypical facial clefts. This rare birth defect affects 1 in every 200,000 live births, and is the result of failed fusion of craniofacial prominences. The patient in question also had cleft palate (CP) as well as micropthalmia and talipes calcaneovarus deformity.

An additional SPECC1L mutation, a *de novo* heterozygous missense mutation, p.Gln415Pro (Q415P), was identified in a male neonate with bilateral atypical facial clefts (Saadi et al., 2011). *In situ* hybridization of mouse *Specc1l* showed prominent expression in the maxillary prominence and lateral nasal processes which fail to fuse in atypical clefts, as well as the eyes and limbs, at embryonic day E9.5-E10.5.

1.4.2 Aberrant adhesion and migration upon *SPECC1L Drosophila* ortholog *CG13366*-kd

Ubiquitous reduction of CG13366, the *Drosophila* ortholog of *SPECC1L*, by RNA interference yielded multiple phenotypes suggestive of impaired cellular adhesion and migration, which the author named the ‘Split discs’ phenotype, due to the failure of dorsal and ventral imaginal discs to properly migrate and adhere to each other. This process is dependent on a class of cell adhesion molecules, integrins. Integrins are important to the processes of migration and adhesion. Many of the *CG13366* knockdown phenotypes suggest defective migration and adhesion in development. Specifically, a wing imaginal disc-specific *CG13366* reduction showed wing

defects involving altered adhesion of the opposing aspects of the developing wing, such as seen in integrin mutants *inflated* and *multiple edematous wings* (Saadi et al., 2011).

1.4.3 *Specc1lb* is implicated in a zebrafish model of oblique facial clefting

Recently, others have employed the zebrafish model to explore how *SPECC1L* disruption results in the rarer and more severe oblique facial clefting described by Saadi et al., (2011), which provided the first and currently one of the only genes implicated in this rare genetic anomaly. *SPECC1L* has two zebrafish homologs, *specc1la* and *specc1lb*. *Specc1lb* is expressed in the epithelia surrounding craniofacial chondrocyte populations; *specc1la* disruption did not yield a craniofacial phenotype. This led to the question of how *Specc1lb* disruption could illustrate its role in the fusion of craniofacial prominences.

The zebrafish ethmoid plate is analogous to the developing palate, which involves the fusion of its median and lateral elements, as the frontonasal and maxillary prominences must converge in palatogenesis. The authors found that morpholino knockdown of *specc1lb* resulted in failure of the median and lateral aspects of the ethmoid plate to fuse, resulting in bilateral clefts. Additionally, the mandible is absent, showing that zebrafish *specc1lb* is required for upper and lower jaw formation, while reinforcing the role demonstrated for *SPECC1L* in human oblique facial clefting (Saadi et al., 2011). Thus, zebrafish *specc1lb* offers currently the only genetic model of oblique facial clefting.

Zebrafish palatogenesis requires a proliferative wave in the pharyngeal structures, to allow convergence and extension in creating mature craniofacial cartilage. *Specc1lb* morphants show a reduction in the extent of such proliferation, with no increase in apoptosis. As the epithelia surrounding chondrocytes play extracellular signaling roles in chondrocyte development, the

authors speculate that *specc1lb* may play a role in that signaling. Thus, upon *specc1lb* knockdown, reduced chondrocyte proliferation is causative in failed extension and subsequent convergence of the ethmoid plate anlage.

Ultimately, the authors posit that *specc1lb* is facilitating different developmental processes in the mandible and maxilla. The absence of a mandible suggests that *specc1lb* enables convergence of the mandibular prominences, and promotes integration of the aspects of the ethmoid plate in the maxilla. Interestingly, zebrafish transcription factor *irf6* is required for this integration. This transcription factor is also implicated in human clefting (Khandelwal et al., 2017).

Still, unresolved questions remain. One example can be found in the absent mandible phenotype, which is not a feature of human oblique facial clefting, suggesting that *specc1lb* serves prominence-specific functions which may be shared with human maxillary, but not mandibular development. Also, a putative role for *specc1la* has not been explored. Although *specc1la* knockdown did not produce the relevant phenotype, there has been no exploration of whether the introduction of *specc1la* mRNA can rescue *specc1lb* defects. Ultimately the nature of this gene duplication may make a zebrafish model of human *SPECC1L* deficiency challenging to interpret.

1.4.4 Mammalian *in vitro* models of *SPECC1L* deficiency

Immunostaining showed that *SPECC1L* associates with the actin and microtubule cytoskeletons and is a cytoskeletal protein. Ectopic Specc1l-GFP localizes to a subset of microtubules containing the acetylated form of α-tubulin. This association is abolished by removal of the carboxyl-terminal Calponin homology domain (CHD), suggesting that endogenous *SPECC1L* associates with the microtubule cytoskeleton via its interactions with actin, which is bound by the CHD of other proteins (Korenbaum et al., 2002). Indeed, overexpression or reduction

of *SPECC1L* results in actin reorganization defects. Overexpression of ObFC patient-mutation Q415P fails to associate normally with microtubules. Endogenous *SPECC1L* also colocalizes with filamentous actin and acetylated α-tubulin of the mitotic spindles, suggesting a role for *SPECC1L* in mitosis which would be further confirmed by a publication of the same year (Mattison et al., 2011).

In vitro models of *SPECC1L* deficiency in mammalian cell lines revealed altered adhesion (Saadi et al., 2011). *SPECC1L*-kd in human embryonic kidney 293 (HEK-293) cells show defective adhesion to the growth substrate, but only upon reaching confluence, when they collectively detach. Interestingly, the introduction of Matrigel substrate does not restore density-based alterations in adhesion. Also, *SPECC1L*-kd HEK-293 cells show reduced filopodia and filamentous actin microspikes, which have been described as indicators of impaired adhesion and motility (Webb et al., 2003).

Actin cytoskeleton reorganization is required for adequate cell adhesion (Calderwood et al., 2000) and migration (Ridley et al., 2003). In wound assays using human osteosarcoma cell line U2OS, *SPECC1L*-kd cells fail to migrate into the wound fully, when compared to WT U2OS cell cultures given the same amount of time. *SPECC1L*-kd U2OS osteosarcoma cells show actin cytoskeletal defects, in the form of an increase in non-cortical, perinuclear actin stress fibers. Promigratory Wnt ligand Wnt5a induces actin cytoskeletal reorganization to facilitate migration (Witze et al., 2008). Upon Wnt5a exposure, *SPECC1L*-kd U2OS fail to reorganize actin at the leading edge, perpendicular to the direction of impending migration, as seen in WT U2OS cells.

In summary, disruption of *SPECC1L* causes severe, atypical clefting. *SPECC1L* deficiency disrupts cell adhesion and migration *in vitro,* offering potential mechanisms underlying defective proliferation within or fusion of craniofacial prominences in the pathogenesis of atypical clefts.

The role played by *SPECC1L* in its association with microtubules is disrupted by SPECC1L mutation. Facilitation of adhesion and migration in the cells which contribute to craniofacial formation would explain the *SPECC1L* disruption induced pathogenesis of ObFC. Thus, SPECC1L plays a critical role in actin-cytoskeleton reorganization that is required for proper facial morphogenesis.

1.4.5 A distinct role for *SPECC1L* in cytokinesis

Complementing the foundational work showing that *SPECC1L* is a cause of orofacial clefting, others described an additional, fundamental role for this protein in cytokinesis. This role was specific to cell cortex stability and the positioning of the mitotic spindles during anaphase (Mattison et al., 2011). These findings have intriguing overlaps with previous research regarding *SPECC1L*, and are also supported by our recent findings, regarding its protein interactors.

Initially, the authors sought to identify and describe the functions of novel substrates of a protein kinase essential for spindle body formation, mono-polar spindle 1 (*MPS1*). *MPS1* localizes to and is involved in centrosome duplication prior to the onset of mitosis. In doing so, they identified MPS1-interacting protein 1 (*MIP1*, *SPECC1L*) as an *MPS1* substrate with dynamic localization throughout cell cycle progression.

This dynamic localization begins with a prominent association with the actin cytoskeleton during interphase, as already described (Saadi et al., 2011). Upon the onset of mitotis early metaphase cells initially show *SPECC1L* association with gamma tubulin found within the microtubule spindle network. Throughout anaphase, *SPECC1L* is associated throughout the development of the ingression furrow and the midbody. The authors note that this mitotic

expression pattern is reminiscent of the actin-binding protein Anillin, which is required for ingression furrow development.

Induced depletion of *SPECC1L* also yielded intriguing insights. *Specc1l* siRNA knockdown in U2OS cells induced a 24 percent increase in bi- and tetra-nucleate cells, after 48 hours, demonstrating defective anaphase separation of chromosomes. Live cell imaging revealed that treated cells exhibited a violent spindle rocking phenotype which often left daughter chromosomes intact within one parent cell only. These results suggest that *SPECC1L* functions in stabilizing or positioning mitotic spindles.

1.5 PI3K-AKT signaling

1.5.1 Introduction

One key signaling pathway influencing many of the cellular phenotypes observed throughout the course of this study is the Phosphatidylinositol-4,5-Bisphosphate 3-Kinase (PI3K) cascade. PI3K is a lipid kinase which generates the specific inositol lipid species required for the activation of downstream kinases, such as the serine-threonine kinase v-akt murine thymoma viral oncogene homolog 1 (AKT/Protein kinase B), a protein of specific relevance to this study.

1.5.2 Extracellular origins of PI3K activation

Inositol lipid signaling via PI3K originates as a response, at the plasma membrane, to a variety of extracellular stimuli. Of importance to embryonic development are extracellular growth factors, such as Fibroblast growth factors (FGFs), epidermal growth factors (EGFs), Platelet-derived growth factors (PDGFs) and insulin, via a class of membrane bound receptors

characterized as receptor tyrosine kinases (RTKs) (Figure 1.4). Upon ligand bound dimerization, RTKs convey growth and survival promoting signaling, in this case, via Ras GTPase, to activate PI3Ks. Another such stimulus, via the focal adhesion kinase (FAK) pathway, is triggered by the dimerization of membrane bound integrins α and β, in response to cellular encounters with components of the extracellular matrix (ECM). A variety of small, signaling molecules, cytokines, stimulate PI3K signaling via cytokine activation of Janus kinase (JAK), in the JAK-STAT signaling pathway. PI3K can also be activated as a pathogenic response to pathogen-associated molecular patterns, via Toll-like receptors (TLR2/4), via Ras-related C3 botulinum toxin substrate 1 (RAC1) signaling to PI3Ks. These are the known ligands and corresponding pathways of the sub-category known as Class IA PI3Ks, the features of which will be described subsequently.

1.5.3 Phosphoinositide chemistry related to PI3K phosphorylation

Embedded within the plasma membrane are a variety of modified phospholipids capable of multiple cellular roles, ranging from membrane deformation in endocytosis to acting as second messengers in key signaling cascades, including PI3K-AKT signaling. The inositol ring of Phosphatidyl inositol (PI) can be modified via kinase phosphorylation at multiple carbons, yielding numerous species. However, it should be noted that other phospho-PI species exist and are generated by enzymes not shown. These pathways will also generate substrates for this and other phospho-PI pathways (Figure 1.5).

As an example of this ATP hydrolysis driven phosphorylation, PI phosphorylation by Phosphatidyl Inositol kinase 4 (PI4K) at 4′-position yields the monophosphate species PI(4)P. Subsequent phosphorylation of the 5′-position by Phosphatidyl Inositol phosphate kinase 1 (PIPK1) yields Phosphoinositol bisphosphate (PtdIns-3,4,5-P_2 or PIP_2). In response to

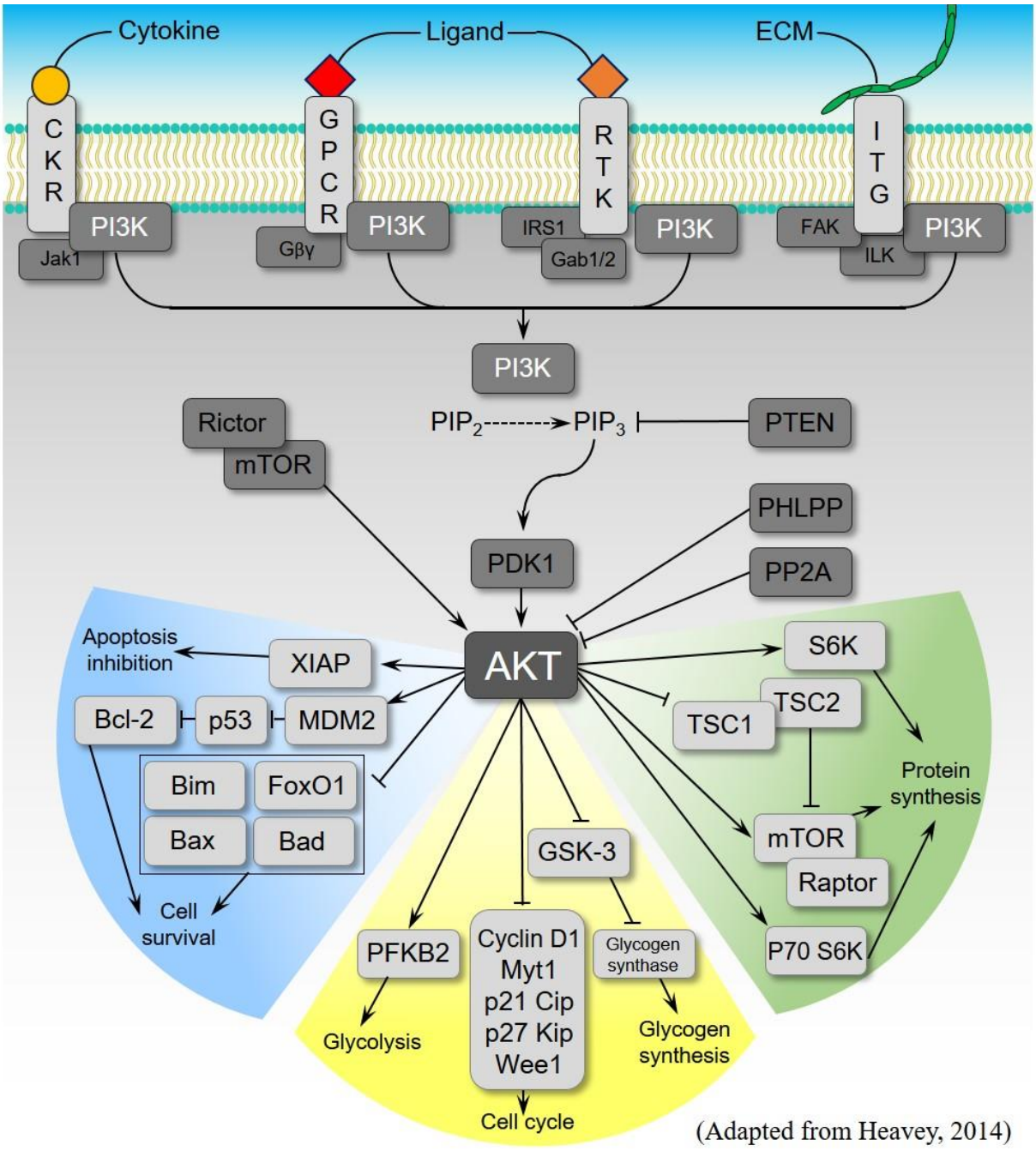

(Adapted from Heavey, 2014)

Figure 1.5. The PI3K-AKT signaling pathway promotes cell growth and survival. (Top) PI3K is activated by multiple extracellular signals, including cytokines, growth factors and contact with the extra-cellular matrix. **(Middle)** Upon activation, lipid kinase PI3K phosphorylates Phosphatidylinositol 4,5-bisphosphate (PIP_2), yielding increased levels of the triphosphate PIP_3. Increased PIP_3 activates PDK1, which activates AKT at the membrane. **(Bottom)** Upon activation, AKT positively and negatively regulates numerous substrates, many of which are involved with cell survival **(blue)**, cell growth and cell cycle control **(yellow)**, as well as protein synthesis **(green)**.

extracellular cues, PI3Ks modify this phospholipid messengers, by phosphorylation of the 3′-position of the inositol ring of Phosphoinositol bisphosphate (PtdIns-3,4,5-P_2 or PIP_2) yielding Phosphoinositol triphosphate (PtdIns-4,5-P_3 or PIP_3). Both species of phospholipid have specific and distinct signaling effects, important to directional migration and cell polarity, generally. Each step in this pathway can be reversed by a competing phosphatase, such as SAC1 Suppressor of Actin Mutations 1-Like (SACM1L), SH2 domain containing inositol 5-phosphatases (SHIPs) or Phosphatase and Tensin Homolog found on Chromosome ten (PTEN). PTEN is the antagonist of PI3Ks, generating PIP_2 from PIP_3 via the cleavage phosphate from the 3′-position of the inositol ring (Figure 1.5). Importantly, with respect to this study, increased PtdIns-3,4,5-P_3 induces the activity of 3-Phosphoinositide dependent protein kinase-1 (PDK-1), ultimately resulting in increased levels of activated AKT at the plasma membrane.

1.5.4 The quaternary structures of PI3K

The quaternary structures of PI3K are highly modular, allowing for multiple configurations of protein subunits, depending upon the needs of the cell. In restricting our consideration to include only Class I PI3Ks, a theme emerges, which is the joining of a catalytic and a regulatory subunit.

The class I PI3Ks, whose *in vivo* substrate is specifically PIP_2, is a dimer of a phospholipid producing p110 catalytic subunit, and a p85 regulatory subunit. The catalytic subunit can be one of four structural variants, p110α, p110β, p110γ and p110δ. All of these, except the γ subunit possess a p85 binding domain, facilitating dimerization. The p110γ lacks this domain and forms a heterodimer with the p101 or p87 regulatory variants.

All p110 subunits are comprised of four other common domains, apart from the amino-terminal p85-binding domain. First is the Ras-binding domain (RBD). The RBD is imagined

playing a primordial function in PI3K activation. Evidence of this is found in the slime mold *Dictyostelium discoideum*, which lacks p85 regulatory subunits entirely, and is primarily activated by GPCR-triggered Ras. The remaining three domains constitute the PI3K core responsible for lipid phosphorylation. The C2 domain is a lipid-binding domain frequently found in proteins associated with the plasma membrane. A proximal helical domain is known to frequently facilitate protein-protein interactions. Finally, a carboxyl-terminal catalytic domain is the site of lipid phosphorylation. These three domains are collectively known as the PI3K core, as they tether lipid kinase activity with the plasma membrane.

Complementing this is the domain architecture of the p85 regulatory subunit. This protein contains multiple Src-homology domains. An amino-terminal Src-homology 3 (SH3) domain is thought to possess a GTPase-activating function, suggesting that PI3Ks can functionally communicate with small GTPases, such as Rho, Rac and Cdc42. Adjacent to this is a single Breakpoint cluster region-homology domain (BH domain). BH domains typically play a role in GTPase functions, although it is yet to be demonstrated that this domain is active in PI3Ks. Finally, three carboxyl-terminal domains constitute the p85 core, which is a p110-binding domain, flanked on each side by a Src-homology 2 (SH2) domain. SH2 domains are typically found in adapter proteins, which interact with RTKs, such as the category of receptors which initiate PI3K signaling (Figure 1.5).

1.5.5 Phospholipid activation of PDK1 and subsequent activation of AKT

In the larger mechanism of phosphoinositide signaling, a less well-understood activity is the intermediate activation of AKT by PDK1, a phosphoinositide-dependent protein kinase. The regulation of AKT-activating phosphorylation is crucial to the proper coordination of multiple

cellular processes, as evidenced by the strong correlation between activating AKT mutations and multiple cancers.

Upon PI3K activation and subsequent phospholipid function, synthesized PIP_3 accumulates within the cytosolic face of the lipid bilayer. Unstimulated cells have large reserves of the monophosphate PtdIns3P. However, upon RTK stimulation, PIP_2 and PIP_3 levels rise, attracting multiple proteins to the membrane, specifically those containing a globular Pleckstrin homology domain (PH domain). Both PDK1 and AKT are mostly cytosolic in distribution, in the non-active state existing prior to stimulation. It is the PH domain of PDK1 and AKT that induces their interaction at the membrane, upon stimulation, as the PH domain has a far higher affinity for PIP_3 and PIP_2, over other PIs (Figure 1.5).

AKT is activated at the plasma membrane, via two activating, post-translational modifications (PTMs). PDK1 phosphorylation of AKT, at Thr^{308}, which resides in the activation loop, or so called T-loop of the kinase domain, is found in combination with another activating phosphorylation. This T-loop is a highly-conserved region of multiple kinases, suggesting regulatory phosphorylation of it is also a conserved process. The second activating phosphorylation is Ser^{473}, in the C-terminal regulatory domain. Interestingly, PDK1 can phosphorylate Thr^{308} directly, but only Ser^{473} when associated with another kinase, Protein kinase N2 (PRK2). There are indications that other kinases, such as the master target of Rapamycin complex 2 (mTORC2), can also phosphorylate this residue. Mutation of either site to Alanine does not abolish phosphorylation of the other, indicating that these are separate, but not necessarily sequential events. Ultimately, activated AKT disassociates from the plasma membrane, to phosphorylate its many cytosolic and nuclear substrates.

1.5.6 Regulation of multiple cellular systems via AKT phosphoregulation

Thus far, there are over 200 verified substrates of AKT phosphoregulation, which participate in multiple cellular systems, as will be subsequently described. Although these substrates are quite varied, a minimal recognition motif has been described for this Serine/Threonine kinase (S/T kinase). AKT phosphorylates the recognition motif RXRXX S/T B, where X is any amino acid and B represents a large hydrophobic amino acid. Interestingly, a minority of AKT substrates lacks this motif, suggesting other methods of regulation by AKT. Its phosphoregulation can be activating, as in the case of IκB kinase and the upregulation of anti-apoptotic genes, or negative as seen in the inactivating phosphorylation of Glycogen synthase kinase 3 (GSK-3). Deficiencies in the PI3K-AKT signaling pathway are associated with embryonic sub-epidermal midline blebbing and cleft palate, as seen in the *Pdgfrα* mouse mutants (Fantauzzo & Soriano, 2014).

Upon verifying that this mutant model was signaling through AKT phosphorylation, in response to Pdgfr activation by PDGF, the authors employed a phosphoproteomic approach, involving primary mouse embryonic palatal mesenchyme (MEPM) as a proxy for palatal shelf response to PDGF exposure. Upon exposure of MEPM cultures to PDGF, control and untreated phosphorylation targets of AKT were identified. Targets of PDGF-mediated AKT phosphorylation largely clustered into a small number of functional classes, with the largest class reflecting abnormal proliferation, potentially explaining the smaller embryonic size or importantly, the reduced palatal shelf size observed in *Pdgfrα* mutants. An additional connection emerged when PDGF-treated MEPMs included *SPECC1L* in the battery of AKT phosphorylation targets (Fantauzzo & Soriano, 2014).

This pathway has been implicated in the regulation of β-catenin required for maintenance of dental mesenchyme, downstream of FGF signaling (Liu et al., 2013). FGF-PI3K-AKT signaling has also been implicated in the development of statoacoustic ganglia in zebrafish otic development (Wang et al., 2015). These works represent a very small number of studies connecting PI3K-AKT signaling with craniofacial development generally or palatogenesis specifically.

1.5.6.1 Inhibition of apoptosis via AKT activation

The pro-survival functions of AKT, in inhibiting apoptosis are described extensively (Kennedy et al., 1999). AKT inhibits pro-apoptotic proteins such as BCL2 associated agonist of cell death (Bad), which reverses the pro-apoptotic signaling of BCL2 apoptosis regulator (Bcl-2) and BCL2-like 1 (Bcl-xl) (Matsuzaki et al., 1999). Also, AKT phosphorylation activates the caspase inhibitory function of X-linked inhibitor of apoptosis (XIAP), either directly or downstream of Nuclear factor kappa B (NF-κB) activation, which also activates XIAP (Asselin et al., 2001). AKT phosphorylation also inhibits transcription factor Forkhead box O3 (FOXO3a), which promotes the transcription of the apoptosis promoting proteins BCL2-like 11 (Bim) and Phorbol-12-Myristate-13-acetate-induced protein 1 (Noxa). Finally, AKT interaction with Master target of Rapamycin (mTOR) induces its activation of BCL2 family apoptosis regulator (MCL-1), a protein with anti-apoptotic activity (Schulze-Bergkamen et al., 2004). Thus, several pathways are activated upon AKT phosphorylation, conveying the pro-survival signals of growth factors.

1.5.6.2 Functions of PI3K-AKT signaling in craniofacial development

The roles of PI3K-AKT signaling in EMT and other cellular processes are well-described (Larue et al., 2005). However, any such functions in craniofacial development generally, are rare.

A prominent exception comes with recent studies investigating the role of platelet-derived growth factor receptor alpha (Pdgfrα) upstream of PI3K-AKT signaling, in a mouse model (Fantauzzo & Soriano, 2014). $Pdgfr\alpha^{PI3K/PI3K}$ homozygous mutant mice expressing a mutated Pdgfrα that is unable to bind and activate PI3K show a variety of phenotypes, including smaller overall size, delayed fusion of the medial nasal process at E11.5-12.5 and delayed maxillary fusion at E13.5. Also of interest was subepidermal blebbing prominent along the facial midline, abnormal neural tube morphology and importantly, smaller than control anterior palatal shelves possibly due to decreased vertical outgrowth (Fantauzzo & Soriano, 2014).

1.6 Adherens junctions

The establishment and maintenance of tissues requires stable cell-cell adhesion (Gumbiner, 1996). Throughout embryogenesis the dynamic nature of these adhesions allows for cell sorting, polarity and the stimulation of intracellular signaling cascades with respect to the developmental requirements of tissues (Baum & Georgiou, 2011). One such type of adhesion, the adherens junction (AJ), is a multimeric complex tethering adjacent cells via homotypic binding of extracellular cadherin proteins. The regulation of AJ stability is a critical feature of CNCC EMT, as AJs must be downregulated to allow their migration away from the neural folds.

1.6.1 Cellular functions of Adherens junctions: Adhesion, signaling and polarity

The AJ is a multimeric protein complex whose fundamental role is in maintaining cell-cell integrity in many tissues, especially those of a stratified epithelium (Lewis et al., 1994). The AJ is

thought to organize around cell-cell contacts, through the heterophilic interactions of cell-adhesion molecule, nectin, which initially link cells at their interface. However, nectin adhesions then show localization of cadherins, homophilic cell adhesion molecules which dimerize with their neighbors via calcium binding (Lewis et al., 1994). Thus, nectins are thought to precede and perhaps recruit cadherins to the developing AJ (Takai et al., 2003). Nectin interacts with Afadin, an actin-binding protein, potentially explaining the first steps in establishing the linkage between the AJ and the actin cytoskeleton (Takahashi et al., 1999). Ultimately, the maturing AJ recruits alpha catenin, which is also an actin binding protein. Alpha catenin serves as the intermediary between the mature AJ and the actin cytoskeleton (Yap et al., 1997). The mature AJ also interacts with the microtubule cytoskeleton, through adaptor protein, such as CAP350. Indeed, depletion of CAP350 causes MDCKII cells to change from an elongated morphology to rounded, suggesting that AJ-microtubule interactions contribute to cell polarity in a stratified epithelium (Robinson, 2015).

The additional critical addition to the AJ is the recruitment of beta catenin (Hartstock & Nelson, 2008). Beta catenin acts both in establishing the stability of the AJ, but also as the mediator which conveys Wnt signaling to the nucleus, organizing transcriptional co-activators to the promoters of Wnt target genes (Nelson & Nusse, 2004). Thus, one model includes the AJ as a component of Wnt signaling, as AJ-bound Beta catenin has been shown to enter into the Wnt signaling pathway, suggesting a shared pool of Beta catenin between adhesion and Wnt signaling (Kam et al., 2009). Thus, AJs effectively sequester beta catenin, as its structural role within them prohibits its nuclear role in activating Wnt signaling.

1.6.2 Regulation of Adherens junction: disassembly

While transcriptional regulation of cadherins is a key point in the regulation of the AJ (Peinando et al., 2004), regulatory recycling of these adhesions involves multiple other mechanisms, including ubiquitination of AJ components, targeting them for endocytic processing (Nanes & Kowalczyk, 2014). For example, the orphaned AJ, which has no binding partner in a neighboring cell, is endocytosed, upon calcium depletion *in vitro* (Kartenbeck et al., 1991). The process of cadherin endocytosis has since been associated with multiple processes both in embryonic development and association with disease and its misregulation (Nanes & Kowalczyk, 2014).

Cadherin endocytosis regulating the AJ is initiated by the binding of adaptor proteins which permit their ubiquitination (Nanes 2014). Upon ubiquitination, the associated AJ is sequestered to an invaginating clathrin-coated pit, in preparation for endocytosis and subsequent recycling (Nanes & Kowalczyk, 2014). This process has relevance for multiple signaling cascades, as seen in the example of the fibroblast growth factor (Fgf) signaling also important to palatogenesis. FGF stimulation was found to induce E-cadherin internalization (Bryant et al., 2005). Other embryogenic patterning pathways also initiate cadherin internalization, as seen in the VEGF-induced internalization of VE-cadherin (Gavard et al., 2006).

1.6.3 The relevance of adherens junctions to embryonic craniofacial development

Cell polarity, a quality marked by the spatial distribution of proteins to either the apical or basal compartments establishes tissue architecture (Yoshida et al., 2012). AJs contribute to the establishment of apico-basal polarization of epithelia (Ohno 2001), which is lost during CNCC

delamination (Park et al., 2010) as AJs are remodeled. This polarization is also relevant to the interactions of the periderm and underlying MEE, in palatal shelf attachment and fusion (Yoshida et al., 2012). Another cell-cell adhesion present in this milieu is the tight junction (TJ). Amongst other functions, TJs promote cell polarization, by creating a lipid boundary restricting membrane-associated proteins to either the apical or basal aspect of the cell (Cereijido et al., 1998). Indeed, this polarizing function of the TJ is patterned by AJs. The recruitment of certain cell adhesion molecules is facilitated by nectins, at developing cell-cell junctions, allowing apical AJs to develop into TJs (Takai et al., 2008). It has been shown that dissolution of the periderm layer coating the MEE of the palatal shelves is initiated by TGF signaling, resulting in a desquamatizing loss of polarity. In support of this, they showed that the localization of a cell polarity marker, GP135, as well as AJ components were dynamic in the periderm between E13.5 and E14.5, and were a response to TGF exposure, thus demonstrating a role for AJs and AJ-relative TJs in the periderm, during palatal shelf adhesion fusion (Yoshida et al., 2012).

Complimenting these findings, proper Beta catenin regulation has been implicated as a requirement for successful lineage transition from NC to *bona fide* mesenchymal stem cells (MSCs). Beta catenin, an AJ component, mediates this transition and its dysregulation results in MSC populations inadequate for proper forebrain development (Choe et al., 2013).

1.6.4 Modulation of adherens junctions through AKT signaling

As the transition from epithelial to mesenchymal cellular features requires the downregulation of cell-cell adhesion complexes, Adherens junctions (AJs), it is important to consider any roles played by AKT in this modulation. AKT performs an inactivating

phosphorylation of Glucose synthase kinase 3 alpha and beta (GSK3α/β) (Lee et al., 2009). Downstream GSK3β kinase function impacts metabolism, cell migration and other features, but is relevant here for its two-fold impact upon EMT. The first impact upon AJs is though transcriptional regulation of genes required for EMT, via Snail family transcriptional repressor 1 (Snail 1). Snail 1 represses expression of the E cadherin gene, important in neural crest development due to the requirement of EMT during CNCC delamination from the neural folds (Cano et al., 2000). However, GSK3β counteracts the transcriptional changes of Snail 1, interrupting EMT progression.

The other half of the GSK3β function in regulating AJs is more direct. GSK3β phosphorylates β-catenin involved with AJs, targeting it for degradation by the β-catenin destruction complex. As a component of this protein complex, GSK3β participates in executing the consequences of an inactive, unstimulated Wnt signaling pathway (Wu & Pan, 2010). Upon phosphorylation, this heteromeric protein complex facilitates the ubiquitination and subsequent proteasomal degradation, modulating AJs (Li et al., 2012). Thus, reduction of upstream PI3K or AKT signaling, in antagonizing GSK3β, affects AJ formation and degradation. This cascade, beginning with receptor tyrosine kinase activation by growth factors, through PI3K-AKT signaling and the subsequent modulation of GSK3β effectively tethers together one aspect of EMT, in the acquisition of a less adhesive and more mobile, mesenchymal phenotype, in response to appropriate developmental stimulation (Thiery & Sleeman, 2006).

CHAPTER TWO:

MUTATIONS IN *SPECC1L*, ENCODING SPERM ANTIGEN WITH CALPONIN HOMOLOGY AND COILED-COIL DOMAINS 1-LIKE, ARE FOUND IN SOME CASES OF AUTOSOMAL DOMINANT OPITZ G/BBB SYNDROME

Chapter Two: Mutations in *SPECC1L*, encoding sperm antigen with calponin homology and coiled-coil domains 1-like, are found in some cases of autosomal dominant Opitz G/BBB syndrome

Paul Kruszka, Dong Li, Margaret Harr, Nathan Wilson, Daniel Swarr, Elizabeth McCormick, Rosetta Chiavacci, Mindy Li, Ariel Martinez, Rachel Hart, Donna McDonald-McGinn, Matthew Deardorff, Marni Falk, Judith Allanson, Cindy Hudson, John Johnson, Irfan Saadi, Hakon Hakonarson, Maximilian Muenke, and Elaine Zackai

Contributions

Manuscript writers: PK, MH, DL, EZ and MM. Study design: MM, EZ, IS, NW and PK. Family A sequencing and data analysis: DL, ML, MF and HH. Family B sequencing and data analysis: AM, RH and PK. Figure construction: MH, DL, EM, IS and NW. Microtubule studies: IS and NW. Patient evaluation and phenotyping Family A: MH, DS, EM, RC, ML, DM, MD, MF, JJ, CH, HH and EZ. Patient evaluation and phenotyping Family B and 24 non-specc1l carriers: PK, MM, EZ and JA. Opitz GBBB study coordinators Children's Hospital of Philadelphia: MH, EM, RC, DM and JJ. Opitz GBBB study coordinators NIH: PK, RH and AM.

2.1 Abstract

2.1.1 Background

Opitz G/BBB syndrome is a heterogeneous disorder characterized by variable expression of midline defects including cleft lip and palate, hypertelorism, laryngealtracheoesophageal

anomalies, congenital heart defects, and hypospadias. The X-linked form of the condition has been associated with mutations in the *MID1* gene on Xp22. The autosomal dominant form has been linked to chromosome 22q11.2, although the causative gene has yet to be elucidated.

2.1.2 Methods and results

In this study, we performed whole exome sequencing on DNA samples from a three-generation family with characteristics of Opitz G/BBB syndrome with negative *MID1* sequencing. We identified a heterozygous missense mutation c.1189A>C (p.Thr397Pro) in *SPECC1L*, located at chromosome 22q11.23. Mutation screening of an additional 19 patients with features of autosomal dominant Opitz G/BBB syndrome identified a c.3247G>A (p.Gly1083Ser) mutation segregating with the phenotype in another three-generation family.

2.1.3 Conclusions

Previously, *SPECC1L* was shown to be required for proper facial morphogenesis with disruptions identified in two patients with oblique facial clefts. Collectively, these data demonstrate that *SPECC1L* mutations can cause syndromic forms of facial clefting including some cases of autosomal dominant Opitz G/BBB syndrome and support the original linkage to chromosome 22q11.2.

2.2 Introduction

Opitz G/BBB syndrome is a genetically heterogeneous, multiple congenital anomalies syndrome diagnosed on the presence of characteristic clinical features. Opitz originally described

two separate syndromes, the BBB syndrome and the G syndrome, which were characterized by hypertelorism, hypospadias and variable other midline defects. Due to the clinical overlap, these two syndromes were later combined into one entity, Opitz G/BBB syndrome or simply Opitz syndrome (Cappa et al., 1987)

Opitz syndrome is inherited in either an autosomal dominant or X linked pattern with multiple reported families showing male-to-male transmission (Funderburk et al., 1978 (2-7)). Linkage analysis of 10 families identified one locus on Xp22 and a second locus on 22q11.2.8 Five families were linked to D22S345 on chromosome 22q11.2 with a LOD score of 3.53 at zero recombination. Crossover events for markers D22S421 and D22S685 placed the Opitz syndrome gene within the 32 cM interval at chromosome 22q11.2, bordered distally by D22S685 and proximally by D22S421.8 The X linked form of Opitz is associated with mutations in the *MID1* gene at chromosome Xp22.2 which encodes a microtubule-associated RING B-box coiled-coil domain protein (Quaderi et al., 1997).

Opitz syndrome is a clinically heterogeneous disorder with variable expression in both the X-linked and autosomal dominant families, and characterized by distinctive facial features including hypertelorism, a prominent forehead, broad nasal bridge and anteverted nares. Congenital anomalies include hypospadias, cleft lip/palate, laryngealtracheoesophageal abnormalities, imperforate anus and cardiac defects. Developmental delay and intellectual disability are variable. Hypospadias and anal anomalies were found more commonly in male patients with *MID1* mutations than in those without (So et al., 2005, Robin et al., 1996).

Using whole exome sequencing (WES), we identified a missense mutation in *SPECC1L* segregating with the phenotype of suspected autosomal dominant Opitz in a three-generation pedigree (see figure 2.1 A). Subsequently, we sequenced the gene in an additional 19 probands

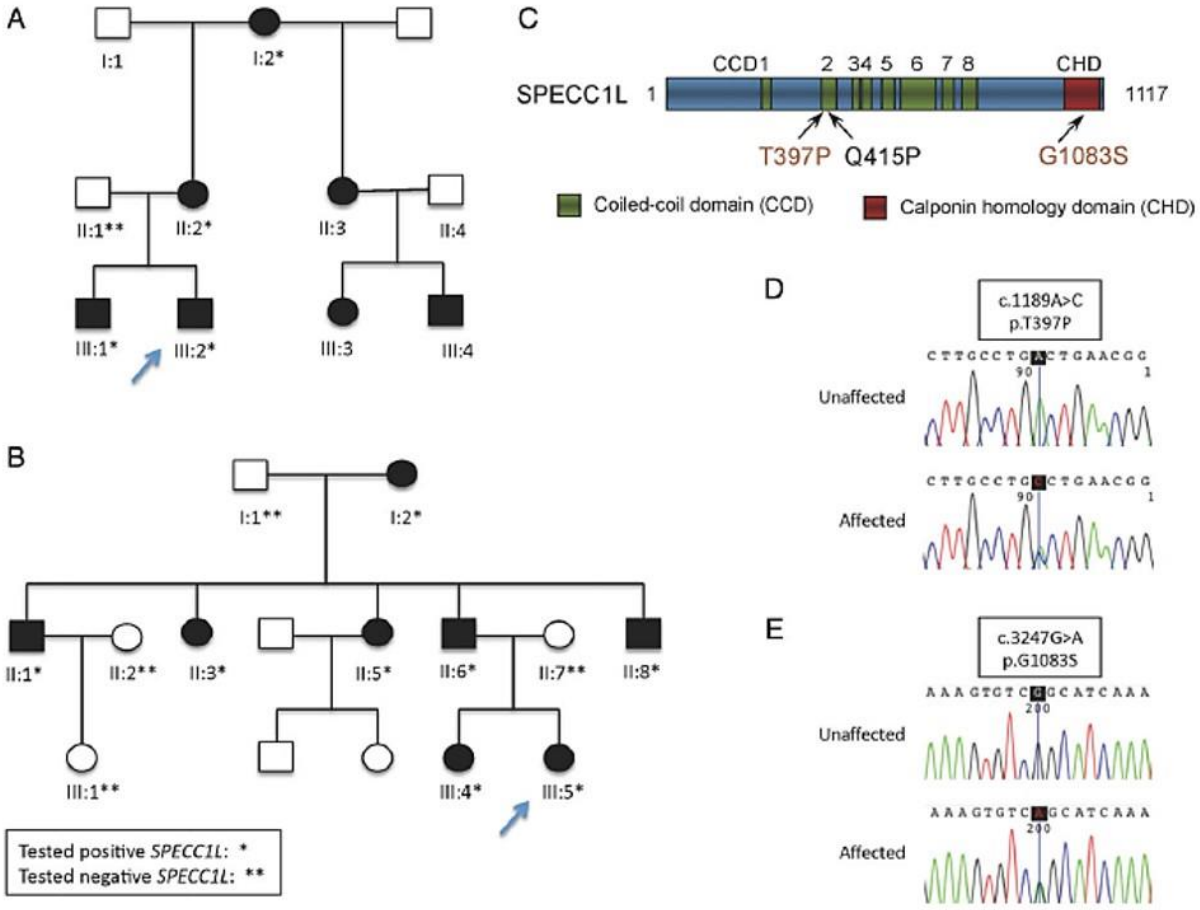

Figure 2.1. Two Opitz G/BBB syndrome families harbor mutations in SPECC1L. (A) Pedigree of Family A. (B) Pedigree of Family B. (C) A schematic of SPECC1L protein showing that the T397P mutation lies in the same coiled-coil domain (CCD) as the previously reported Q415P mutation and that the G1083S mutation lies in C-terminal calponin homology domain (CHD). (D) DNA analysis. Trace from proband, AIII.2 and (E) trace from proband BIII.5.

and identified a second family with a novel missense mutation in *SPECC1L* and clinical features of Opitz.5 This second family also had a three-generational pedigree with the *SPECC1L* mutation segregating with the distinguishing phenotype (see figure 2.1 B). This study provides further evidence that Opitz is a genetically heterogeneous syndrome and that *SPECC1L* mutations account for a subset of the autosomal dominant cases.

2.3 Patients and methods

2.3.1 Patients

2.3.1.1 Family A

Family A presented to genetics at the Children's Hospital of Philadelphia after the birth of their second child. The proband, individual III.2 (figure 2.2 A), was the second boy born to a 24-year-old G2 mother (figure 2.2 C) and was referred to genetics for multiple congenital anomalies including a congenital diaphragmatic hernia (CDH), bilateral cleft lip and palate, micrognathia, and dysmorphic facial features. Echocardiogram and brain MRI were normal, and he required monitoring for right grade two vesicoureteral reflux, and possible left sided hearing loss. At 12 months of age, his height was at the 15th centile, weight was at the 30th centile and head circumference was at the 85th centile. He was noted to have a prominent forehead, hypertelorism, broad nasal bridge, down-slanting palpebral fissures, extra ear crus bilaterally and micrognathia. Bilateral cleft lip had been repaired. He had truncal hypotonia with some delay of motor milestones, but his speech and cognition were felt to be age appropriate.

The proband's brother (figure 2.2 B) had a history of tracheomalacia, inguinal and umbilical hernias, metopic craniosynostosis, critical aortic stenosis, and subsequent poststenotic dilation of the aortic root. Surgical repair of the metopic synostosis was first attempted at 12

Figure 2.2. Facial dysmorphologies of affecteds from two Opitz G/BBB syndrome families. (A) (B)

months of age but was not completed due to tracheomalacia and complications with intubation. Repair was then pursued around 20 months of age due to persistent presentation of headaches.

Mild delays in speech acquisition were noted although cognition was appropriate for age. His facial features included hypertelorism, prominent forehead with prominent metopic suture shown in figure 2 B and in a 3D head CT in online supplementary figure, broad nasal bridge, widow's peak hairline, arched eyebrows, down-slanting palpebral fissures and a vertical groove in the nasal tip. There was no history of hypospadias in either boy. The mother (figure 2.2 C) had a history of bilateral cleft lip and palate, congenital umbilical hernia and bicornuate uterus. In addition, she had hypertelorism, a prominent forehead, broad nasal root and repaired bilateral cleft lip. She reported that her mother, sister and the sister's children all had similar facial features.

Genetic testing to date had been uninformative and included a normal male karyotype, normal SNP genome-wide microarray, and *MID1* sequencing and deletion/duplication testing negative for Opitz syndrome in both brothers. Sequencing of *EFNB1* for craniofrontonasal dysplasia was also normal in the proband. Sequencing of *GPC3* for Simpson–Golabi–Behmel syndrome and *TGFBR1* and *TGFBR2* sequencing for Loeys–Dietz syndrome were normal in the brother.

2.3.1.2 Family B

Family B was previously described by Judith Allanson in 1988 and is reported as Family 1 in the Robin *et al* 1995 article establishing the linkage of the autosomal dominant form of Opitz to chromosome 22q11.2.5811 The proband, individual III.5 (figure 2.2 D; table 1), was an affected girl with swallowing difficulties, stridor, micrognathia, cleft palate, bilateral hearing loss, mild ventricular dilatation, sagittal craniosynostosis (without history of surgery), ureteral reflux,

umbilical hernia and cardiomegaly, thought to be secondary to chronic hypoxia. Her facial features included a broad prominent nasal root and bridge, mild central groove in the tip of the nose, prominence of the metopic suture and both parietal areas, marked widow's peak, downslanting palpebral fissures, hypertelorism, posteriorly rotated ears, and a wide and poorly defined philtrum. The proband's father and his four siblings were also felt to be affected based on the findings of megalencephaly, hypertelorism, down-slanting palpebral fissure, high broad nasal bridge, wide nasal base with a hooked tip, and long columella. The father was reported to have a congenital upper gastrointestinal obstruction. One paternal uncle had a unilateral cleft lip and palate. Hypospadias was not present in the father or two affected uncles. The proband's sister had hypertelorism and high broad nasal bridge.

2.3.2 Methods

2.3.2.1 Exome sequencing and bioinformatics variant

After written informed consent was obtained, genomic DNA was extracted from the peripheral-blood lymphocytes of the proband and both parents, and from the saliva of the affected brother and maternal grandmother in Family A. Exome capture was carried out for the proband and both parents using NimbleGen SeqCap EZ Human Exon Library V.3.0 (Roche NimbleGen, Madison, Wisconsin, USA), guided by the manufacturer's protocols. In brief, the qualified genomic DNA was isolated from peripheral-blood samples and randomly sheared to 200–300 bp fragments, followed by end-repair, a-tailing and pair-end index adapter ligation. The libraries were subsequently clustered on the cBOT instrument, multiplexing four samples per flowcell lane and sequenced using pair-end reads for 101 cycles with a paired-end mode on the Illumina HiSeq2000 following the manufacturer's instructions (Illumina, San Diego, California, USA). Base calling

was performed by the Illumina CASAVA software (V.1.8.2) with default parameters. All the raw reads were aligned to the reference human genome (UCSC hg19) using the Burrows–Wheeler aligner and single nucleotide variants (SNVs) and small insertions/deletions (indels) were identified using the Genome Analysis Tool Kit (GATKv2.6) (Li & Durbin, 2009, DePristo et al., 2011). The kinship coefficient was calculated between every two samples via KING to confirm reported relationships (Manichaikul et al., 2010). Annovar11 and SnpEff were used to functionally annotate the variants and to categorize them into missense, nonsense, splice-altering variants and coding frameshift indels, which are likely to be deleterious compared with synonymous and non-coding variants (Wang et al., 2010, Cinqoani et al., 2012). Under autosomal dominant mode of inheritance, we excluded variants that: (1) were synonymous variants; (2) present in unaffected father; (3) had a minor allele frequency of >0.005 in 1000 Genomes Project, 6503 exomes from the NHLBI Exome Sequencing Project (ESP6500SI; http://evs.gs.washington.edu/EVS/) or our inhouse database of >1500 sequencing exomes; (4) had a conservation score GERP++ < 2; and (5) were predicted by SIFT/PolyPhen2 scores to be benign variants (Davydov et al., 2010, Adzhubei et al., 2010, Liu et al., 2011).

2.3.2.2 Sanger sequencing

Validation of the mutation candidate was performed by Sanger sequencing in all the available family members using the standard techniques of PCR amplicons with primer set 5′ CTACCAGCCCCTCACATCG 3′ and 5′ AGTTCCTGGGTAATGTGCTGT 3′.

This study was approved by the Institutional Review Boards at The Children's Hospital of Philadelphia and the National Human Genome Research Institute, the National Institutes of Health.

2.3.2.3 Sequencing of additional patients with Opitz G/BBB

After written informed consent was obtained, genomic DNA was extracted from the peripheral-blood lymphocytes of 25 additional families with clinically diagnosed Opitz syndrome. Six probands were found to have *MID1* mutations and all probands had normal chromosomal microarrays. The remaining 19 probands without *MID1* mutations were sequenced for *SPECC1L* mutations by Sanger sequencing for exons 1–17 with standard techniques of PCR (see online supplementary table S1 for primer sets).

2.3.2.4 Mutagenesis

The p.Thr397Pro and p.Gly1083Ser mutations were created in full-length in a murine SPECC1L-GFP expression construct, described previously (Saadi et al., 2011) using the Q5 site-directed mutagenesis kit (NEB, Ipswich, Massachusetts, USA) according to manufacturer's protocol. The p.Gln415Pro and C-terminal calponin homology domain truncated (ΔCHD) constructs were created previously (Saadi et al., 2011).

2.3.2.5 Cell culture

SPECC1L-GFP expression constructs containing either wildtype or Thr397Pro, Gly1083Ser, Gln415Pro and ΔCHD mutations were transfected into U2OS osteosarcoma cells (ATCC, Manassas, Virginia, USA) using Viafect (Promega, Madison, Wisconsin, USA) or TransIT (Mirus Bio, Madison, Wisconsin, USA) according to manufacturer's protocol. U2OS cells were grown in standard DMEM supplemented with 10% fetal bovine serum (FBS). Transfections and immunostaining were carried out on coverslips in 24-well plates. Cells were fixed in 4% paraformaldehyde (PFA) for 10 min, and blocked in phosphate buffered saline (PBS) with 1% goat

serum and 0.1% Tween. Acetylated α-tubulin antibody (Sigma, St Louis, Missouri, USA) was used at 1:1000 dilution. After staining, coverslips were mounted in VectaShield containing DAPI (Vector Labs, Burlingame, California, USA).

2.4 Results

2.4.1 Identification of *SPECC1L* mutation in Family A by WES

The WES generated a total of 50 443 SNVs and 4799 indels in the proband, 50 533SNVs and 4808 indels in the mother and 50 592 SNVs and 4811 indels in the father. We applied the filtering strategy as described in the Patients and methods section, filtering variants to exclude those who had a minor allele frequency (MAF) >0.5% or predictive of benign variant. Of these, 27 variants (see online supplementary table S2) were shared between the two affected patients (proband and mother), but not in the healthy father (figure 2.1 A). Those variants included a missense variant c.1189A>C (p.Thr397Pro) in *SPECC1L* (Mendelian inheritance in man (MIM) 614140; NM_015330.3), which is required for proper facial morphogenesis (Saadi et al., 2011).

The mutation was absent from 1000 Genomes Project, ESP6500SI, or additional exome sequencing data of over 1500 WES samples that we had previously sequenced in our inhouse database. Sanger sequencing of five family members, consisting of one unaffected and four affected individuals, confirmed its presence in proband, affected brother, mother and maternal grandmother (figure 2.1 D).

2.4.2 Screening of additional patients

To further establish the association between *SPECC1L* and Opitz syndrome, we sequenced its coding region in an additional 19 patients with features of Opitz syndrome. The sequencing analysis identified a heterozygous missense mutation, c.3247G>A (p.Gly1083Ser), in one proband (Family B); Family B has been previously linked to 22q11.2 by Robin *et al*.8 We tested one other family linked to 22q11.2 besides Family B and did not find a mutation in *SPECC1L*. Mutation screening of additional family members confirmed segregation of the mutation with the phenotype. The p.Gly1083Ser mutation occurs in the CHD of *SPECC1L* (figure 2.1 C) and predicted to be damaging with high probability according to the pathogenic score algorithms SIFT, Polyphen2, LRT and MutationTaster, and is not found in the 1000 Genomes Projects ESP6500SI or our inhouse database.

2.4.3 Functional analysis

Expression of SPECC1L-GFP results in stabilization of a subset of microtubules (figure 3A) that appear in a lattice-like pattern and colocalize with acetylated α-tubulin (figure 2.3B, C), as previously described.20 We used this property of *SPECC1L* as a functional assay to assess the effect of *SPECC1L* Thr397Pro and Gly1083Ser mutations. Both Thr397Pro-GFP (figure 2.3D–F) and Gly1083Ser-GFP (figure 2.3G–I) mutant proteins show a drastic reduction in their ability to stabilize microtubules, consistent with these variants being pathological. The altered expression pattern of both Thr397Pro-GFP and Gly1083Ser-GFP mutant proteins is similar to that of the previously described Gln415Pro mutation (figure 2.3J–L). All three mutant SPECC1L-GFP proteins show a largely punctate expression pattern with poor, non-contiguous association with stabilized microtubules, in contrast to a robust, elaborate network of stabilized microtubules seen

with wildtype SPECC1L-GFP. Interestingly, while Gln415Pro and Thr397Pro lay in the second coiled-coil domain, the Gly1083Ser mutation is located in the C-terminal CHD which was also previously shown to be required for *SPECC1L* stabilization of microtubules (figure 2.3M–O).20 Synthetic mutations outside these domains do not strongly affect microtubule stabilization (data not shown). Thus, mutations affecting the second coiled-coil domain or the CHD are likely to affect the same aspect of *SPECC1L* function and result in similar phenotypes.

2.5 Discussion

Here we report mutations in *SPECC1L* as a cause of autosomal dominant Opitz syndrome in a subset of patients. WES analysis identified a novel mutation in *SPECC1L* on chromosome 22q11.23 to be the most probable disease causing mutation in a family with features suggestive of autosomal dominant Opitz syndrome. Sanger sequencing confirmed this result and the mutation was found to segregate with the clinical findings in three generations. Gene sequencing in 19 additional patients with suspected autosomal dominant Opitz syndrome revealed one additional novel mutation which segregated with the phenotype in a three-generation pedigree. Importantly, the *SPECC1L* gene, located at chromosome 22q11.23, is within one Mb of the D22S345 marker, which was previously linked to autosomal dominant Opitz syndrome.8 From Robin *et al*, we tested two families that were linked to 22q11.2; the other family did not have a mutation in *SPECC1L*, which may be due to locus heterogeneity associated with autosomal dominant Opitz syndrome or due to a mutation in a non-coding area of the *SPECC1L* not captured by our analysis such as a promoter region or intron. Interestingly, there have been case reports of patients with the Opitz syndrome phenotype and 22q11.2 deletions (McDonald 1995, Fryburg et al., 1996, Lacassie et al., 1996); however, *SPECC1L* is not contained within the 2.54 Mb typically deleted region associated

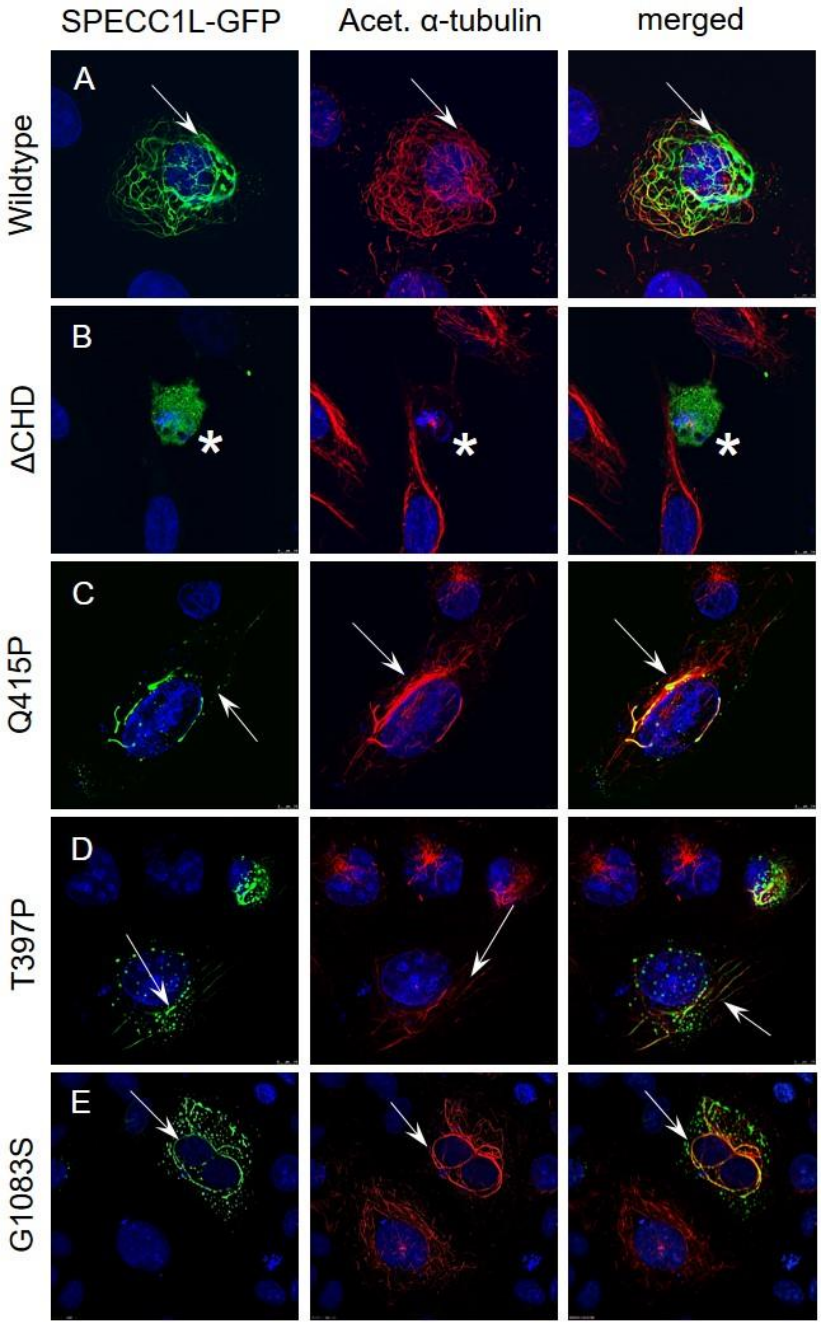

Figure 2.3. SPECC1L-T397P and SPECC1L-G1083S mutant proteins are defective in stabilising microtubules. U2OS cells were transfected with wildtype or mutant green fluorescent protein (GFP)-tagged Specc1l expression constructs. Wildtype SPECC1L-GFP expression (A; green) stabilises a subset of microtubules that colocalise with acetylated-α-tubulin (B, C; red). Compared with wildtype protein (A–C), both SPECC1L-T397P (D–F) and SPECC1L-G1083S (G–I) mutant proteins fail to stabilise microtubules efficiently and show a punctuate expression pattern, similar to SPECC1L-Q415P mutant protein (J–L). SPECC1L-ΔCHD shows a diffuse expression pattern with near complete absence of microtubule stabilisation (M–O). Nuclei are stained with DAPI (blue).

with 22q11.2 deletion syndrome. Further study is needed to inquire whether there are other Opitz syndrome causing genes on chromosome 22.

The *SPECC1L* gene was first identified by Saadi *et al* (2011) to be disrupted by a balanced translocation, t(1;22)(21.3;q11.23) in a female patient with bilateral oromedial-canthal (Tessier IV) clefts, cleft palate, bilateral ocular hypoplasia and unilateral calcaneovarus foot deformity. The coding regions of *SPECC1L* were subsequently sequenced in 23 patients with oblique facial clefts and a de novo missense mutation, c.1244A>C (p.Gln415Pro), was identified in one individual (Saadi 2011). This mutation is located within the second coiled-coil domain of the *SPECC1L* protein, similar to the c.1189A>C (p.Thr397Pro) identified in Family A of this report.

SPECC1L gene encodes a 'cross-linking' protein that functionally interacts with both microtubules and the actin cytoskeleton and is necessary for cell adhesion and migration (Saadi 2011) Morpholino-based knockdown of a *SPECC1L* ortholog in zebrafish (*specc1lb*) results in loss of mandible and bilateral clefts between median and lateral elements of the ethmoid plate, which are structures analogous to the frontonasal process (FNP) and the paired maxillary processes (MxP), respectively (Gfrerer et al., 2014). Lineage tracing analysis revealed that cranial neural crest cells contributing to the FNP fail to integrate with the MxP populations, while cells contributing to lower jaw structures were able to migrate to their destined pharyngeal segment but failed to converge to form mandibular elements (Gfrerer et al., 2014). The function of *SPECC1L* in migration and adhesion of FNP and MxP is consistent with our patient phenotypes of hypertelorism and orofacial clefting. It is unclear why mutations in *SPECC1L*, and even the same domain, result in the two distinct phenotypes of Opitz syndrome and oblique facial clefts. Although facial malformations are major portions of the phenotype in both conditions, a larger cohort of patients with SPECC1L mutations will be needed to examine genotype–phenotype correlation.

Saadi et al (2011) demonstrated that the c.1244A>C (p.Gln415Pro) mutation identified in the patient with oblique facial cleft significantly interfered with the ability of SPECC1L to bind to and stabilize microtubules in an in vitro cell assay. Similarly, the Thr397Pro-GFP mutant protein (Family A) and Gly1083Ser-GFP (Family B) mutant proteins show a drastic reduction in their ability to stabilize microtubules. It is important to note that the p.Thr397Pro and the p.Gln415Pro mutations are both located in the second coiled-coil domain and manifest a similar inability in microtubule stabilization. In contrast, the p.Gly1083Ser mutation is located in the CHD, located at the C-terminus, which has been shown to facilitate actin binding (Saadi et al., 2011). However, Saadi et al (2011) demonstrated that expression of a truncated form of SPECC1L protein lacking the CHD (SPECC1L-ΔCHD) completely abolished the formation of stabilized microtubules as well. Thus, the second coiled-coil domain and the CHD interaction with actin cytoskeleton are required for microtubule stabilization function of SPECC1L. It is therefore consistent that the two mutations we report here, in the second coiled-coil domain and the CHD respectively, manifest similar patient phenotypes.

The combination of hypertelorism, facial cleft and CDH has previously been reported in Opitz G/BBB with MID1 mutation as well as in other craniofacial disorders with midline defects including craniofrontonasal dysplasia with EFNB1 mutation and Simpson–Golabi with GPC3 mutation (Taylor et al., 2010, Brooks et al., 2002, Slavotinek, 2007). Many of the other genes associated with CDH, including EFNB1, GPC3 and SLT3, have been found to be critical to cell migration (Slavotinek, 2007). Given SPECC1L's involvement in cell adhesion and migration, it is therefore reasonable to speculate that the SPECC1L mutation might also explain the CDH seen in the proband of Family A.

MID1 and SPECC1L mutations result in Opitz syndrome and both of their gene products are involved in microtubule stability. Using the green fluorescent protein (GFP) as a tag, MID1 has been shown to be a microtubule-associated protein that affects microtubule dynamics in MID1 overexpressing cells (Schweiger et al., 1999). The MID1 protein consists of a tripartite motif at the N-terminal which includes a RING finger, two B-boxes, and a coiled-coil domain. The C-terminus has a fibronectin Type III domain, a cells (simian CV-1) in origin, and carrying the Simian virus 40 (SV40) (COS) domain and a B30.2 domain Short 2006). Most mutations in X linked Opitz syndrome are found in the C-terminus domains and when these mutations are introduced into in vitro cellular assays, they abolish microtubule association of these proteins (Schweiger et al., 1999). It is clear that mutations in MID1 and SPECC1L have a similar cellular and clinical phenotype.

The two families presented in this report show many of the classic features associated with Opitz syndrome, but also show some unusual features. The brother of the proband in Family A had surgical repair of metopic craniosynostosis and the original proband in Family B was reported to have a prominent metopic ridge and sagittal craniosynostosis, which were not surgically repaired. A detailed history of the sagittal craniosynostosis documented in Allanson's 1988 paper (Allanson, 1988) in the proband in Family B and why it was not surgically repaired was difficult to ascertain, making further natural history studies important to further clarify the significance of this finding. Synostosis of the cranial sutures is not a common feature of Opitz and the presence of this finding may help distinguish cases caused by *SPECC1L* mutations, especially hypertelorism associated with metopic synostosis as this type of synostosis usually results in hypotelorism (see online supplementary figure). Hypospadias is a common finding in both autosomal dominant and X linked Opitz G/BBB syndrome (So et al., 2005) but was not seen in any of the affected male

patients in either family in this report. Therefore, absence of hypospadias in a family with suspected autosomal dominant Opitz syndrome should also lead a clinician to consider the possibility of *SPECC1L* mutation. Further studies are indicated to determine the prevalence of *SPECC1L* mutations in patients with syndromic clefting including those with autosomal dominant Opitz syndrome.

Table 2.1. Prevalence of phenotypic features in patients with *MID1* mutations compared with phenotypic features of Family A and Family B

Patient	Prevalence:	AIII.2	AIII.1	AII.2	BIII.5	BII.6
Sex	Opitz G/BBB	M	M	F	F	M
Relationship	syndrome	Index	Brother	Mother	Index	Father
Phenotypic feature:						
Facial features						
Ocular hypertelorism	+++	+	+	+	+	+
Prominent forehead	++	+	+	+	+	+
Widow's peak	++	-	+	-	+	+
Broad nasal bridge	++	+	+	+	+	+
Anteverted nares	++		-	-	+	
Micrognathia	+	+	+	+	+	
Down-slanted papebral fissures	+	+	+	+	+	+
Central groove in nasal tip		-	+	-	+	
Posteriorly rotated ears		-	-		+	+
LTE anomalies	+++	-	+	-	+	
Hypospadias	+++	-	-	N/A	N/A	-
Cleft lip or cleft palate	++	+	-	+	+	-
Congenital heart defect	++	-	AS	-		
Imperforate or ectopic anus	++	-	-	-		
Midline brain defects	++	-				
Diaphragmatic hernia	+	+	-	-	-	
Umbilical / inguinal hernia	+	+	+	+	+	
Craniosynostosis		-	Metopic	-	Sagittal	
Hearing loss		?			+	
Developmental delay	++	Mild	Mild	-	Mild	
Intellectual disability	++	-	-	-	-	-
Other			Aortic dilation	BU	Cardio-megaly	Congenital GI obstruc-tion
Family history		AI.2: HT, BU AII.3 and AIII.3: HT, UT, hip dysplasia	BIII.8: HT, CL/CP BI.2, BII.1, BII.3, BII.5, BIII.4: HT			

+++ major feature, ++ minor features; * previously reported/present in patient.

AS, aortic stenosis; GI, gastrointestinal; LET, laryngealtracheoesophageal; BU; bicornuate uterus, HT; hypertelorism; N/A, not applicable; UT; Undescended testicle.

CHAPTER THREE:

SPECC1L DEFICIENCY RESULTS IN INCREASED ADHERENS JUNCTION STABILITY AND REDUCED CRANIAL NEURAL CREST CELL DELAMINATION

Chapter Three: SPECC1L deficiency results in increased adherens junction stability and reduced cranial neural crest cell delamination

Nathan R Wilson, Adam J Olm-Shipman, Diana S Acevedo, Kanagaraj Palaniyandi, Everett G Hall, Edina Kosa, Kelly M Stumpff, Guerin J Smith, Lenore Pitstick, Eric C Liao, Bryan C Bjork, András Czirók, Irfan Saadi

Contributions

NW and IS conceived and designed the experiments. NW, AO, DA, KP, EH, EK, KS, GS, EK, LP, BB, A. and IS performed the experiments. NW, AO, EL, BB, AC and IS analyzed the data. BB, EL and AC edited the manuscript. NW and IS wrote the paper. All authors reviewed the manuscript.

3.1 Abstract

Cranial neural crest cells (CNCCs) delaminate from embryonic neural folds and migrate to pharyngeal arches, which give rise to most mid-facial structures. CNCC dysfunction plays a prominent role in the etiology of orofacial clefts, a frequent birth malformation. Heterozygous mutations in *SPECC1L* have been identified in patients with atypical and syndromic clefts. Here, we report that in *SPECC1L*-knockdown cultured cells, staining of canonical adherens junction (AJ) components, β-catenin and E-cadherin, was increased, and electron micrographs revealed an apico-basal diffusion of AJs. To understand the role of SPECC1L in craniofacial morphogenesis, we generated a mouse model of *Specc1l* deficiency. Homozygous mutants were embryonic lethal

and showed impaired neural tube closure and CNCC delamination. Staining of AJ proteins was increased in the mutant neural folds. This AJ defect is consistent with impaired CNCC delamination, which requires AJ dissolution. Further, PI3K-AKT signaling was reduced and apoptosis was increased in *Specc1l* mutants. *In vitro,* moderate inhibition of PI3K-AKT signaling in wildtype cells was sufficient to cause AJ alterations. Importantly, AJ changes induced by *SPECC1L*-knockdown were rescued by activating the PI3K-AKT pathway. Together, these data indicate SPECC1L as a novel modulator of PI3K-AKT signaling and AJ biology, required for neural tube closure and CNCC delamination.

3.2 Introduction

Cranial neural crest cells (CNCCs) are specified in the dorsal neuroectoderm and delaminate from the neuroepithelium of the developing neural folds through a process that involves epithelial-mesenchymal transition (EMT) (Le Dourain, 1982, Saint-Jeannet, 2006, Trainor, 2014). Premigratory epithelial CNCCs break down their cell-cell junctions and become migratory mesenchymal CNCCs, which populate the first and second pharyngeal arches, and give rise to the majority of craniofacial cartilage. Thus, genes that modulate CNCC function are frequently perturbed in the etiology of craniofacial congenital malformations such as orofacial clefts (Trainor, 2014, Cordero et al., 2011, Bolande, 1997, Mangold et al., 2011, Minoux & Rijli, 2010), which are among the most frequent birth malformations affecting 1/800 births in the U.S. alone (Dixon et al., 2011).

CNCC delamination occurs simultaneously with anterior neural tube closure between mouse embryonic days 8.5 and 9.5. Many mouse mutants of genes associated with orofacial clefts

also manifest some form of neural tube defects, including *Irf6* (Ingraham et al., 2006, Peyrard-Janvid et al., 2014), *Grhl3* (Peyrard-Janvid et al., 2014), *Cfl1* (Harris & Tepass, 2010) and *Pdgfra* (Fantauzzo & Soriano, 2014). However, the neural tube closure and CNCC delamination processes can be considered independent since the *Splotch* (*Pax3*) mouse mutant shows neural tube closure defects without any effect on CNCC delamination or migration (Copp et al., 2003, Murdoch & Copp, 2010). Additional mouse models with defects in CNCC delamination and neural tube closure will help delineate the shared molecular underpinnings of these two processes.

Delamination of CNCCs from the neural epithelium requires dissolution of adherens junctions (AJs), composed of a protein complex, containing E-cadherin, β-catenin, α-E-catenin and α-actinin among others, tethered to actin filaments[2]. Studies where E-cadherin is overexpressed in the neural folds, show reduced or delayed delamination of CNCCs. Conversely, down-regulation of E-cadherin results in early delamination (Taneyhill, 2008, Theveneau & Mayor, 2012). Many factors that mediate EMT during CNCC delamination are transcription factors (AP2α, Id2, FOXD3, SNAIL, TWIST, SOX10) and extracellular matrix (ECM) remodeling proteins such as matrix metalloproteases (MMPs), however, direct cytoskeletal regulators of CNCC AJs are not yet known. The PI3K-AKT pathway is known to antagonize E-cadherin levels, primarily from cancer studies (Laure et al., 2005). Recent studies show that loss of murine PDGFα based PI3K-AKT signaling leads to craniofacial malformations including cleft palate and neural tube defects (Fantauzzo & Soriano, 2014). However, a link between the PI3K-AKT pathway and AJ stability in CNCC delamination is not clear.

Previously, we identified *SPECC1L* as the first gene mutated in two individuals with a severe cleft that extends from the oral cavity to the eye, termed Oblique Facial Cleft (ObFC) or

Tessier IV clefts (Saadi et al., 2011). *SPECC1L* mutations have since been identified in two multi-generation families with autosomal dominant Opitz G/BBB syndrome (OMIM #145410), where affected individuals manifest hypertelorism and cleft lip/palate (Kruszka et al., 2014), and in a family with Teebi hypertelorism syndrome (OMIM #145420) (Bhoj et al., 2015). More than half of Opitz G/BBB syndrome cases are X-linked (OMIM #300000), caused by mutations in *MID1* gene (So et al., 2005), which encodes a microtubule-associated cytoskeletal protein (Short & Cox 2006). We proposed that SPECC1L, also a microtubule and actin cytoskeleton-associated protein, may mediate transduction of signals required to remodel the actin cytoskeleton during cell adhesion and migration (Saadi et al., 2011). Using *in vitro* and *in vivo* studies, we now describe SPECC1L as a novel regulator of AJ stability through PI3K-AKT signaling. At the cellular level, SPECC1L deficiency resulted in reduced levels of pan-AKT protein and increased apico-basal AJ dispersion, which was rescued by chemical activation of the AKT pathway. *In vivo, Specc1l*-deficient embryos showed neural tube closure failure and reduced CNCC delamination. Thus, SPECC1L functions in the highly-regulated cell adhesion based signaling required for proper CNCC function during facial morphogenesis.

3.3 Materials and Methods

3.3.1 Cell lines and antibodies

U2OS osteosarcoma control and *SPECC1L*-kd cells were previously described (Saadi et al. 2011). Anti-SPECC1L antibody was also previously characterized (Saadi et al. 2011). Antibodies against β-catenin (rabbit; 1:1000; Santa Cruz, Dallas TX) (mouse; 1:1000; Cell Signaling Technology, Danvers, MA), Myosin IIb (1:1000; Sigma-Aldrich, St. Louis, MO), E-

cadherin (1:1000; Abcam, Cambridge, MA), AP2A (1:1000; Novus Biologicals, Littleton, CO), SOX10 (1:1000; Aviva Systems Biology, San Diego, CA), DLX2 (1:1000; Abcam, Cambridge, MA), phospho-Ser473-AKT (1:1000; Cell Signaling Technology, Danvers, MA), pan-AKT (1:1000; ThermoFisher Scientific, Waltham, MA), KI67 (1:1000; Cell Signaling Technology, Danvers MA), cleaved Caspase 3 (1:1000; Cell Signaling Technology, Danvers, MA), and β-actin (1:2500; Sigma-Aldrich, St. Louis, MO) were used as described. Actin filaments were stained using Acti-stain rhodamine phalloidin (Cytoskeleton, Denver, CO).

3.4 Results

3.4.1 SPECC1L is localized at cell boundaries in cultured cells upon confluency

To characterize the role of SPECC1L at the cellular level, we used the SPECC1L-deficient U2OS osteosarcoma stable cell line described previously (Saadi et al., 2011). These stable *SPECC1L*-knockdown (kd) U2OS cells have a moderate (60–70%) reduction in *SPECC1L* transcript and protein levels with defects in migration and actin cytoskeleton reorganization (Saadi et al., 2011). In contrast, a severe transient reduction in *SPECC1L* has been shown to cause mitotic defects (Mattison et al., 2011). Upon further characterization, we find that our stable *SPECC1L*-kd cells changed morphology upon very high confluency (Fig. 3.1). Individual control and kd cells at low confluency appeared similar (Fig. 3.1A, D). Twenty-four hours after confluency, control cells maintained their cuboidal shape (Fig. 3.1B, E), while *SPECC1L*-kd cells elongated (Fig. 3.1C, F). The extent of this cell shape change was captured by *in vivo* live-imaging of control and kd cells (Supplemental Movie 3.1). To determine the role of SPECC1L in confluent cells, we first examined its expression. We found that SPECC1L protein level was increased upon confluency (Fig. 3.1G) without an increase in *SPECC1L* transcript levels (Fig. 3.1H).

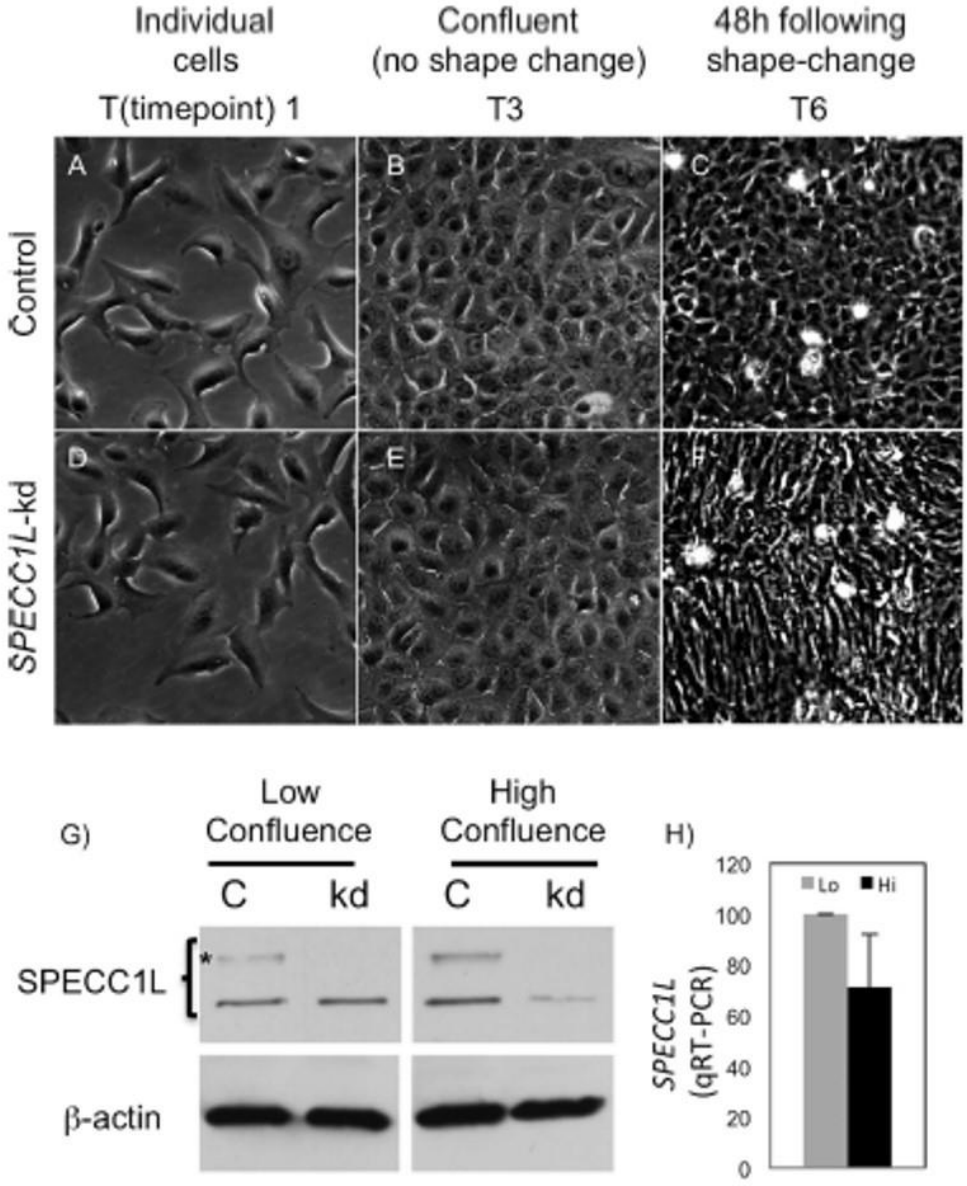

Figure 3.1. SPECC1L-knockdown cells elongate upon high confluency. (**A–F**) Compared to control U2OS cells (**A–C**), *SPECC1L*-knockdown cells (**D–F**) elongate upon high confluency (**F**). Three (T1, T3, T6) of the six time-points we chose for various cell densities are shown here. (**G**) Western blot analysis shows that SPECC1L protein is stabilized at high, compared to low confluency, in control cells. SPECC1L immunoblot shows an expected 120 kD band and a higher molecular weight band (*) that is likely modified post-translationally. The western blot analyses were performed under the same conditions for low and high confluence. The images shown for SPECC1L at low and high confluence are taken from a single blot. The same blot was stripped and re-probed with β -actin antibody. (**H**) Quantitative RT-PCR analysis shows no significant change in *SPECC1L* transcript levels. Error bars represent SEM from four independent experiments.

Furthermore, SPECC1L protein accumulated at cell-cell boundaries with increasing cell density (Fig. 3.2A–E), in a pattern overlapping with that of membrane-associated β-catenin (Fig.3. 2A'–E'). Given the association of SPECC1L with actin cytoskeleton (Saadi et al., 2011, Mattison et al., 2011), we hypothesized that SPECC1L interacts with actin-based adherens junctions (AJs).

3.4.2 *SPECC1L*-kd cells show altered apico-basal dispersion of AJ proteins

Next, we sought to determine the effects of SPECC1L deficiency on AJs. We used several markers associated with AJs, including canonical components F-Actin, Myosin IIb, β-catenin, and E-cadherin (D'Souza-Schorey, 2005, Stepniak et al., 2009, Nishimura & Takeichi, 2009, Strobl-Massulla & Bronner, 2012). As previously reported, actin stress fibers were increased in *SPECC1L*-kd cells (Fig. 3.3A, B) (Saadi et al., 2011). Myosin IIb, associated with actin filaments, showed a similar increase in *SPECC1L*-kd cells *in vitro* (Fig. 3.3C, D). AJ-associated β-catenin, which binds to cadherins at the cell membrane, showed a normal "honey-comb" pattern of expression in control cuboidal cells (Fig. 3.3E, G). Interestingly, in planar images using confocal microscopy, β-catenin (Fig. 3.3E, F) and E-cadherin (Fig. 3.3G, H) staining at the cell membrane in confluent SPECC1L-deficient cells showed a drastically expanded staining pattern. This expansion in AJ-associated β-catenin staining in kd cells was most evident upon confluency, but appeared to precede the cell shape change (Fig. 3.2 F–J, F'–J'). To determine the physical nature of this expanded AJ staining, we examined the cell boundaries in the apico-basal plane of *SPECC1L*-kd U2OS cells (Fig. 3.3I, J) using transmission electron microscopy (TEM). Compared to control cells (Fig. 3.3I), which had distinct electron-dense regions indicating AJs (arrowheads), the kd cells (Fig. 3.3J) showed a large contiguous region of high electron density, suggesting extensive

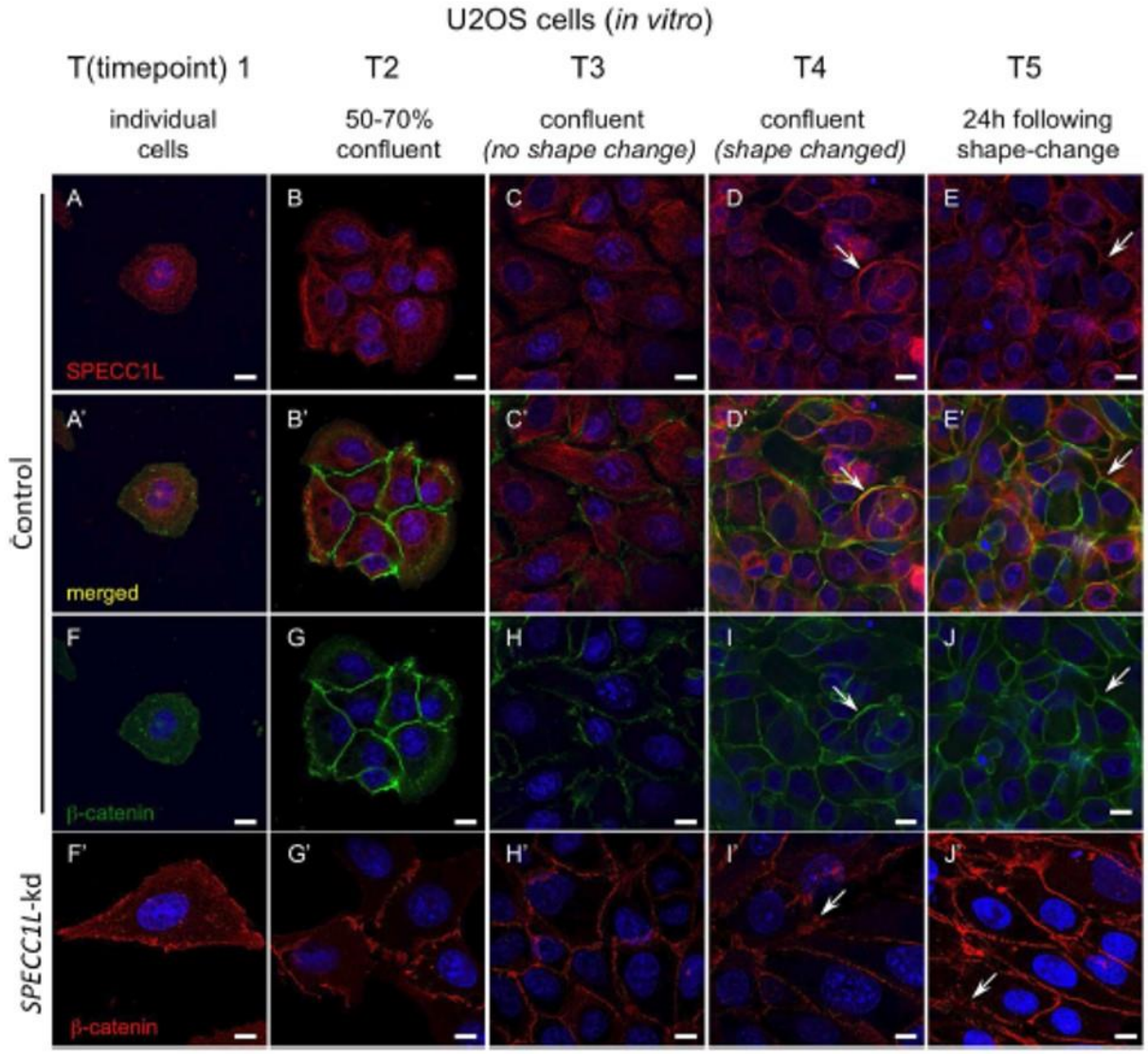

Figure 3.2. SPECC1L is stabilized at cell-cell boundaries similarly to β-catenin. (**A–E**) We picked six timepoints (T1–T6) representing a range of cell densities to standardize analysis of cell shape and AJ change in *SPECC1L*-knockdown (kd) U2OS cells. First five of these time-points include individual cells (T1), 50–70% confluency with small cell clusters (T2), confluency without kd cell shape change (T3), shape change in kd cells (T4), and 24 hrs post shape change in kd cells (T5). SPECC1L protein is mostly dispersed within the cytoplasm at T1 (**A**), but is observed to accumulate at cell-cell boundaries at subsequent time-points (**B–E**), arrows). (**F–J**) β -catenin shows a similar accumulation at cell-cell boundaries in association with AJ complex. (**A'–E'**) SPECC1L and β -catenin show overlapping staining at cell boundaries at high cell densities (arrows). (**F'–J'**) In *SPECC1L*-kd cells, β -catenin staining appears normal at low cell densities (**F'**–**H'**), but is expanded upon cell shape change (**I'**,**J'**; arrows), indicating altered AJs. Bars = 10 μ m.

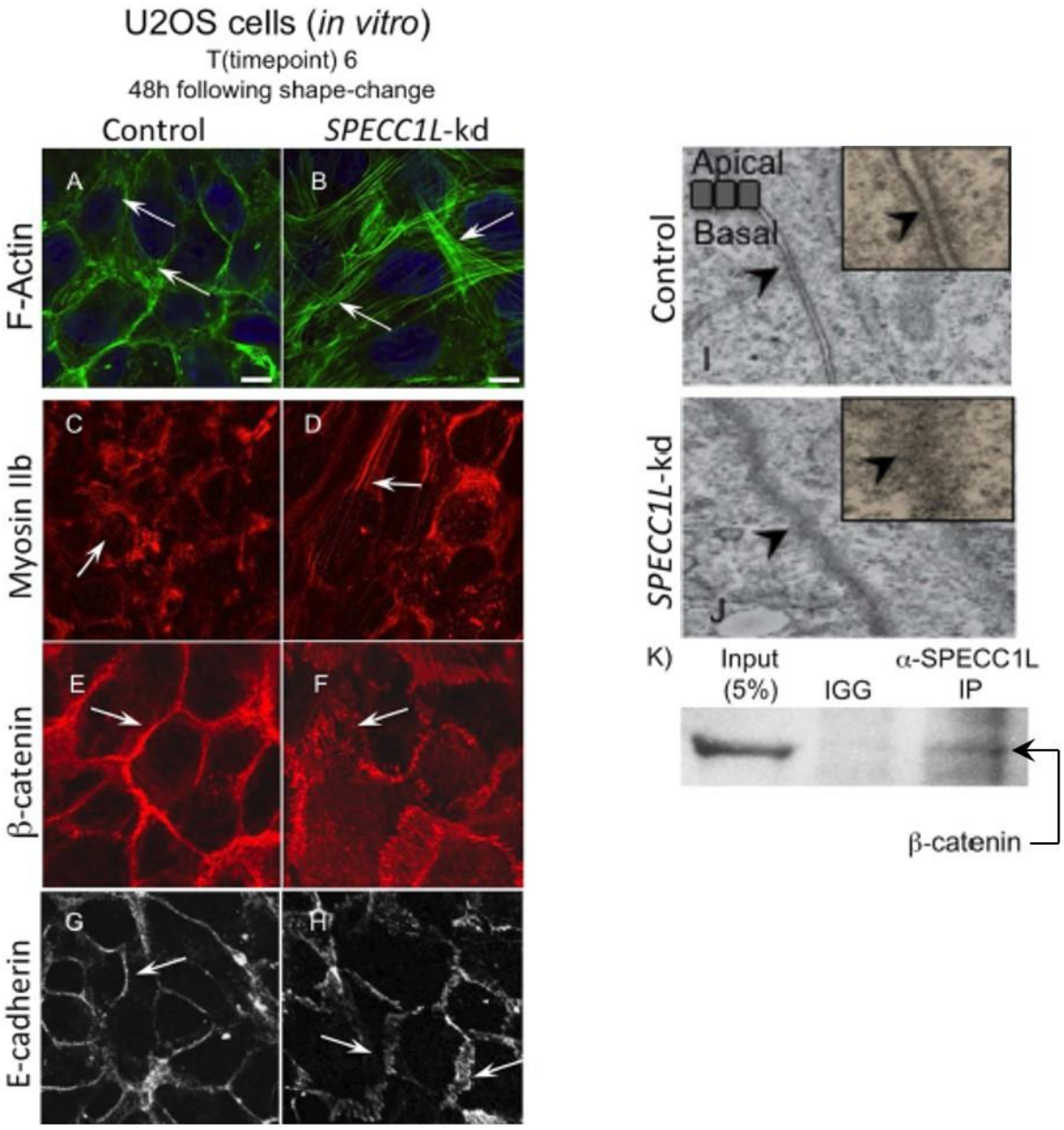

Figure 3.3. *SPECC1L*-kd U2OS cells show altered expression of adherens junction markers. (**A–H)** Increased F-actin staining in kd cells at 48 hours post-confluency (T6; **A**,**B**). Altered F-actin associated Myosin IIb staining (**C**,**D**). Smooth pattern of β -catenin and E-cadherin membrane staining in control cells (**E**,**G**) is expanded in *SPECC1L*-kd cells (**F**,**H**). Bars = 10 μ m. (**I–J)** Electron micrographs looking at apico-basal cell-cell boundary. Control cells show distinct electron-dense regions, indicating adherens junctions (**I**, arrow). In contrast, the entire apico-basal boundary appears electron-dense in *SPECC1L*-kd cells (**J**, arrows), suggesting increased density and dispersion of adherens junctions. (**K**) β -catenin co-immunoprecipitation with *SPECC1L* in lysates from confluent U2OS cells. The image is taken from a single blot, and represents one of four independent experiments.

dispersion of AJs along the apico-basal plane. Also, in lateral sections, we observed widespread ruffling of the cell membrane in the kd cells (Fig. 3.9A, B), accounting for the expanded striated pattern of β-catenin and E-cadherin staining (Fig. 3.3F, H). In support of a role for SPECC1L in AJs, β-catenin co-immunoprecipitated with SPECC1L in lysates from confluent U2OS cells (Fig. 3.3K). Together with expanded immunostaining of AJ markers, the TEM analysis is consistent with our hypothesis that SPECC1L deficiency increased apico-basal density and dispersion of AJs.

3.4.3 *Specc1l* deficiency shown neurulation defect and reduced CNCC delamination

To understand the role of SPECC1L in craniofacial morphogenesis, we created a mouse model of *Specc1l* deficiency using two independent gene-trap ES cell lines - DTM096 and RRH048 (BayGenomics, CA), which trap *Specc1l* transcripts in introns 1 and 15 respectively (Fig. 3.4A, Fig. 3.10A, B). Genomic location of gene-trap vector insertion was identified by whole-genome sequencing and verified by PCR (Fig. 3.10, C, D). Both gene-trap constructs also afford in-frame *Specc1l-lacZ* reporter fusion upon trapping. Thus, *lacZ* expression, as determined by X-gal staining, was used as a proxy for *Specc1l* expression. Both alleles show a similar *lacZ* expression pattern with the DTM096 gene-trap in intron 1 showing stronger expression than RRH048 in intron 15 (not shown). *Specc1l* is expressed broadly, however, expression is particularly robust in the neural folds at E8.5 (Fig. 3.4B), the neural tube and facial prominences at E9.5 and E10.5 (Fig. 3.4C, D), and in the developing limbs and eyes at E10.5 (Fig. 3.4D). We previously reported that SPECC1L expression in the first pharyngeal arch at E10.5 is present in both the epithelium and the underlying mesenchyme (Saadi et al., 2011), consistent with CNCC lineage. To validate expression of SPECC1L in CNCCs, we co-stained for SPECC1L and NCC markers AP2-alpha (AP2A) and SOX10 in E8.5 neural folds (Fig. 3.4E–J) and in E9.5 cranial sections

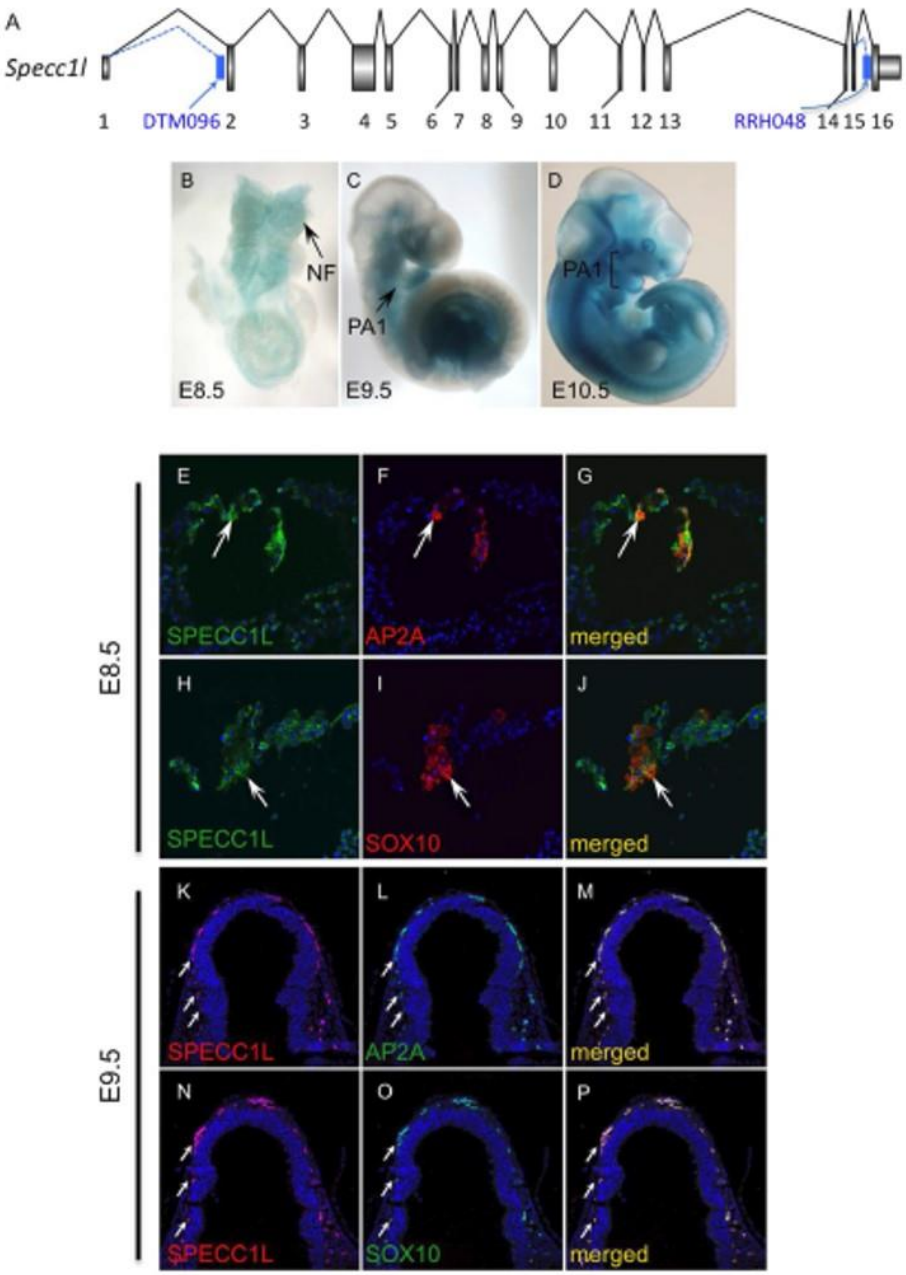

Figure 3.4. ***Specc1l*** **expression and overlap with the neural crest cell lineage.** (**A**) Schematic representation of murine *Specc1l* gene indicating insertion of genetrap vectors in ES cell clones DTM096 (intron 1) and RRH048 (intron 15). (**B–D**) Heterozygous *Specc1l*^{DTM096} embryos stained for *lacZ*, representing *Specc1l* expression, from E8.5 to E10.5. NE = neuroectoderm, NF = neural folds, PA1 = 1st pharyngeal arch. (**E–P**) Co-immunostaining of SPECC1L with NCC markers AP2A and SOX10 in E8.5 neural folds (NF; **E–J**) and in E9.5 cranial sections (**K–P**). SPECC1L staining is broadly observed in the E8.5 neural folds (**E**,**H**; arrows), including in cells marked by AP2A (**F**,**G**; arrows) and SOX10 (**I**,**J**; arrows). At E9.5, SPECC1L strongly stains migrating CNCCs (**K**,**N**; arrows) marked by AP2A (**L**,**M**; arrows) and SOX10 (**O**,**P**; arrows).

(Fig. 3.4K–P). At E8.5, SPECC1L stains the neural folds broadly (Fig. 3.4E, H), including cells stained with the NCC markers (Fig. 3.4G, J). At E9.5, SPECC1L (Fig. 3.4K, N) strongly stains migratory CNCCs co-stained with AP2A (Fig. 3.4L, M) or SOX10 (Fig. 4O, P).

Intercross matings between *Specc1l*$^{DTM096/+}$ and *Specc1l*$^{RRH048/+}$ heterozygous mice showed that the two gene-trap alleles failed to complement each other, and that compound heterozygous and embryos homozygous for either gene trap allele are embryonic lethal (Table 3.1). The Mendelian ratios indicate reduced survival of heterozygotes at birth (1.34 vs. 2.0 expected). We noted a low incidence of perinatal lethality in heterozygotes; some with craniofacial malformations (Fig. 3.11, E). However, the low penetrance of these perinatal craniofacial phenotypes makes it difficult to study the underlying pathophysiological mechanism. Therefore, we focused on the embryonic lethal phenotype of the *Specc1l* homozygous mutant.

The majority of *Specc1l*$^{DTM096/RRH048}$compound heterozygous or homozygous mutant embryos failed to thrive beyond E9.5–10.5 (Fig. 3.5A–D), with a failure of the neural tube to close anteriorly (Fig. 3.5B, D), and sometimes posteriorly (not shown). This cranial neural tube closure defect was accompanied by a large proportion of CNCCs, marked by DLX2, to remain in the neural folds at E10.5, suggesting a failure to delaminate (Fig. 3.5A'–D'). To determine if there was also a reduction in overall specification of CNCCs, we marked the CNCC lineage with GFP in our gene-trap lines with *Wnt1-Cre* and *ROSA*^{mTmG}. We flow-sorted the GFP+ NCCs and GFP- (RFP+) non-NCCs from whole embryos. At E9.5, the proportion of flow-sorted GFP-labeled CNCCs did not change significantly between WT and mutant embryos (not shown), indicating normal CNCC specification. Thus, we hypothesized that the residual staining with *Wnt1*-Cre and DLX2 in the open neural folds (Fig. 3.5B') was due to a defect in CNCC delamination, possibly

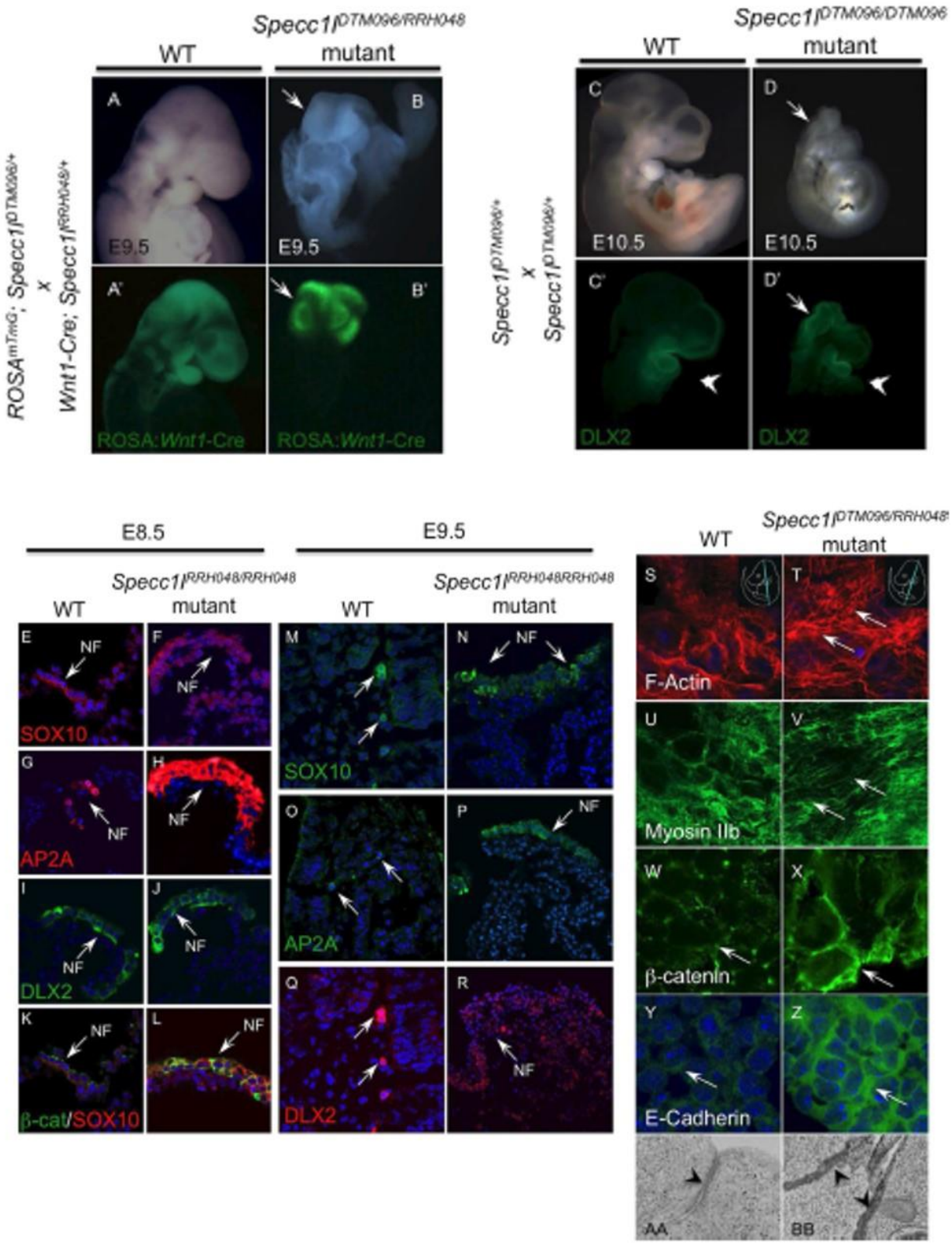
Specc1l DTM096/RRH048
WT
mutant
ROSA mTmG; Specc1l DTM096/+
x
Wnt1-Cre; Specc1l RRH048/+
A
B
E9.5
E9.5
A'
B'
ROSA:Wnt1-Cre
ROSA:Wnt1-Cre
Specc1l DTM096/DTM096
WT
mutant
Specc1l DTM096/+
x
Specc1l DTM096/+
C
D
E10.5
E10.5
C'
D'
DLX2
DLX2
E8.5
E9.5
Specc1l RRH048/RRH048
WT
mutant
WT
Specc1l RRH048/RRH048
mutant
E
F
NF
NF
SOX10
M
N
NF
SOX10
G
H
NF
NF
AP2A
O
P
NF
AP2A
I
J
NF
NF
DLX2
Q
R
NF
DLX2
K
L
NF
NF
β-cat/SOX10
Specc1l DTM096/RRH048
WT
mutant
S
T
F-Actin
U
V
Myosin IIb
W
X
β-catenin
Y
Z
E-Cadherin
AA
BB

Figure 3.5

Figure 3.5. *Specc1l* deficiency leads to defects in neural tube closure, cranial neural crest cell delamination and AJs. (**A,B'**) E9.5 WT (**A**) embryo with migratory cranial neural crest cells (CNCCs) marked with *Wnt1*-Cre (**A'**). In contrast, *Specc1l* mutant embryo shows open neural folds (**B**, arrow) with CNCCs that have still not migrated (**B'**, arrow). (**C,D'**) Brightfield images (**C,D**) and CNCC marker DLX2 immunostaining (**C',D'**) of E10.5 WT (**C,C'**) and *Specc1l* mutant (**D,D'**) embryos. In E10.5 WT embryo, DLX2 positive CNCCs populate the branchial arches (**C'**, arrowhead), while in the mutant significant staining remains in open neural folds (**D'**, arrow) with some staining in the 1st pharyngeal arch (**D'**, arrowhead), indicating poor CNCC delamination and migration. **E-R**) Sections from WT and *Specc1l* mutant embryos at E8.5 (**E–L**) and at E9.5 (**M–R**) were stained with NCC markers SOX10 (**E,F,M,N**), AP2A (**G,H,O,P**), and DLX2 (**I,J,Q,R**). At E8.5, NCC staining is observed in the neural folds (NF) of WT and mutant sections. Co-staining of SOX10 and β -catenin in E8.5 WT (**K**) and mutant (**L**) shows increased β -catenin staining at cell boundaries in the neural folds. At E9.5, migratory CNCC staining is observed in WT (**M,O,Q**), while in mutants undelaminated CNCCs stain the open neural folds (**N,P,R**). (**S–Z**) Analysis of AJ markers *in vivo* in WT and *Specc1l*$^{DTM096/RRH048}$ mutant E9.5 embryo coronal sections. The approximate plane of section is indicated in the top-right corner. Increased F-actin (**S,T**) and Myosin IIb (**U,V**) staining is observed in mutant tissue sections. Similarly to *in vitro* results in Fig. 3, expanded β -catenin (**W,X**) and E-cadherin (**Y,Z**) membrane staining is observed *in vivo* in mutant embryos. (**AA-BB**) Electron micrograph of WT embryo section looking at apico-basal cell boundary shows a distinct electron-dense region indicating adherens junction (**AA**, arrowhead). In contrast, the entire apico-basal boundary appears electron-dense in *Specc1l* mutant embryo section (**BB**, arrowheads), suggesting increased density and dispersion of adherens junctions.

due to increased density or dispersion of AJs, as observed in *SPECC1L*-kd cells. We used NCC markers SOX10, AP2A, and DLX2 to confirm the presence of CNCCs in the neural folds (Fig. 3.5E–R). At E8.5, neural fold staining is observed with all three NCC markers in both WT (Fig. 3.5E, G, I) and *Specc1l* mutant (Fig. 3.5F, H, J) sections. At E9.5, while NCC markers stain migratory NCCs in WT sections (Fig. 3.5M, O, Q), residual NCC staining is present in the open neural folds of *Specc1l* mutant embryos (Fig. 3.5N, P, R). Since SOX10 and DLX2 mark migratory CNCCs, this result indicates that SPECC1L deficient CNCCs attain post-migratory specification but fail to emigrate from the neural folds.

3.4.4 *Specc1l* mutant tissue recapitulates *in vitro* adherens junction changes

To test our hypothesis that reduced delamination is due to altered AJs, we investigated the AJ markers in the open neural folds of *Specc1l* mutant embryos (Fig. 3.5S–Z). We observed increased actin stress fibers (Fig. 3.5S, T) and concomitant increased localization of Myosin IIB staining to the actin fibers (Fig. 3.5U, V). Importantly, we saw increased staining of β-catenin (Fig. 3.5W, X) and E-cadherin (Fig. 3.5Y, Z) at cell-cell boundaries. We also examined β-catenin staining of NCCs in the neural folds of E8.5 embryos (Fig. 3.5K, L). The β-catenin staining appears more robust in *Specc1l* mutant neural folds (Fig. 3.5L vs. K), suggesting that changes in AJs have commenced. In electron micrographs of cranial sections from E9.5 embryos, we again observed an increase in dispersed electron-dense staining in *Specc1l* mutant embryos compared to WT (Figs 3.5AA, BB and 3.9, E–H). Taken together, these results validate our *in vitro* findings in *SPECC1L*-kd U2OS cells, and indicate that abnormal staining of AJs precedes CNCC delamination in our mutant embryos.

3.4.5 Reduced PI3K-AKT signaling and increased apoptosis in SPECC1L deficient cells

Given the known antagonistic relationship of AKT activity to E-cadherin stability (Larue et al., 2005, Thomas-Tikhonenko, 2010), we hypothesized involvement of PI3K-AKT signaling. In addition, we observed sub-epidermal blebbing in some of our mutant embryos that escape E9.5–10.5 lethality (<5%), and instead arrest at approximately E13.5 (Fig. 3.11). Sub-epidermal blebbing is a hallmark of reduced PDGFRα-based PI3K-AKT signaling (Fantauzzo & Soriano, 2014). Fantauzzo *et al*. (2014) reported that disruption of PDGFRα-based PI3K activation in $Pdgfra^{PI3K/PI3K}$ mutant embryos results in sub-epidermal blebbing, neural tube defects, and cleft palate phenotypes. Indeed, pan-AKT and active phospho-Ser473-AKT levels were reduced *in vivo* in *Specc1l* mutant tissue (Fig. 3.6A–D), prior to embryonic arrest at E9.5. Reduced phospho-Ser473-AKT level was likely entirely due to reduced pan-AKT levels *in vivo* (Fig. 3.6E) and *in vitro* (Fig. 3.6F). The *in vitro* reduction was only present at high confluency of U2OS cells upon cell shape and AJ density changes (Fig. 3.6D). Thus, our data suggest SPECC1L is a novel positive regulator of PI3K-AKT signaling in craniofacial morphogenesis.

We next examined markers of proliferation and apoptosis. We did not observe any differences in proliferation in E9.5 embryos (Fig. 3.6E, G vs. I) as measured by KI67 staining, with a proliferative index of 82.5% for WT and 86.5% for *Specc1l* mutant ($p < 0.56$, Fisher exact test). Similarly, we did not observe any difference in apoptosis as measured by cleaved Caspase 3 staining in neural folds at E8.5, prior to embryonic arrest (not shown). In contrast, apoptosis was markedly increased throughout the E9.5 mutant embryo (Fig. 3.6F, H vs. J). This global increase in apoptosis is consistent with reduced PI3K-AKT signaling and early embryonic lethality (Zeitlin et al., 1995, Mueller et al., 2002, Gladdy, 2006).

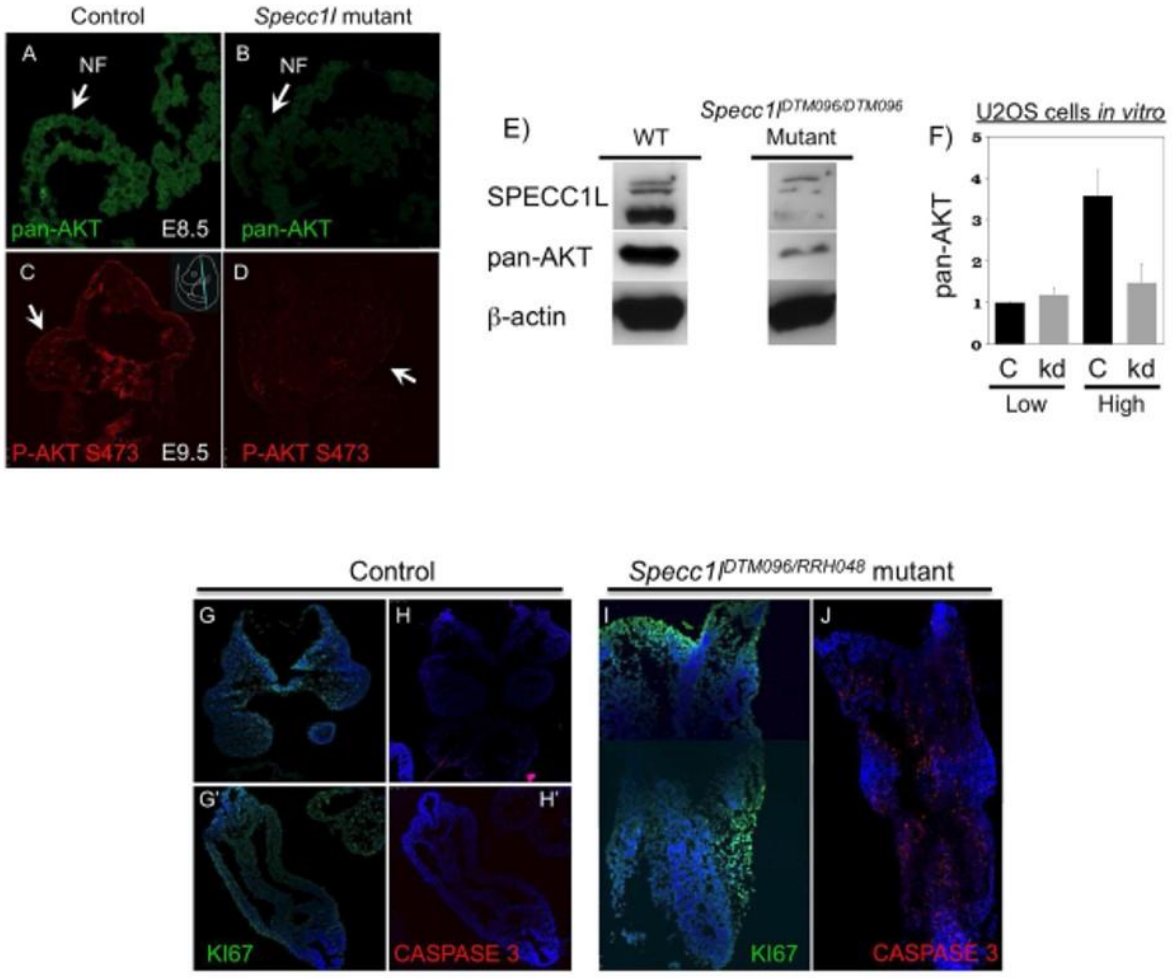

Figure 3.6. ***Specc1l*** **mutant embryos show reduced PI3K-AKT signaling and increased cell death.** (**A–E**) E8.5 (**A,B**) and E9.5 (**C,D**) cranial sections or E9.5 lysates (**E**) from *Specc1l* mutant embryos show decreased levels of active phospho-S473-AKT and pan-AKT protein, compared to WT control. The western blot analyses were performed under the same conditions for WT and mutant lysates. The images shown for SPECC1L are taken from a single blot. The same blot was stripped and re-probed with pan-AKT and then β -actin antibodies. Pan-AKT level in E8.5 neural folds (**A**,**B**) and phospho-S473-AKT level in E9.5 cranial section are markedly reduced. (**F**) A similar reduction is seen in pan-AKT levels in *SPECC1L*-kd U2OS cell lysates collected at high confluency. The error bars represent SEM from quantitation of three independent western blots. (**G–J**) Sections of WT embryos at E9.5 show cell proliferation (**G**,**G'**) with negligible apoptotic activity (**H**,**H'**) through KI67 and cleaved Caspase 3 staining, respectively. In *Specc1l* mutant embryos, there is comparable cell proliferation (**I**), however, there is a striking increase in cells undergoing apoptosis (**J**).

3.4.6 Upregulation of PI3K-AKT pathway rescues *SPECC1L*-kd phenotype

Next, to confirm a causal role for PI3K-AKT signaling in AJ change in our kd cells, we chemically altered the pathway in control and kd cells (Fig. 3.7A–F). We used the cell shape change phenotype observed in confluent *SPECC1L*-kd cells as a marker, which we quantified using the ratio of the longest dimension (length) and the corresponding perpendicular dimension (width). A relatively round or cuboidal cell would be expected to give a ratio of 1 (Fig. 3.7G). In addition to cell shape, we confirmed the effect on AJs through β-catenin staining (Fig. 3.7A'–F'). Inhibition of the PI3K-AKT pathway using Wortmannin was sufficient to alter cell shape (Fig. 3.7A, C) and AJs (Fig. 3.7A') in control cells. The PI3K-AKT activator, SC-79, did not affect cell shape (Fig. 3.7A, E) or AJ expansion (Fig. 3.7A') in control cells. In *SPECC1L*-kd cells, further down-regulation of PI3K-AKT pathway resulted in increased apoptosis (Fig. 3.7B, D) with drastically expanded staining for β-catenin (Fig. 3.7B'), consistent with our severe mutants *in vivo*. Importantly, upregulation of the PI3K-AKT pathway drastically ameliorated the cell shape (Fig. 3.7B, F) and AJ (Fig. 3.7B'') phenotypes. As stated above, changes in cell shape were quantitated as a cell circularity ratio (CCR), and compared for significance (Fig. 3.7G). Indeed, in control cells (Fig. 3.7G, CCR = 1.56), Wortmannin treatment was sufficient to significantly change cell shape (Fig. 3.7G, CCR = 3.61, $p < 2.4 \times 10^{-9}$), which was similar in extent to that seen in *SPECC1L*-kd cells (Fig. 3.7G, CCR = 3.46). Wortmannin treatment of *SPECC1L*-kd cells (Fig. 3.7G, CCR = 3.60, not significant) did not affect cell elongation any further than untreated kd cells (Fig. 3.7G, CCR = 3.46, not significant) or Wortmannin-treated control cells (Fig. 3.7G, CCR = 3.61, not significant). Most important, SC-79 AKT activator rescued the elongated cell shape phenotype of *SPECC1L*-kd cells (Fig. 3.7G, CCR = 1.74, $p < 6.2 \times 10^{-12}$). These results substantiate that

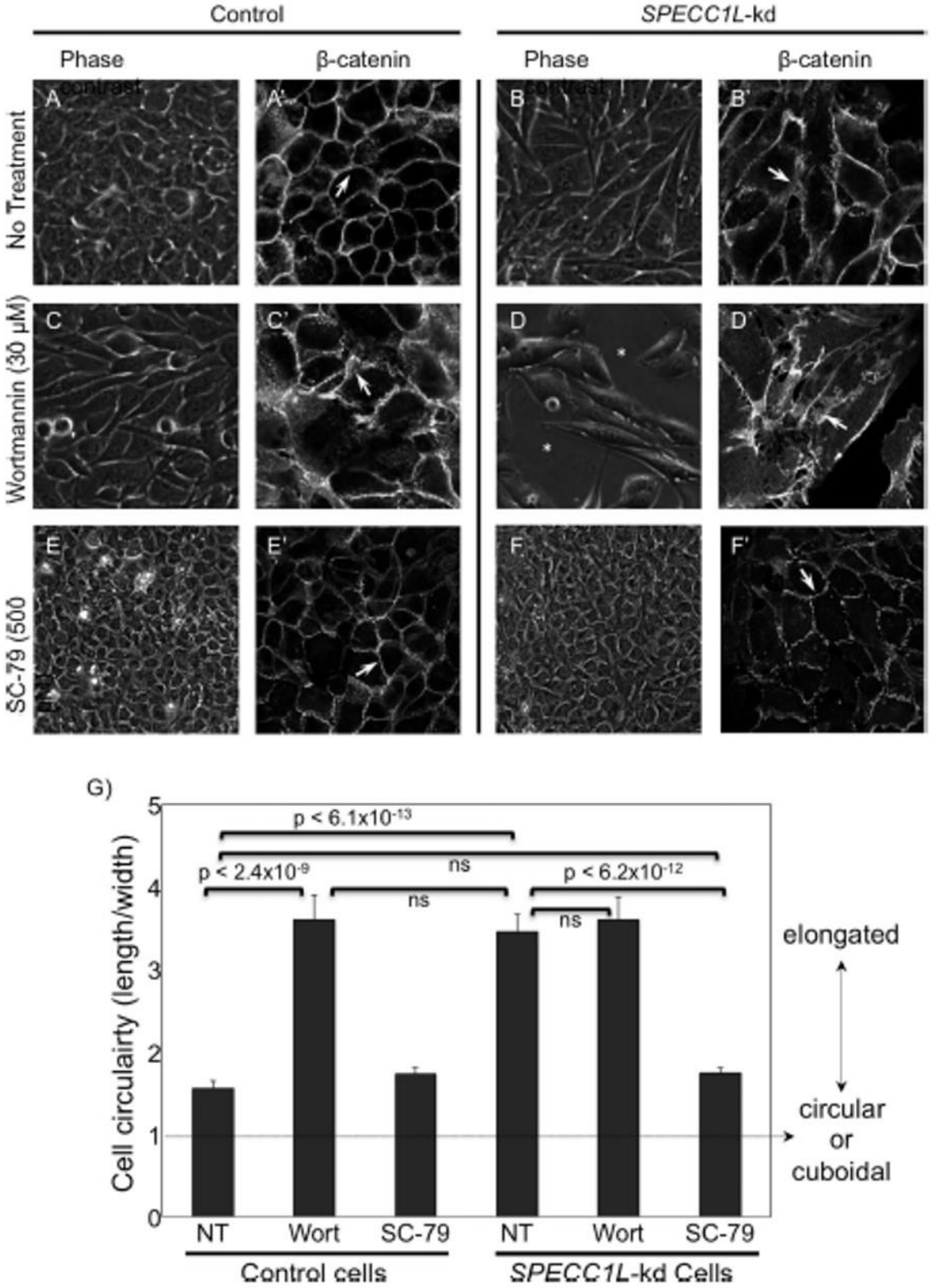
Control
SPECC1L-kd
Phase contrast
β-catenin
Phase contrast
β-catenin
No Treatment
Wortmannin (30 μM)
SC-79 (500
A
A'
B
B'
C
C'
D
D'
E
E'
F
F'
G)
Cell circulairty (length/width)
p < 6.1x10-13
p < 2.4x10-9
ns
p < 6.2x10-12
ns
ns
elongated
circular or cuboidal
NT
Wort
SC-79
NT
Wort
SC-79
Control cells
SPECC1L-kd Cells

Figure 3.7

Figure 3.7. Upregulation of PI3K-AKT pathway can rescue *SPECC1L*-kd phenotype *in vitro*. (**A–F'**) Control (**A**,**C**,**E**) and *SPECC1L*-kd (**B**,**D**,**F**) cells were treated with PI3K-AKT pathway inhibitor Wortmannin (**C**,**D**) or activator SC-79 (**E**,**F**). Untreated control cells are cuboidal (**A**) with normal honey-comb pattern of β -cat staining (**A'**), while kd cells are elongated (**B**) with expanded β -cat staining (**B'**). Upon down-regulation of PI3K-AKT pathway, control cells are elongated (**C**) with β -cat expansion (**C'**), while kd cells begin to undergo apoptosis (**D**), similarly to our severe mutant embryos, and show extremely expanded β–cat staining (**D'**). Upon up regulation of PI3K-AKT pathway, control cells remain cuboidal (**E**) with normal β-cat staining (**E'**), while kd cells show much improved cell shape (**F**) and β -cat staining (**F'**), indicating rescue. (**G**) The extent of cell shape change in (**A–F**) were quantitated using a cell circularity ratio (CCR) of longest dimension (length) and the corresponding perpendicular dimension (width) using MetaMorph software. The no treatment (NT) *SPECC1L*-kd cells (CCR = 3.46) were significantly elongated than control cells (CCR = 1.56, $p < 6.1 \times 10{-}13$). Wortmannin (Wort) inhibition of PI3K-AKT pathway in control cells was sufficient to cause a similar elongation of cell shape (CCR = 3.61, $p < 2.4 \times 10{-}9$). Similarly, AKT activation with SC-79 in *SPECC1L*-kd cells was able to rescue the elongated cell shape back to control level (CCR = 1.74, $p < 6.2 \times 10{-}12$). Wortmannin treatment of *SPECC1L*-kd cells resulted in increased apoptosis, but did not cause further increase in cell shape change (CCR = 3.60) beyond that observed in untreated kd (CCR = 3.46, ns) or Wortmannin-treated control cells (3.61). ns = not significant. Measurement of 50 cells + /− S.E.M. is shown. Statistical differences were calculated using a Student's t-test.

SPECC1L regulates PI3K-AKT signaling, and indicate that moderate reduction in SPECC1L affects cell adhesion, while severe reduction can lead to apoptosis (Fig. 3.8).

3.5 Discussion

Dissolution of AJs is required for pre-migratory CNCCs to delaminate from the neural epithelium of the anterior neural folds (Le Douarin, 1982, Taneyhill, 2008, Theveneau & Mayor, 2011). The increased staining of AJ components and loss of apico-basal asymmetrical distribution of AJs in SPECC1L-deficient cells *in vitro* and *in vivo*, combined with physical proximity of SPECC1L with β-catenin indicates a role for SPECC1L in maintaining localized stability of AJs by properly organizing the actin cytoskeleton. The association of SPECC1L with the actin cytoskeleton and β-catenin combined with an increase in condensed actin filaments upon SPECC1L deficiency are consistent with the observed increase in AJ density. Another possibility is that increased actin fibers in SPECC1L deficient cells lead to altered tension between cells. As cell tension can impact AJ dynamics (Harris et al., 2014), a change in tension may lead to more dispersed AJs (Engl et al., 2014). Either alteration can consequently affect CNCC delamination.

Wnt1 is expressed in the early neural folds that give rise to neural crest cells. Thus, *Wnt1*-cre lineage tracing marks both pre-migratory and migratory NCCs (Chai et al., 2000). However, *Wnt1* also marks lineage of dorsal brain tissues that also arise from the early neural folds (Chai et al., 2000, Brault et al., 2001), leaving a possibility that the *Wnt1*-marked staining in our E9.5 mutant open neural folds were not CNCCs. Our positive staining with NCC markers AP2A and SOX10 confirms that the open neural folds of the *Specc1l* mutant embryos indeed contain CNCCs. Furthermore, since AP2A and SOX10 are markers for early migrating NCCs, the positive staining indicates that these cells are post-migratory CNCCs that fail to delaminate by E9.5.

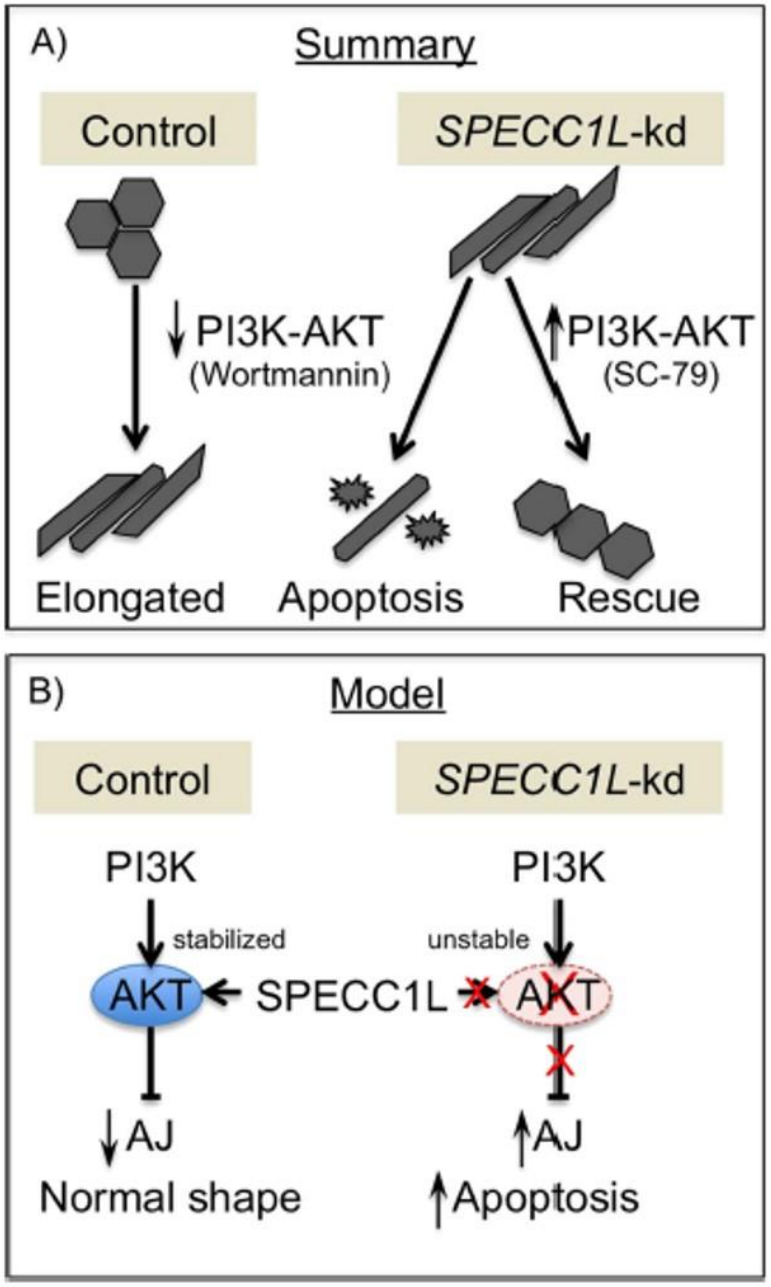

Figure 3.8. Model of SPECC1L modulation of PI3K-AKT pathway and AJs. (**A**) Schematic summary of PI3K-AKT pathway inhibition and activation leading to AJ change and rescue, respectively. (**B**) A model proposing that SPECC1L stabilizes AKT protein.

Our data indicate that the molecular regulation of AJs by SPECC1L is mediated by PI3K-AKT signaling. AKT signaling is reduced in SPECC1L-deficient cells and tissue. A direct role for PI3K-AKT signaling in craniofacial morphogenesis is supported by the findings of Fantauzzo *et al*. (2014) showing that lack of PDGFRα-based activation of PI3K-AKT signaling leads to cleft palate phenotype. We also showed that inhibition of the PI3K-AKT pathway is sufficient to alter AJs and cell shape in U2OS cells. Consistent with our findings, Cain *et al*, (2010) have shown that in endothelial cells down-regulation of PI3K α110 subunit led to a similarly expanded pericellular β-catenin staining, termed as increased "junctional index". However, in their endothelial cells with already highly organized actin filaments, the down-regulation of PI3K-AKT pathway resulted in a relaxation of cell shape. In contrast, the *SPECC1L*-kd U2OS cells show elongated cell shape. This difference is likely cell-type specific. While down-regulation of PI3K-AKT signaling consistently affects the actin cytoskeleton, the effect on cell shape is dictated by altered tension resulting from changes in central actin fiber density and organization. In U2OS cells, we used the cell shape change only as a marker of the SPECC1L-deficient AJ change and rescue. Taken together, we propose that suppression of AKT pathway upon SPECC1L deficiency increases AJ stability and reduces delamination of the CNCCs.

Interestingly, pan-AKT levels are reduced in addition to phospho-473-AKT levels *in vitro* and *in vivo* upon SPECC1L deficiency, thus indicating regulation of PI3K-AKT signaling at the level of AKT protein stability or turnover. Both *SPECC1L* and *MID1* genes, implicated in Opitz/GBBB Syndrome, encode proteins that stabilize microtubules (Saadi et al., 2011, Short & Cox, 2006). The mechanism through which SPECC1L and MID1 mediate microtubule stabilization is not entirely clear. In the case of SPECC1L, this stabilization involves enhanced acetylation of a subset of microtubules (Saadi et al., 2011). Perhaps SPECC1L utilizes a similar

mechanism to stabilize other proteins such as AKT. Acetylation of lysine residues in AKT protein has been shown to result in reduced membrane localization and phosphorylation (Sundaresan et al., 2011). In addition, K63 chain ubiquitination of the same lysine residues on AKT is required for its membrane localization and activation (Yang et al., 2009, Chan et al., 2014). Of the few SPECC1L protein interactors identified in different high throughput yeast two-hybrid screens, four-CCDC8 (Hanson et al., 2014), ECM29 (Gorbea et al., 2010), APC and UBE2I (Bandyopadhyay et al., 2010) - participate in protein turnover or stability through ubiquitination or sumoylation. It is possible that SPECC1L participates in the post-translational modification of AKT lysine residues, affecting AKT stability. However, a definitive role for SPECC1L in AKT protein localization and stability is yet to be elucidated.

A severe deficiency in SPECC1L expression *in vivo* results in increased AJ marker staining and defective CNCC delamination, as well as in increased apoptosis and early embryonic lethality. Previous reports have shown that mouse mutants with increased levels of apoptosis have associated neural tube (Homanics et al., 1995, Ikeda et al, 2001, Ruland et al., 2001, Migliorini et al., 2002) and craniofacial defects (Jeong et al., 2004). It is proposed that excessive cell death in the neural folds or pharyngeal arches may result in insufficient number of cells required for proper morphogenetic movement (Jeong et al., 2004, Copp, 2005, Harris & Juriloff et al., 2007). In contrast, our SPECC1L-deficient cell lines with moderate reduction in *SPECC1L* expression show only AJ changes without evidence of increased cell death. However, chemical inhibition of PI3K-AKT pathway in these kd cells does indeed lead to increased apoptosis. Thus, a moderate reduction in SPECC1L expression or function allows cell viability. This is consistent with the observation that rare *Specc1l* mutant embryos that escape E9.5 arrest - likely due to reduced gene-trapping efficiency - are able to close their neural tubes and arrest later in development, frequently with

craniofacial defects (Fig. 3.11). Also, consistent with this is the rare occurrence of *Specc1l* heterozygous embryos with craniofacial malformation - likely due to increased gene-trapping efficiency - and findings in zebrafish where morphants for one of two *SPECC1L* orthologs (*specc1lb*) lead to late embryonic phenotypes including a loss of mandible and bilateral clefts (Gfrerer et al., 2014). Thus, heterozygous *SPECC1L* loss-of-function mutations identified in human patients may lead to mild perturbation in SPECC1L function during craniofacial morphogenesis, sufficient to account for their orofacial clefts. SPECC1L-based modulation of cell-cell contacts may also play a role in palatogenesis and pharyngeal arch fusion. Further studies of SPECC1L function will help elucidate the role of transient cell-cell contacts in neuroepithelial cell movement during neural tube closure and in CNCCs during craniofacial morphogenesis.

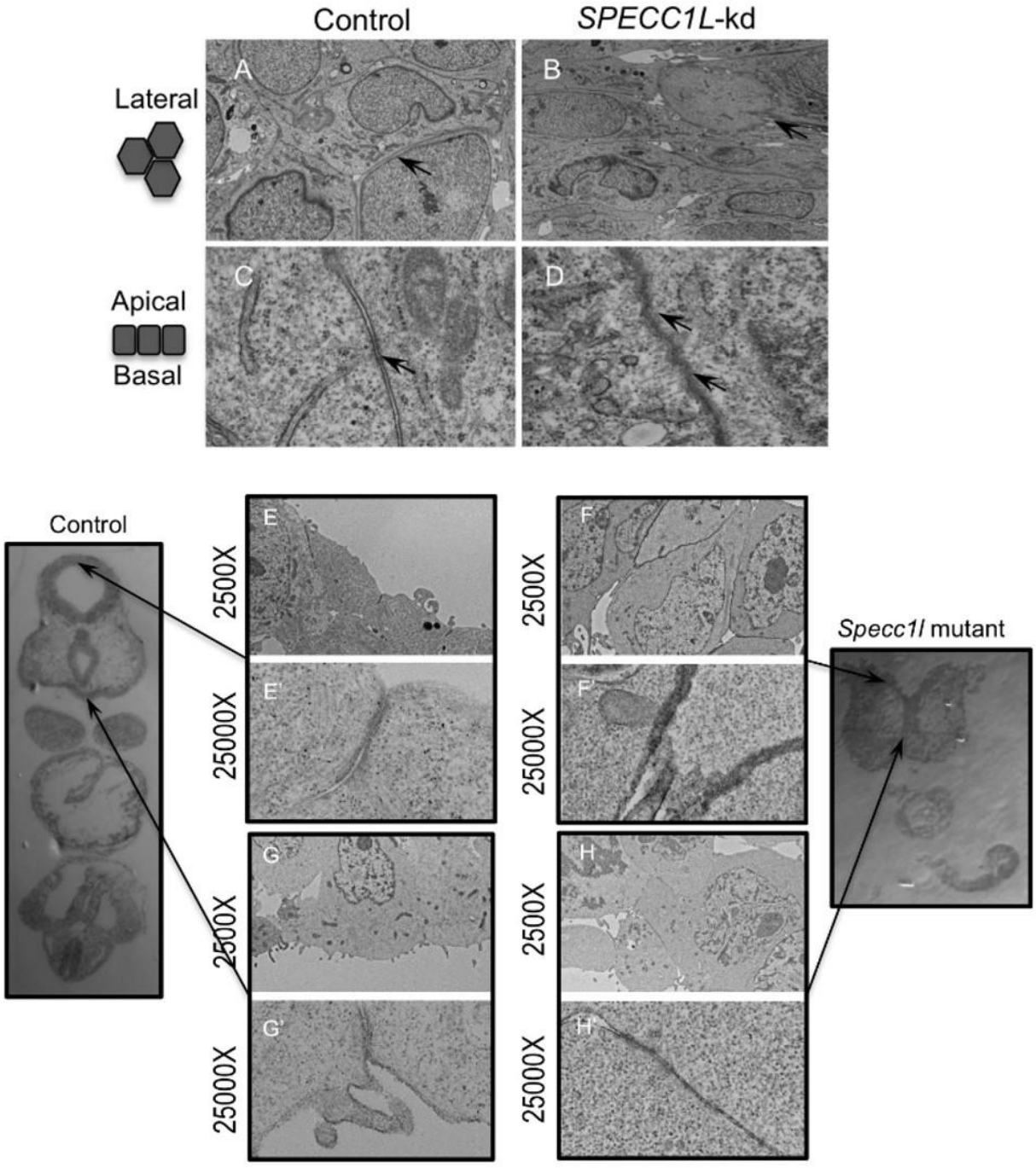

Supplemental Figure 3.9

Supplemental Figure 3.9. *SPECC1L*-kd cells and tissue show altered cell-cell boundaries in electron micrographs. Low magnification analysis of transverse sections show the normal honeycomb pattern for Control U2OS cells (**A**, arrow). However, *SPECC1L*-kd U2OS cells show jagged edges that appear intercalated (**B**, arrow). Higher magnification sections looking at the apical-basal boundary shows distinct electron-dense regions indicating adherens junctions (**C**, arrow). In contrast, the entire apical-basal boundary appears electron-dense in *SPECC1L*-kd U2OS cells (**D**, arrows), suggesting increased density of adherens junctions (**E-H**). Importantly, the same increased density was noted *in vivo* in *Specc1l* mutant E9.5 embryo sections. Regions shown for control and wildtype embryos (**E, G**) were taken from dorsal hindbrain (**E**) and maxillary pharyngeal arch **(G)** epithelia, while those for mutant embryos were taken from the open neural folds (F, H). Corresponding higher magnification images are shown in **E'-H'**, indicating increased electron dense regions in the mutatnt cell-cell boundaries compared to those between control cells.

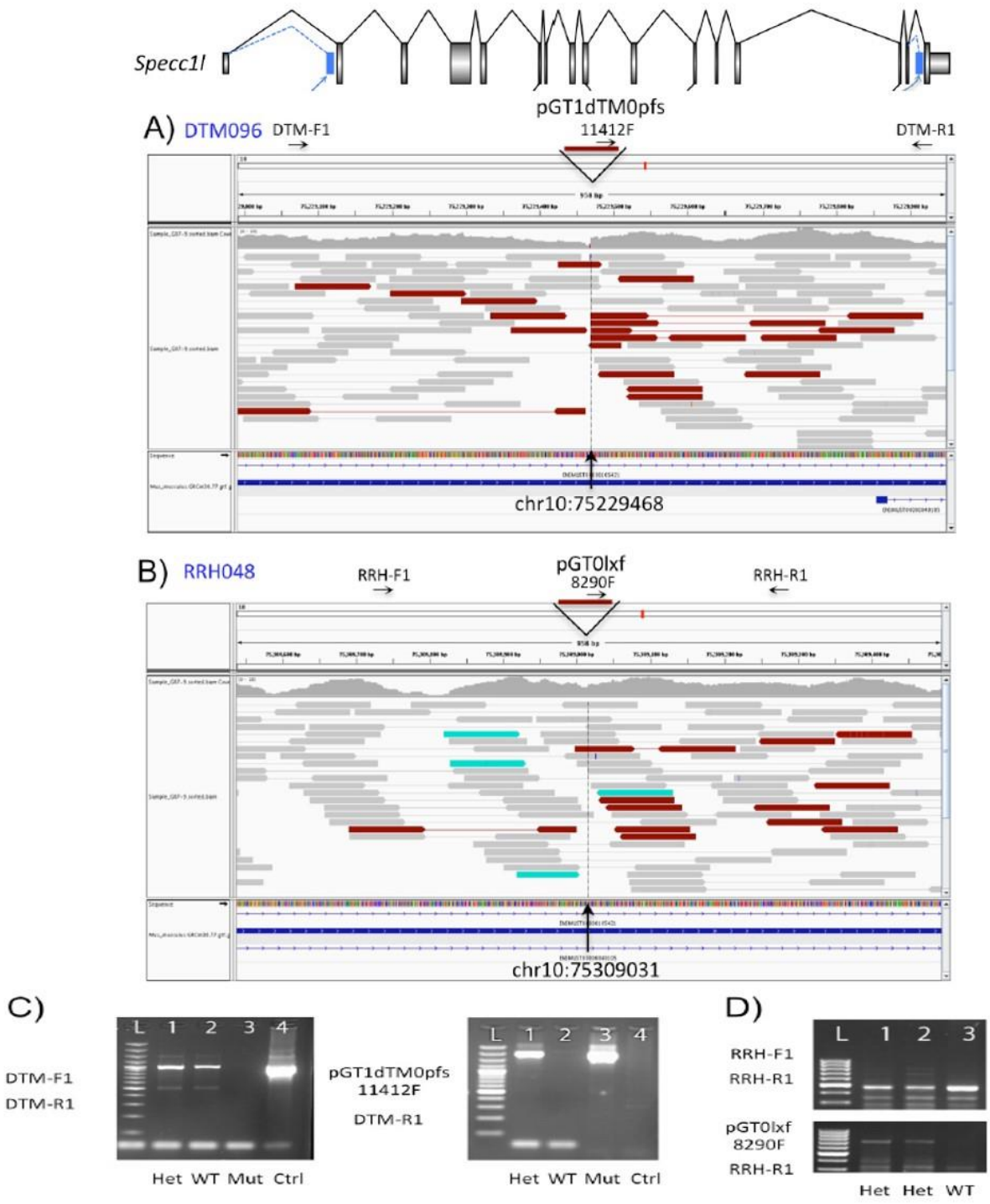

Primer Sequences	DTM-F1	GCTGCTTTGTGGCATTCTCA
	DTM-R1	CCACCACCTGCTTTCAGTCT
	pGT1dTM0pfs-11412F	CGTAAGGAGAAAATACCGCATCA
	RRH-F1	AGGGGCCATAAAATGCTGCT
	RRH-R1	GGGCTGTCCTGAGCAAGTTA
	pGT0lxf-8290F	ACCTCTGACACATGCAGCTC

Supplemental Figure 3.10

Supplemental Figure 3.10. Confirmation of genomic locations of *Specc1l* DTM096 and RRH048 genetrap constructs. Genomic DNA from *Specc1lDTM096/RRH048* mutant embryo was analyzed by whole genome sequencing. As expected, disrupted mapping with clustering of un-mapped paired-ends was observed in *Specc1l* intron 1 and 15 corresponding to DTM096 (**A**) and RRH048 (**B**) reported locations. These insertions were confirmed by conventional PCR using a primer in the vector, thus establishing specific genotyping protocols for *Specc1l*^{DTM096} (**C**) and *Specc1l*^{RRH048} (**D**), respectively. Primer sequences and approximate locations are indicated for reference.

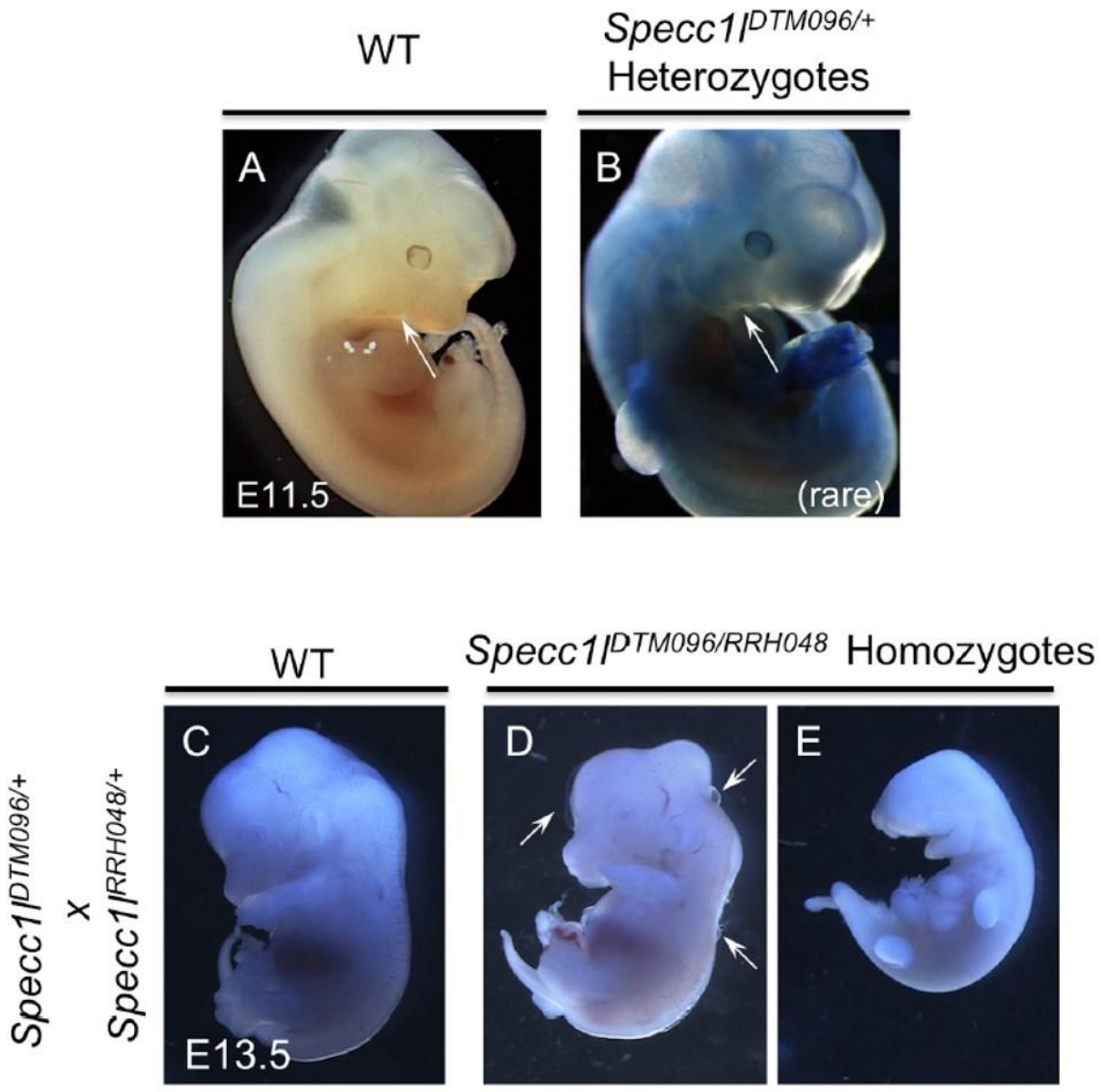

Supplemental Figure 3.11. Rare late gestational phenotypes of heterozygous and homozygous *Specc1l* deficient embryos. **A**, **B**) In very rare cases, heterozygous *Specc1l* embyos show perinatal lethality. Shown are lacZ stained control 11.5 wildtype (**A**, clear) and a heterozygous littermate with hypoplastic facial processes (**B**, blue stained). **C-E**) in some cases, homozygous mutants escape early growth arrest and show a range of phenotypes including sub-epidermal blebbing (**D**, arrows) and severe craniofacial, limb and spine malformation (**E**), compared to WT littermate (**C**).

Analysis at birth:		WT	Het	Hom	Litters
Specc1l$^{DTM/+}$ x *Specc1l*$^{DTM/+}$		29	43	0	13
Specc1l$^{DTM/+}$ x *Specc1l*$^{RRH/+}$		34	43	0	12
Specc1l$^{RRH/+}$ x *Specc1l*$^{RRH/+}$		16	20	0	8
	Total	**79**	**106**	**0**	**33**
Mendelian Ratio	**Observed**	**1**	**1.34**	**0**	
	Expected	**1**	**2**	**1**	

Supplemental Table 3.1. *Specc1l*^{DTM} and *Specc1l*^{RRH} heterozygotes show reduced Mendelian ratio and homozygous mutants do not survive until birth.

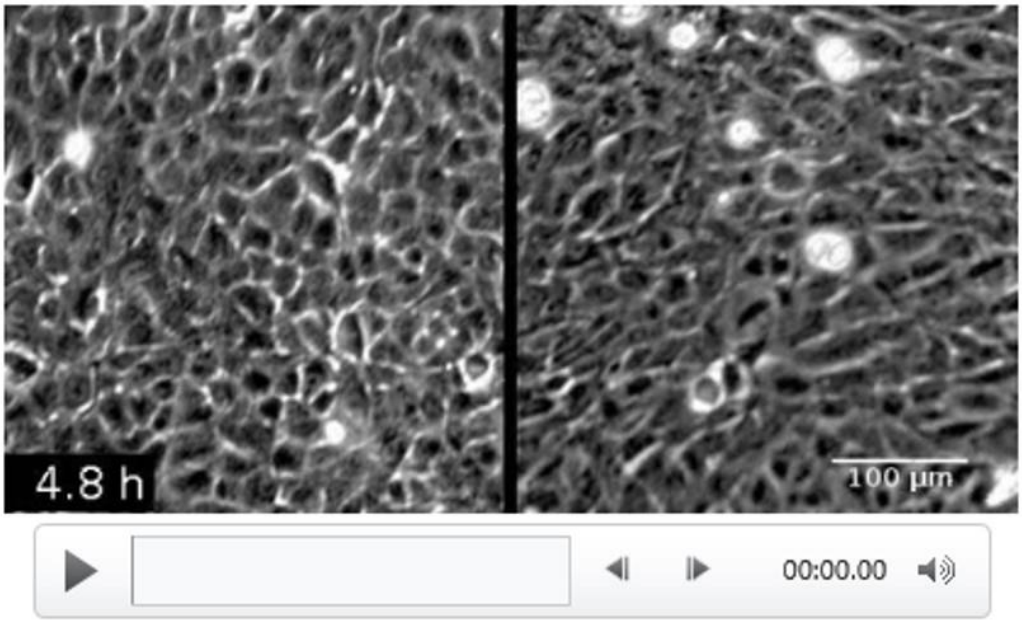

Supplemental Movie 3.1. SPECC1L-kd U2OS cells elongate upon high confluency. Equal number of Control (**left**) and SPECC1L-kd cells (**right**) were plated onto 35mm dishes and imaged. While control cells stay cuboidal, *SPECC1L*-kd cells elongate upon high confluency. Elapsed time is shown in hours.

This video can be accessed at:
http://www.nature.com/article-assets/npg/srep/2016/160120/srep17735/extref/srep17735-s1.mov

CHAPTER FOUR:

MODERATE DEFICIENCY OF *SPECC1L* IMPAIRS COLLECTIVE MIGRATION OF PRIMARY PALATAL MESENCHYME CELLS

Chapter Four: Moderate deficiency of *Specc1l* impairs collective migration of primary palatal mesenchyme cells

Nathan Wilson, Everett Hall, Edina Kósa, Dona Greta Isai, Jeremy Goering, András Czirók, Irfan Saadi

Contributions

Mouse crosses and palatal shelf dissection was performed by EH, Cell culture was performed by NW, Live imaging was performed by NW and EK, cell tracking was performed by EK, JG and NW, computational analyses were performed by EK, GI and AC.

4.1 Abstract

Cranial neural crest cells (CNCCs) migrate from the embryonic neural folds to the pharyngeal arches, contributing to maxillofacial development. Collective cell migration is a cooperative process fundamental to embryonic development, which shapes and populates emerging tissues. Unlike directional migration, during which each cell acts as an independent player, collective migration requires dynamic relationships between members in the coordination of movement. The collective migration required for CNCC infiltration of the pharyngeal arches is relevant to the aberrant development seen in orofacial clefting, as demonstrated by deficiency of the tumor suppressor Merlin, one of the few known proteins which disrupts collective migration, *Merlin* mutant mice have cleft palate, among other defects (Gritli-Linde et al., 2008, Das et al., 2015). *SPECC1L*-kd U2OS cells show impaired wound healing, taking longer to fill wounds than wildtype U2OS cells (Saadi et al., 2011). We have shown that this impairment is dependent upon the elongated cell shape change, which occurs in *SPECC1L*-kd U2OS cells (Chapter Three). The

extent of collective cell migration can be quantified by measurement of correlation length, which represents the distance from an observed cell where its neighbors continue migrating in the same direction as it (Szabó et al., 2010). Here we report that *SPECC1L*-kd U2OS cells show reduced correlation lengths when compared with wild type counterparts, indicating a defect in collective migration. Compound mutant mice harboring severe gene trapped *Specc1l*$^{RRH/-}$ and hypomorphic deletion *Specc1l*$^{\Delta 300/-}$ alleles (*Specc1l*$^{RRH/\Delta 300}$) show incompletely penetrant CP. Wound assays using wild type and *Specc1l*$^{RRH/300}$ embryonic palatal mesenchyme cells (MEPM) showed a comparable reduction in correlation length, indicating defects in collective migration. Previously, we reported that these U2OS *SPECC1L*-kd cells exhibit adherens junction and morphological phenotypes due to downregulation of PI3K-AKT signaling pathway. We report that the delayed wound closure time seen in *SPECC1L*-kd U2OS cells is partially rescued by AKT activation, *in vitro*. Together, these data indicate SPECC1L as a novel modulator of the functions of PI3K-AKT signaling in CNCC migration.

4.2 Introduction

CNCCs, differentiating within the dorsal neuroectoderm, subsequently delaminate and migrate into the pharyngeal arches, where they contribute to most craniofacial cartilage and bone (Trainor et al., 2000). However, many questions remain concerning CNCC collective cell migration, a process marked by cell-cell interactions (Theveneau & Mayor, 2012).

Frequently the disruption of genes regulating CNCC functions is associated with craniofacial malformations such as orofacial clefts, a common congenital deformity affecting approximately 1/800 live births. Of interest are genes which affect collective migration and

associate with facial clefting, such as Filamin A, which disrupts epithelial migration (Simpson et al., 2008) and is also associated with the syndromic cleft palate of Otopalatodigitial type 1 syndrome (Passos-Bueno et al., 2009). Neural crest-specific *Filamin A* knockout in mouse causes abnormalities of the cardiac outflow tract (Feng et al., 2006).

Collective cell migration requires cell-cell and cell-ECM interactions (Rorth, 2009). Migratory CNCCs interact with each other through transient adhesions involving N-cadherin (Xu et al., 2001). These interactions may negate CNCC proliferation throughout migration, as cells at the leading edge enter mitosis more frequently than those following them. Migratory CNCCs also show chemotactic responses to secreted factors such as VEGF and Sdf1 (Kulesa & McLennan, 2015), as well as other cell-environment signals including contact with Ephrins and Semaphorins, as well as proteoglycans (Kulesa & McLennan, 2015).

Proper migration, proliferation and differentiation of CNCCs are required for palatogenesis. The disruption of any of these processes can cause facial clefting (Ito et al., 2003). Previously, *SPECC1L* was identified as the first gene mutated in severe, atypical facial clefting which extend from the oral cavity to the eye, in two human patients (Saadi 2011). *SPECC1L* mutations have been identified in two families affected by autosomal dominant Opitz G/BBB syndrome (OMIM #145410) (Kruszka & McLennan, 2015), which manifest cleft lip/palate. Other Opitz G/BBB syndrome cases are X-linked (OMIM #300000) and are caused by mutations in *MID1*, encoding a protein associated with the microtubule cytoskeleton (Schweiger et al., 1999). *SPECC1L* also interacts with both the microtubule and actin cytoskeletons. Indeed, cytoskeletal regulation is critical in neural crest migration, such as seen in the disruption of actin depolymerizing protein n-cofilin, which causes defective neural tube closure and impaired neural crest migration (Gurniak et al., 2004). Recently we described a role for *SPECC1L* in modulation

of the actin cytoskeleton and subsequent cell shape, through a PI3K-AKT dependent mechanism (Chapter Three). Specifically, *SPECC1L*-kd U2OS cells change from a cuboidal to an elongated cell shape, upon high confluence. *SPECC1L*-kd phenotypes also include increased apico-basal adherens junction (AJ) dispersion, with severe mouse mutants showing impaired delamination of CNCCs from the open neural folds. These phenotypes were reversible *in vitro*, through reactivation of AKT signaling by a small molecular activator, SC79, complementing our finding that severe mutants show reduced pan-AKT levels.

Previously we reported the homozygous lethal phenotypes of *Specc1l* gene trapped mouse embryos. This lethality occurs prior to embryonic day 9.5 (E9.5), marked by phenotypes which include reduced embryonic size relative to developmental stage and importantly, failure of CNCCs to delaminate from the still open neural folds (Chapter Three). Thus, this severe model of *SPECC1L* deficiency prohibits the investigation of post E9.5 developmental processes.

To expand our understanding of additional roles played by *SPECC1L* in CNCCs, we generated zinc finger deletions in *Specc1l* to allow modeling of less severe, moderate *SPECC1L* disruptions likely more reflective of human clefting pathogenesis. The *SPECC1L*$^{RRH\Delta 300}$ mouse shows delayed palatal fusion in approximately 50% of embryos and frequently show sub-epidermal blebbing associated with defects in the PI3K-AKT signaling pathway (Fantauzzo & Soriano, 2014). We used *in vitro* studies of *SPECC1L*-kd U2OS cultured cells and *SPECC1L*$^{RRH\Delta 300}$ mouse-derived primary MEPM cells to demonstrate a defect in collective migration, as identified through reduced correlation lengths of migratory streams. We report that this defect is responsive to modulation of the PI3K-AKT signaling pathway, complementing our previous findings showing the same responsiveness to the shape and AJ changes seen in *SPECC1L*-kd U2OS cells (Chapter Three).

4.3 Materials and methods

Cell lines

U2OS osteosarcoma control and *SPECC1L*-kd cells were previously described (Saadi et al., 2011).

Cell shape change in U2OS cells

U2OS control and SPECC1L-kd cells were cultured in standard DMEM high glucose media supplemented with 10% fetal bovine serum (Life technologies, Carlsbad, CA). To modulate the PI3K-AKT pathway, cells were cultured in described concentrations of PI3K-AKT inhibitor, Wortmannin (TOCRIS Biosciences, Minneapolis, MN), or activator, SC-79 (TOCRIS Biosciences, Minneapolis, MN). Media with chemicals was replaced daily.

Primary culture of mouse embryonic palatal mesenchyme (MEPM)

Mice heterozygous for the severe *Specc1l* gene trap allele $Specc1l^{RRH/-}$ were mated with heterozygous mutants of the hypomorphic $Specc1l^{\Delta 300/-}$ deletion allele, yielding compound mutant $Specc1l^{RRH/\Delta 300}$ embryos for primary culture. At E13.5, WT, heterozygotes and $Specc1l^{RRH/\Delta 300}$ embryos were harvested for excision of the palatal shelves. Subsequent incubation in Liberase DL (Roche, Basel, Switzerland) allowed mechanical separation of palatal shelf epithelium and dissolution of remaining mesenchyme into single-cell suspension. Primary MEPM cultures were seeded onto fibronectin treated tissue culture plastic vessels in 3D-printed rings with the same dimensions as one well of a standard 96 well plate. Upon overnight incubation in standard conditions, MEPM cultures were wounded with a 2 µl micropipette tip.

Live-imaging

Time-lapse recordings were performed of live control and kd cells in regular culture conditions with a phase contrast image collected every 10 minutes over a period of seven days. Images were taken with a computer-controlled Leica DM IRB inverted microscope equipped with a powered stage and a 10 × N-PLAN objective, coupled to a QImaging Retiga-SRV camera. During imaging, cell cultures were kept at 37C in a humidified 5% CO2 atmosphere.

Live-imaging analysis

Live-imaging of U2OS cells and primary MEPM cultures were manually tracked to identify the position of each cell migrating into the wound, per frame, until wound closure, using tracking software developed at the University of Kansas Medical Center (Dr. András Czirók, Ph.D.). Resulting coordinate tables were then analyzed using particle image velocimetry, as previously described (Zamir et al., 2005) and correlation length analysis using software developed by Dr. András Czirók, Ph.D.

4.4 Results

4.4.1 *Specc1l* deficiency impairs the collective migration of U2OS cells

Prior work showed that *SPECC1L*-kd U2OS cells are defective in wound closure, compared to WT U2OS cells, establishing a role for *SPECC1L* in cell migration (Saadi et al., 2011). Thus, we first explored which qualities of cell migration were disrupted, since embryonic migration, can largely be disrupted by many factors, including disruptions between individual cells and their neighbors (Saadoun et al., 2015), individual cells and their environment (Kulesa & McLennan, 2015), as well as disruption of the ability of cells to collectively migrate as a group

(Das et al., 2015). The latter is especially important to craniofacial development, given the migratory patterns they exhibit, which specifically feature formation of migratory streams, where each individual cell physically interacts with its neighbors, during migration (Belvindra et al., 2007).

Due to the functional importance that the actin cytoskeleton serves in establishing cell shape, we first investigated cell migration, considering the altered actin cytoskeleton and morphology of *SPECC1L*-kd cells. *SPECC1L*-kd U2OS alteration is density dependent. Thus, we performed wound healing assays, using wild type and *SPECC1L*-kd U2OS cell cultures, both before and after these changes. Interestingly, frame rate counting and kymographs derived from live cell imaging show wound closure rates equivalent between wild type and *SPECC1L*-kd U2OS cells, before shape change (Fig. 4.1 A). However, in cultures wounded after high density and subsequently altered morphology, *SPECC1L*-kd U2OS cells exhibited notably increased time in closing the wound, when compared with their wild type counterparts (Fig. 4.1 B).

To investigate what aspect of cell migration this density-dependent change perturbs, we employed particle image velocimetry (PIV), an analytic method commonly employed in understanding the dynamics present in fields of individual objects in dynamic movement (Zamir et al., 2005). PIV generates coordinate tables describing the position of individual objects in motion, over time. These coordinates allow the calculation of correlation length, which represents how effectively cells are migrating in each direction, with respect to each other (Zamir 2005), and is considered a measurement of collective cell migration (Das et al., 2015).

Such analyses were performed on low and high density fields, without wounds, as well as for wounds made before and after the *SPECC1L*-kd shape change phenotype. Wild type and

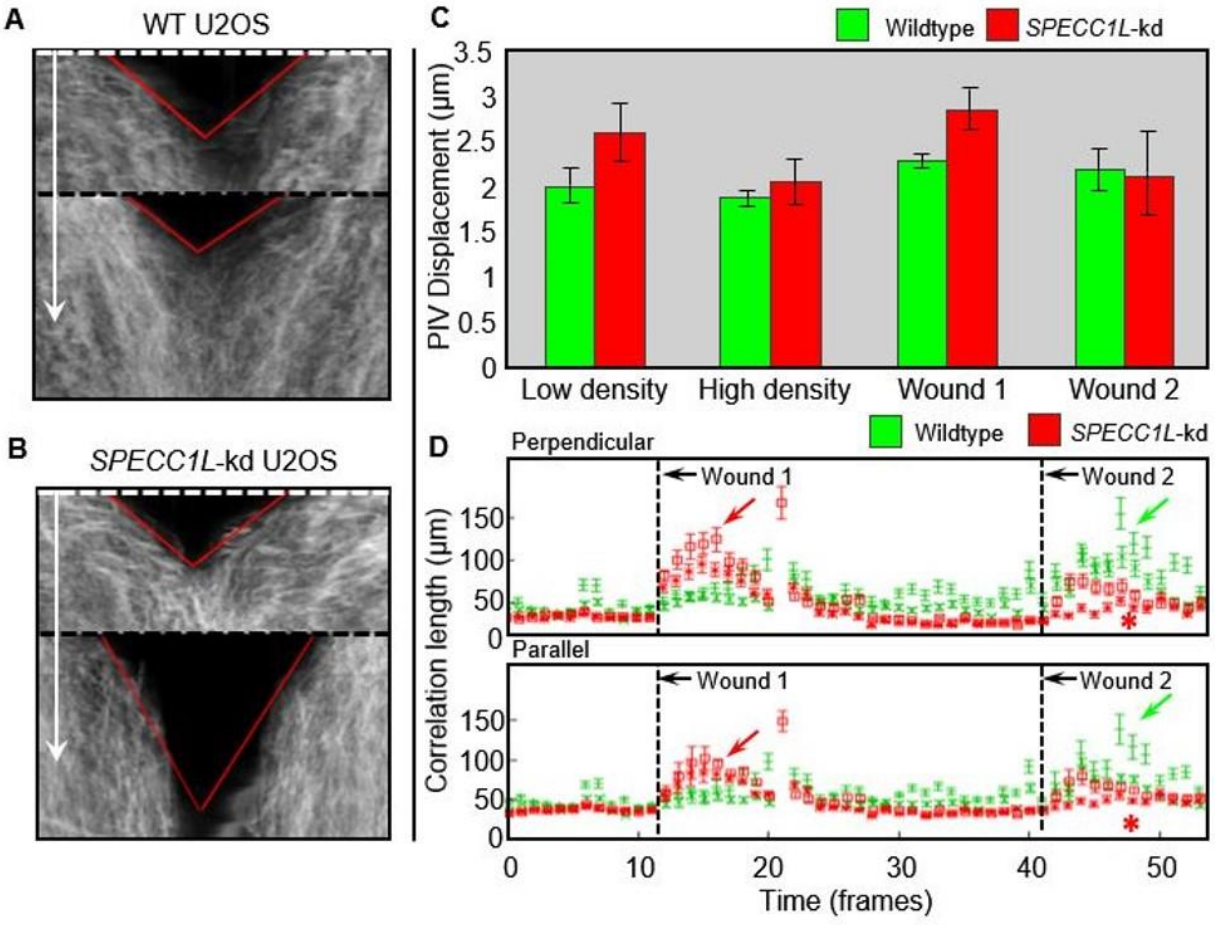

Figure 4.1. SPECC1L-kd wound closure delay and reduced collective cell migration occur upon shape change. Kymographs show delayed wound closure in SPECC1L-kd (**B**) when compared with WT U2OS cells (**A**). Cultures wounded before SPECC1L-kd cells change shape (**A**, **B**, white hashed line) show no delay in the rate of wound closure (red funnel) observed over time (white arrow). SPECC1L-kd cells (**B**) show delayed wound closure only when wounded after shape change (black hased line). **C**) SPECC1L-kd displacement (red) is higher than WT (green) in the initial pre-shape change wound (Wound 1) and in low density controls (Low density). The equivalent displacement shown by WT and SPECC1L-kd post-shape change wounds (Wound 2) show displacement itself does not explain delayed wound closure (**B**, red funnel). **D**) Comparing correlation lengths between WT (green) and SPECC1L-kd (red) wounds made before (Wound 1, black hashed line) show that SPECC1L-kd correlation lengths are not reduced (red arrows). Only wounds made after shape change (Wound 2, black hashed line) show reduced correlation lengths (red asterisk) when compared with WT (green arrows).

SPECC1L-kd U2OS cells do not show a disparity in PIV displacement which can explain the impaired wound closure. *SPECC1L*-kd cells show increased displacement upon wounds made before shape change and comparable displacement in wounds made after this change, showing that *SPECC1L*-kd cells have the displacement potential necessary to close wounds as quickly as their wild type counterparts (Fig. 4.1C). An example of such a finding can be seen when correlation length is reduced upon deficiency of Merlin, which is also accompanied by an increase in velocity (Das et al., 2015). As a difference in velocity cannot explain impaired collective migration in *SPECC1L*-kd U2OS cells, we next examined collective cell migration (Fig. 4.1D).

Measuring the correlation lengths of migratory cell streams is a measure of collective migration. Correlation lengths can be assessed directionally, describing the lengths of streams of cells moving perpendicular or in parallel with each other (Slater et al., 2013). Correlation length measurements show that wild type and *SPECC1L*-kd cells provide similar stream lengths, in wounds made before cell shape change, (Fig. 4.1D, Wound 1). Wounds made after *SPECC1L*-kd induced shape change (Fig. 4.1D, Wound 2) show wild type U2OS correlation lengths do not change between low and high confluence. However, *SPECC1L*-kd cells show a notable decrease in correlation lengths (Fig. 4.1D, Wound 2), suggesting that defective wound healing after *SPECC1L*-kd induced shape change is due to defects in the ability of these cells to collectively migrate. Directional measurement of correlation lengths involving parallel and perpendicular streams support this (Fig. 4.1D) as well as non-directional analyses of the same experiments (not shown).

4.4.2 Moderate *Specc1l* mutants show altered adhesion in a model of CNCC migration

As severe deficiency of Specc1l results in an embryonic lethal phenotype prohibiting investigation of neural crest migration, we generated a hypomorphic *Specc1l* allele to allow this (Fig. 4.2A). The hypomorphic *Specc1l*$^{\Delta 300/-}$ allele generates a 57-amino acid in-frame deletion between coiled coil domains 5 and 6 (Fig. 4.2A), which transcribes a protein of reduced molecular weight detectable by Western blotting (Hall, et al., in preparation). Understanding the underlying hypomorphic function of this allele is work still ongoing.

Mating of *Specc1l*$^{RRH/-}$ with *Specc1l*$^{\Delta 300/-}$ heterozygous mice yields compound mutant *Specc1l*$^{RRH/\Delta 300}$ embryos which are perinatal lethal, showing incompletely penetrant (~50%) delayed palatal shelf elevation (Hall, et al., in preparation). We then investigated *in vitro* neural crest progenitor migration by combining these alleles on a background which genetically labels a cell population including neural crest progenitors, using the *Wnt1*-GFP marker background. Using established neural crest explanation technique, we investigated whether hypomorphic *Specc1l* disruption impacts migration.

Upon excision of the neural folds from E8.5 WT, *Specc1l*$^{RRH/-}$, *Specc1l*$^{\Delta 300/-}$ and *Specc1l*$^{RRH/\Delta 300}$ mouse embryos, they were placed upon fibronectin-coated plastic, to facilitate adhesion and migration of *Wnt1*-GFP cells out of the tissue. Neural folds isolated from WT embryos quickly adhered to this substrate, showing adhesion and subsequent outward cell migration (Fig. 4.2D, upper panel). *Wnt1*-GFP expressing cells can be seen migrating out of the adhering explant, migrating away from its bulk in constant waves (Fig. 4.2D, lower panel). Interestingly, *Specc1l*$^{RRH/300}$ compound mutant neural fold explants never adhered completely, with most never adhering long enough for analysis. The few that did adhered transiently, and

produced almost no *Wnt1*-GFP positive migratory cells (Fig 4.2E, lower panel, Supplemental video).

Although visible in phase contrast, the *Wnt1*-GFP signal in these explants is harder to visualize, as the non-adhering tissue is outside of the live imaging focal plane (Fig.4.2 E). We also verified that neural crest induction does occur, as *Wnt1*-GFP expressing cells are present in the neural folds of *Specc1l*$^{DTM/DTM}$ mutant embryos. Additionally, fluorescence assisted cell sorting of embryonic lysates show that wild type and severe *Specc1l*$^{DTM/DTM}$ mutant embryos show equivalent proportions of *Wnt1*-GFP positive and negative cells (Fig.4.2 B, C).

4.4.3 Wound assays show reduced collective migration in *SPECC1L*$^{RRH/300}$ MEPMs

Culturing of explanted neural fold tissues was an unsuited technique to assess migration of CNCCs from Specc1l deficient embryos. Thus, we employed an extensively used method, primary culture of embryonic palatal mesenchyme, as described (Yu et al., 2005). MEPM cells were used as a proxy for CNCCs, as they are derived from the neural crest. MEPMs isolated from wild type and *SPECC1L*$^{RRH/300}$ palatal shelves were isolated from E13.5 embryos and cultured for wound assays.

Wound assays performed upon cultured wild type and *SPECC1L*$^{RRH/300}$ MEPM cell cultures showed that *SPECC1L*$^{RRH/300}$ MEPM cells show reduced speed of wound closure, as seen in kymographic representation of frame by frame cell movements (Fig 4.3. A, B). Like our U2OS displacement results (Fig. 4.1, C), SPECC*1L*$^{RRH/300}$ MEPMs show increased displacement, as shown by PIV analyses of live-cell imaging (Fig 4.3, C). This increased displacement was consistent throughout the wound closure process. This increase in displacement corresponds to a

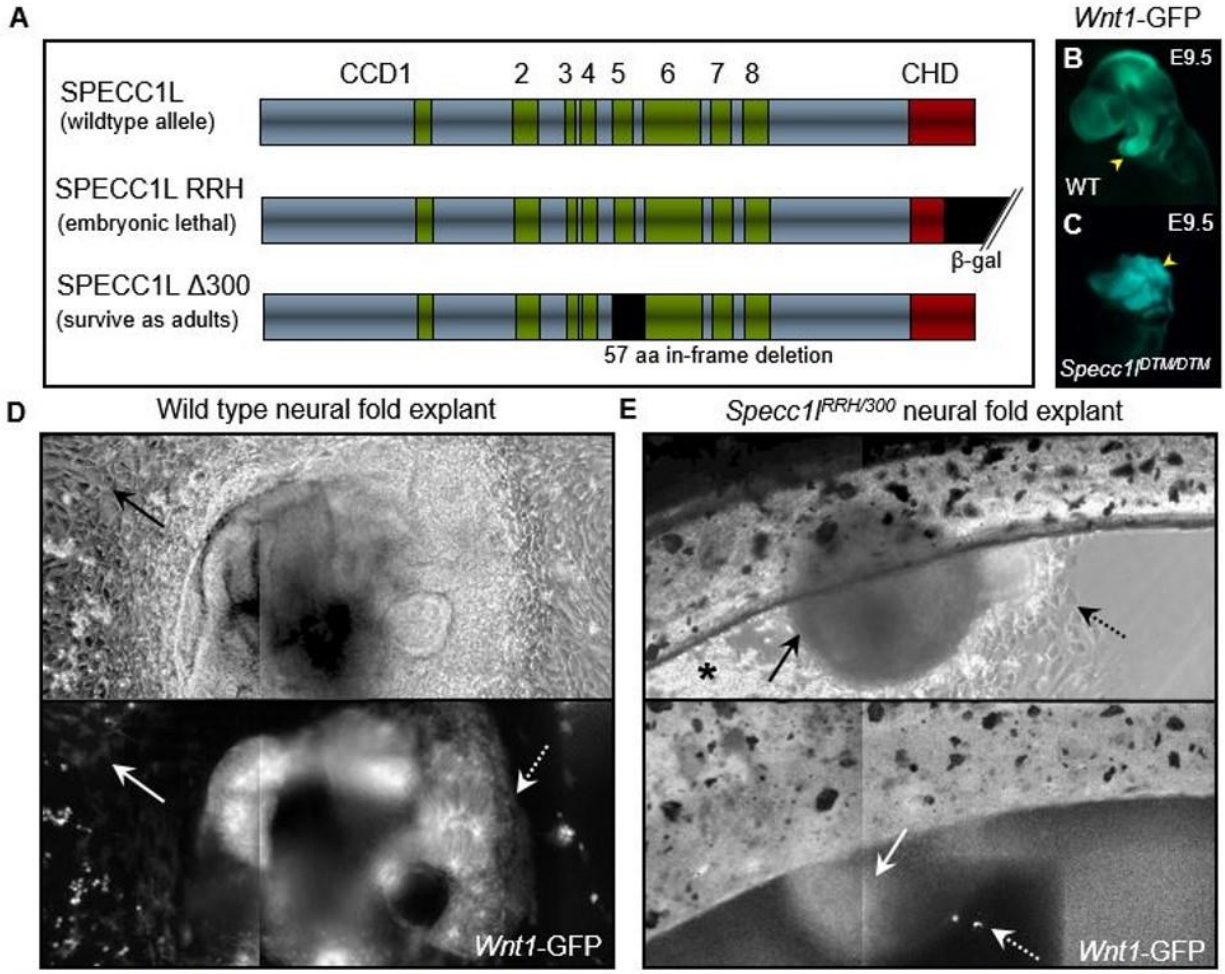

Figure 4.2. Moderate *Specc1l* mutants show defective adhesion in an in vitro model of neural crest migration. Alleles employed in generating moderate Specc1l mouse mutants (**A**). Cultured neural fold explants from a *Wnt1*-GFP expressing reporter mouse line show adhesion (**D**, upper panel, solid black arrow) and subsequent migration of *Wnt1*-GFP-positive neural crest precursors (**D**, lower panel, white arrow) and neural fold adhesion (**D**, lower panel, hashed arrow) (n=8). In contrast, moderate mutant *Specc1l*$^{RRH/300}$ neural folds show a general defect in explant adhesion (**E**, upper panel, solid black arrow) with reduced migration of adhesive cells (**E**, upper panel, hashed black arrow) and increased shedding of non-adhesive cellular material (**E**, upper panel, black asterisk). Very rarely, a small number of *Wnt1*-GFP expressing cells would successfully migrate from the explant (**E**, lower panel, hashed white arrow), showing erratic movements. The bulk of *Wnt1*-GFP expressing cells remain within the explant (**E**, lower panel, solid white arrow), which shows weak GFP signal due its impaired adhesion leaving it outside of the focal plane (n=4). Previous experiments have shown that Specc1l deficiency doesn't noticably impact *Wnt1*-GFP expression in the developing neural folds, using FACS analyses to compare the proportion of GFP positive and negative cells from dissociated wild type (**B**) and *Specc1l*$^{DTM/DTM}$ mutant E9.5 embryos (**C**). S*pecc1l*$^{DTM/DTM}$ mutant embryos show impaired delamination of GFP positive cells from the developing neural folds (**C**, yellow arrow) when compared with the delaminated GFP postive population shown in wild type embryos (**B**, yellow arrow).

higher average velocity of SPECC*1L*$^{RRH/300}$ MEPMs, when compared with their wild type counterparts (Fig 4.3, D). Superficially it would seem as though cells with higher average velocity would be able to close a wound more rapidly and would not show a notable delay in closure time. However, *SPECC1L*$^{RRH/300}$ MEPMs show reduced correlation lengths when compared with their wildtype counterparts (Fig 4.3, E), indicating impaired collective migration.

4.4.4 Activation of AKT rescues delayed wound closure in SPECC1L-kd U2OS cells

Previously, we reported that severe *Specc1l* gene trapped mouse mutants show reduced pan-Akt protein level, which is independent of *Akt* transcription (Chapter Three). Modulation of the PI3K-AKT signaling cascade with molecular activators and inhibitors could rescue or phenocopy, respectively, the morphological and adhesive phenotypes associated with *SPECC1L* deficiency, in U2OS cells (Chapter Three). Specifically, we found that inhibition of Phosphatidyl-inositol kinase 3 (PI3K) with Wortmannin (Abbas et al., 1998), induced in wild type U2OS cells an elongated morphology and an increase in the density of adherens junctions, which are the hallmarks of *SPECC1L*-kd. Additionally, we reported that activation of downstream PI3K effector V-Akt murine thyoma viral oncogene homolog 1 (AKT) with the small molecule modulator SC79 (Jo et al., 2012) in *SPECCC1L*-kd U2OS cells rescued the elongated morphology and altered AJs. Thus, we next investigated the possibility that modulating PI3K-AKT signaling could also rescue delayed wound closure.

Upon examination of the number of frames required for wound closure, pretreatment of wild type U2OS cell cultures with Wortmannin caused a robust negative effect on wound closure speed seen in untreated wild type wounds (Fig 4.4 A-C'), at the same concentration (30 μM) used previously (Fig 4D). Complimenting this finding, *SPECC1L*-kd cell cultures pretreated with SC79

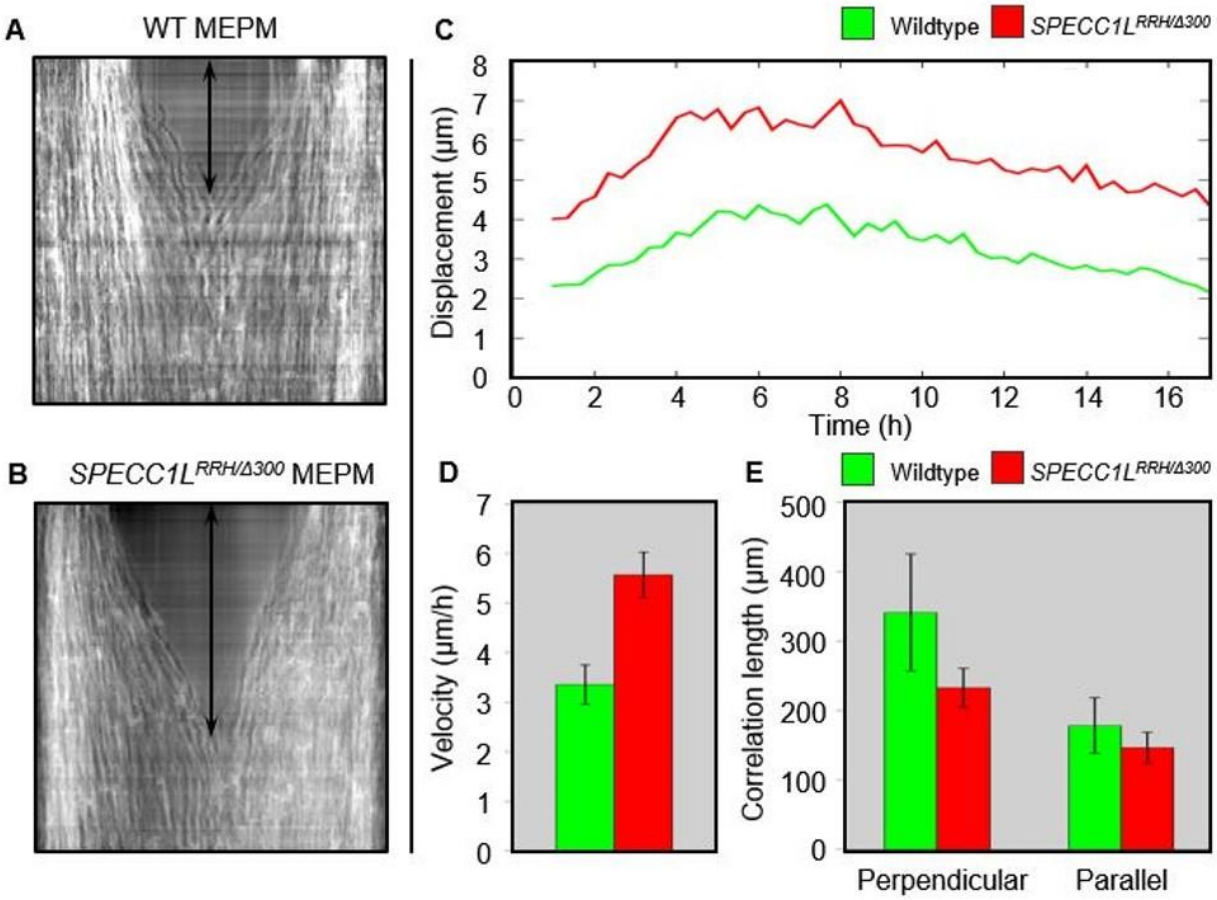

Figure 4.3. Wound assays show reduced collective migration in *Specc1l*$^{RRH/300}$ mouse embryonic palatal mesenchyme cultures. Kymographs show the rate of wound closure for wildtype mouse embryonic palatal mesenchyme (MEPM) cell cultures (**A**, black arrow) and moderate mutant *Specc1l*$^{RRH/300}$ MEPMs (**B**, black arrow). Note the reduced wound closure rate shown by mutants (B, black arrow), when compared with wild type (**A**, black arrow). Particle image velocimetry analyses of MEPM wound closure show that *Specc1l*$^{RRH/300}$ MEPM (red) show consistently increased displacement (µm) over their wild type counterparts (green). Elevated *Specc1l*$^{RRH/300}$ MEPM displacement is consistent throughout wound closure **(C)**. Distinct from displacement, *Specc1l*$^{RRH/300}$ MEPM (red) velocity (µm/h) is greater than their wild type counterparts (green) (**D**). Measurement of correlation length **(E)**, a quantification of collective migration, shows decreased correlation length (µm) of *Specc1l*$^{RRH/300}$ MEPM (red) when compared with their wild type counterparts (green), whether correlation length was measured with respect to perpendicular (**left**), parallel (**right**) stream length or when analyzed in bulk, without respect to directionality (not shown).

show an improvement in wound closure speed when compared with vehicle treated wound cultures (Fig 4D'). These experiments were conducted at the same concentration of SC79 (500 μM) required to rescue morphological and adhesion defects we reported previously (Chapter Three).

Thus, we have demonstrated SPECC1L deficiency causes defects in the collective migration of U2OS and MEPM cells which results from a reduction in the parallel and perpendicular correlation lengths of migrating streams. This defect, as assessed by wound closure time, is rescued upon AKT activation, suggesting a common mechanism underlying this defect and the morphological and adhesion phenotypes. Previously, others have shown an increase in wound closure time correlating with AJ density, in retinal pigment epithelial cells (Kaida et al., 2000), suggesting that *SPECC1L*-kd U2OS altered AJs may cause reduced wound closure. Given the temporal sensitivity of various aspects of tissue morphogenesis relative to collective cell migration, these results contribute to furthering our understanding of the link between cellular phenotypes and both normal and aberrant embryonic craniofacial development.

4.5 Discussion

Collective migration of CNCCs is required for the contribution of CNCCs to the developing maxilla and mandible (Chai et al., 2000). The reduction in correlation lengths shown by S*PECC1L*-kd U2OS cells and *SPECC1L*$^{RRH/300}$ MEPMs support a role for *SPECC1L* in collective cell migration, as stream formation is a fundamental event in CNCC migration (Tang et al., 2007). Protein interactions with SPECC1L support this role as well, as an siRNA mass screening for genes which inhibit epithelial migration found 42 contributing factors, which all

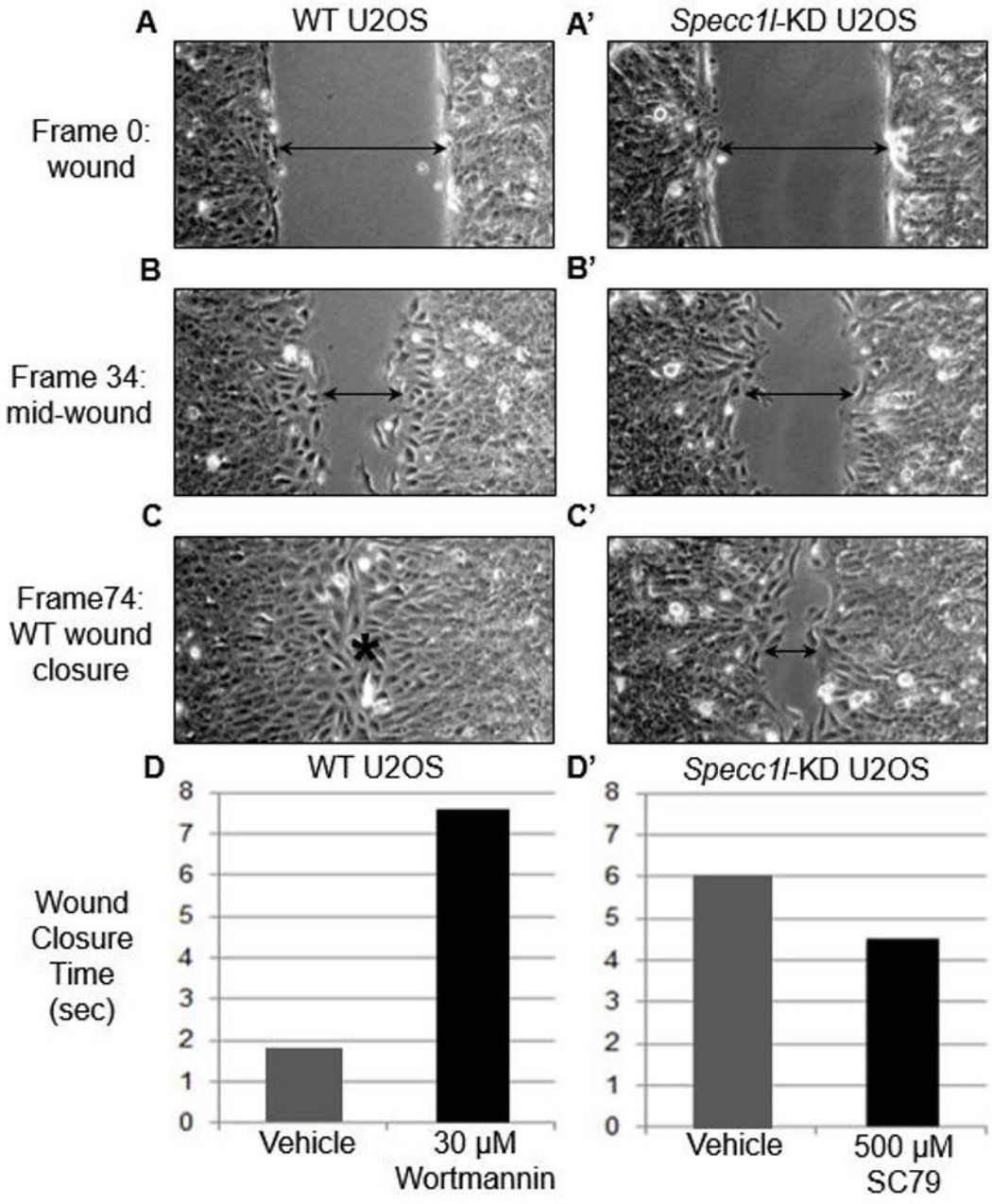

Figure 4.4. Activating PI3K-AKT signaling rescues delayed wound closure in *SPECC1L*-kd U2OS cells. *SPECC1L*-kd cell wounds show increased time to wound closure (**A'**, **B'**, **C'**) when compared with wild type (**A**, **B**, **C**), as previously described. At the onset of wound closure (**A**, **A'**, arrows), *SPECC1L*-kd cell wounds show reduced closure by mid wound (**B, B'**, arrows) and delayed closure (**C'**, arrow) upon wild type wound closure (**C**, asterisk). Using this model, modulation of the PI3K-AKT signaling cascade partially rescues *SPECC1L*-kd induced closure delay upon pre-treatment with 500 µM SC79, an AKT activator (**D'**, black), when compared with vehicle treatment alone (**D'**, grey). Pretreatment with 30 µM Wortmannin, a PI3K inhibitor shows an increase in the wound closure time of wild type U2OS cells (**D**, black), when compared with vehicle pretreatment (**D**, grey).

correlated with three major signaling hubs, actin, integrin β1 and β-catenin (Simpson et al., 2008). These findings support a novel role for SPECC1L in collective migration, given its regulation of AJs, highlighting the importance of cell-cell interactions in CNCC collective migration (Rørth, 2009).

The responsiveness of our U2OS model to PI3K-AKT modulation compliments our previous reports highlighting its role in rescuing *SPECC1L*-kd morphological and AJ phenotypes (Chapter Three). A tempting speculation involves the reported role of PI3K-AKT signaling in collective migration, where others have shown that PI3K inhibition leads to a reduction in AKT regulation of Paxillin α (Paxa), resulting in impaired cytoskeletal reorganization and subsequent migration defects (Chung et al., 2001).

Impaired cytoskeletal reorganization has already been implicated in impaired collective migration (Tobin et al., 2008). Interestingly, others have recently reported that in MDCK epithelial cells, migrating streams can be understood as a 'leader' cell at the forefront of migration being followed by numerous 'follower' cells. In accord with the aforementioned screen for genes responsible for collective migration, PI3K and Integrin β1, are upregulated in leader but not follower cells, as well as their specific localization to the leading-edge guiding stream migration, which is not observed in follower cells (Yamaguchi et al., 2014). Thus, we propose a novel role for SPECC1L in the process of collective migration of CNCCs, through its regulation of AJs and the actin cytoskeleton.

CHAPTER FIVE:

DISCUSSION

Chapter Five: Discussion

5.1 Discovery of *SPECC1L* disruption in atypical facial clefting

Prior to my studies, the gene encoding the cytoskeletal protein *Sperm antigen with calponin homology and coiled-coil domains 1-like* (*SPECC1L*) was the first gene implicated in severe atypical facial clefting (Saadi et al., 2011). *SPECC1L* was identified in this study, from a balanced chromosomal translocation between chromosomes 1 and 22, harbored by a neonate with atypical facial clefting (Dasouki et al., 1988). Mouse *in situ* hybridization shows prominent expression of *Specc1l* in the maxillary prominence and lateral nasal processes which fail to fuse in ObFC, as well as the eyes and limbs, at embryonic day E9.5-E10.5 (Saadi et al., 2011). Further support for SPECC1L involvement in atypical facial clefts came with the identification of a *de novo* heterozygous missense mutation in *SPECC1L*, p.Gln415Pro (Q415P), in a neonate also born with severe facial clefts, setting the stage for discovery of multiple *SPECC1L* mutations in less severe forms of clefting (Saadi et al., 2011).

5.2 *SPECC1L* mutations identified in syndromic clefting

5.2.1 Role of *SPECC1L* in the pathogenesis of non-X linked Opitz G/BBB syndrome

Recently we collaborated with a research group at the Children's Hospital of Philadelphia, on a whole exome sequencing analysis project (Chapter Two). Opitz G/BBB syndrome is a developmental disorder primarily characterized by defects in midline development, including cleft lip and palate, hypospadias, laryngeal cleft and cardiac defects. This syndrome is known to have two inheritance patterns, either X-linked or autosomal dominant. The causative gene inducing the X-linked form of Opitz has been identified as *Mid1* encoding a microtubule-associated protein with E3 ubiquitin ligase activity. Previously, the gene responsible for the autosomal dominant form

of Opitz was only known to reside within a 32 cM sequence of chromosome 22q11.2. Results from two families with three generations of reported Opitz-like features also negative for *MID1* disruption revealed two separate heterozygous mutations within the coding region of *SPECC1L*.

The proband of Family A was identified through multiple defects, including congenital hypertelorism and cleft lip and palate. Sequencing analysis revealed that the proband harbored a heterozygous missense mutation in *SPECC1L*, c.1189A>C (T397P), in the second coiled coil domain whose disruption was previously shown to cause severe atypical facial clefting (Saadi et al., 2011).

Adding to this relationship was the discovery of an additional heterozygous missense mutation in *SPECC1L*, c.3247G>A (G1083S), in the Calponin homology domain (CHD) previously shown to abolish microtubule binding *in vitro*, when removed via mutagenesis (Saadi et al., 2011). This mutation in the proband of Family B was a female identifiable by defects including cleft lip and palate, as well as hypertelorism.

These findings were further validated using mutagenesis and transfection of GFP-tagged mouse *Specc1l* constructs for the canonical allele, the mutations identified above, T397P and G1083S, as well as the Q415P mutation previously identified in the second coiled coil domain. This mutation was found in a neonate with severe atypical facial clefting (Saadi et al., 2011). Protein localization analyses suggest that the second coiled coil domain and the CHD are involved in microtubule interactions. Lastly, *Specc1l* lacking the carboxyl terminal Calponin homology domain (*Specc1l* ΔCHD) was included as a reference to a complete lack of microtubule association (Saadi et al., 2011).

Ectopic wild type *specc1l*-GFP associates with a lattice of perinuclear microtubules stabilized through the acetylation of α-tubulin. Figure 2.3 shows the results of this and patient

mutation *Specc1l*-GFP transfection. All patient mutations, T397P, G1083S and Q415P show a punctate expression indicating failed microtubule stabilization, when compared with wildtype SPECC1L-GFP.

MID1 and SPECC1L are microtubule-associated proteins. Complimenting this similarity are reports showing that MID1 associated patient mutations also show defective microtubule stabilization, in similar assays, suggesting a specific role for microtubule regulation in midline development which either MID1 or SPECC1L disruption can impair, resulting in Opitz G/BBB syndrome.

5.2.2 Role of *SPECC1L* in Teebi hypertelorism syndrome

Additional findings have shown a specific role for this protein in the subtler aspects of midfacial development which are less severe than orofacial clefting. Teebi hypertelorism syndrome is an autosomal dominant disorder first described by Dr. Ahmad Teebi (Teebi et al., 1987). It includes a range of phenotypes include hypertelorism, prominent forehead, long palpebral fissures, heavy and broad eyebrows, widow's peak, broad and depressed nasal bridge, short nose, mild interdigital webbing, and shawl scrotum. Developmental delays have also been observed, but not in all cases.

Through whole exome sequencing of 19 families with syndromic craniofacial phenotypes, two families previously diagnosed with Teebi hypertelorism syndrome were found to harbor deleterious mutations in *SPECC1L*. The first patient, a 15 year old male, harbored an E420D variant obtained through maternal inheritance. The mother of patient one also showed hypertelorism and unilateral ptosis, as well as preauricular pits. Patient one was born with the following craniofacial abnormalities – hypertelorism, a larger than average distance between the

ocular orbits, natal teeth, a premature emergence of neonatal teeth which typically emerge after birth, micrognathia, as well as preauricular pits. The patient also had bilateral ptosis and craniosynostosis which were surgically addressed previously.

Non-craniofacial findings included two-vessel cord, a deformation of the umbilical cord causing it to lack one of the two arteries typical of the three-vessel structure observed in normal development, as well as protruding umbilicus and shawl scrotum, small hands, hypersegmented vertebrae and cardiac defects, surgically addressed previously.

The second patient harbors a *de novo SPECC1L* mutation which deletes Isoleucine 400 in the I400 and Histidine 401 (I400_H401del) in the second coiled coil domain. The second patient shared many of the same features seen in the first, including hypertelorism, natal teeth and upslanted palpebral fissures and cardiac deformities. Findings unique to Patient one included omphalocele, the need for tracheostomy and assisted ventilation in the first six months of life, as well a later diagnosis of autism and behavioral issues.

SPECC1L mutations observed in these Teebi syndrome patients are of further interest because they are within the second coiled coil domain disrupted by *SPECC1L* mutations observed in more severe Opitz G/BBB syndrome at T397P (Kruszka et al., 2015), as well as the most severe atypical facial clefting mutation Q415P (Saadi et al., 2011), both of which involve orofacial clefting. Interestingly, no molecular pathogenetic mechanism has been proposed to describe Teebi hypertelorism prior to this study, which caused the authors to suggest that this syndrome may be in fact a milder phenotype in a range of *SPECC1L* phenotypic severity where severe atypical clefting is the most deleterious manifestation. These results support including *SPECC1L* mutation screening in future genetic workups of Teebi hypertelorism patients. Placing Teebi hypertelorism into a range of phenotypic severity associated with SPECC1L disruption is supported by the

description of a family with Teebi hypertelorism where all six affecteds showed a high arched palate, with one affected showing cleft lip and palate (Morris et al., 1987).

5.3 *SPECC1L* patient mutations may disrupt a conserved coiled coil domain

5.3.1 Conserved domains within SPECC1L harbor human mutations

One explanation for the impact of the described human mutations involves the two highly conserved regions within SPECC1L which harbor them. Although no known orthologs of *Specc1l* more ancient than the *CG13366* gene found in *Drosophila melanogaster* (Saadi et al., 2011) have been described, the sequences of the second coiled-coil domain and calponin-homology domain (CHD) containing human patient mutations share high homology across the animal kingdom.

Chordate and insect species along with a platyhelminth and an echinoderm all express proteins which contain conserved domain architectures similar to *SPECC1L*, including a conserved coiled coil domain and a singular carboxyl-terminal CHD. The orientation of these domains offers a point of initial interest, as CHDs are frequently amino-terminal and often found in repetition, with singular carboxyl-terminal compositions less frequent (Korenbaum & Rivero, 2002). Analysis of proteins with putative Specc1l homology show that the insect species *Anopheles gambiae* (gi 158290650 ref XP), *Drosophila melanogaster* (gi 24638896 ref NP5), *Tribolium castaneum* (gi 91085061 ref XP 9) and *Apis mellifera* (gi 110766125 ref XP) share higher homology to each other than to the echinoderm *Strongylocentrotus purpuratus* (gi 115627978 XP), the platyhelminth *Schistosoma mansoni* (gi 256073851ref XP) or *Homo sapiens* (gi 300669640 sp Q69Y), as would be expected from their respective phyla (Fig. 5.1A).

The previously reported coiled coil mutations T397P (Kruszka et al., 2015), Q415P (Saadi et al., 2011), I400_H401del and E420D (Bhoj et al., 2015) all mutate an approximately 40 amino

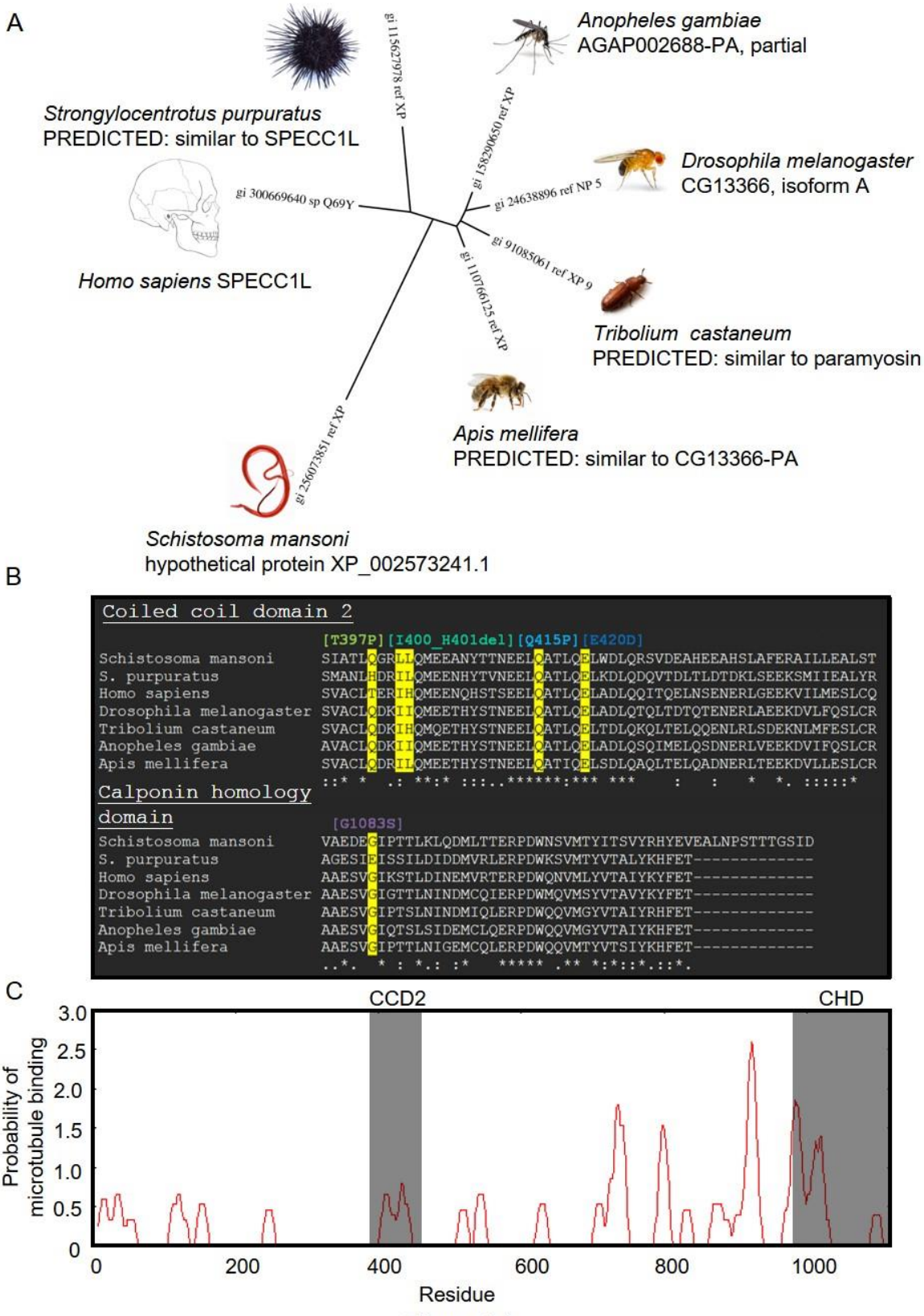
A
Anopheles gambiae
AGAP002688-PA, partial
Strongylocentrotus purpuratus
PREDICTED: similar to SPECC1L
gi 115627978 ref XP
gi 158290650 ref XP
gi 300669640 sp Q69Y
gi 24638896 ref NP 5
Drosophila melanogaster
CG13366, isoform A
gi 91085061 ref XP 9
Homo sapiens SPECC1L
gi 110766125 ref XP
Tribolium castaneum
PREDICTED: similar to paramyosin
Apis mellifera
PREDICTED: similar to CG13366-PA
gi 256073851 ref XP
Schistosoma mansoni
hypothetical protein XP_002573241.1
B
Coiled coil domain 2
[T397P][I400_H401del][Q415P][E420D]
Schistosoma mansoni SIATLQGRLIQMEEANYTTNEELQATLQELWDLQRSVDEAHEEAHSLAFERAILLEALST
S. purpuratus SMANLHDRILQMEENHYTVNEELQATLQELKDLQDQVTDLTLDTDKLSEEKSMIIEALYR
Homo sapiens SVACLTERIHQMEENQHSTSEELQATLQELADLQQITQELNSENERLGEEKVILMESLCQ
Drosophila melanogaster SVACLQDKIIQMEETHYSTNEELQATLQELADLQTQLTDTQTENERLAEEKDVLFQSLCR
Tribolium castaneum SVACLQDKIHQMQETHYSTNEELQATLQELTDLQKQLTELQQENLRLSDEKNLMFESLCR
Anopheles gambiae AVACLQDKIIQMEETHYSTNEELQATLQELADLQSQIMELQSDNERLVEEKDVIFQSLCR
Apis mellifera SVACLQDRILQMEETHYSTNEELQATIQELSDLQAQLTELQADNERLTEEKDVLLESLCR
Calponin homology domain
[G1083S]
Schistosoma mansoni VAEDEGIPTTLKLQDMLTTERPDWNSVMTYITSVYRHYEVEALNPSTTTGSID
S. purpuratus AGESIEISSILDIDDMVRLERPDWKSVMTYVTALYKHFET----------
Homo sapiens AAESVGIKSTLDINEMVRTERPDWQNVMLYVTAIYKYFET----------
Drosophila melanogaster AAESVGIGTTLNINDMCQIERPDWMQVMSYVTAVYKYFET----------
Tribolium castaneum AAESVGIPTSLNINDMIQLERPDWQQVMGYVTAIYRHFET----------
Anopheles gambiae AAESVGIQTSLSIDEMCLQERPDWQQVMGYVTAIYKHFET----------
Apis mellifera AAESVGIPTTLNIGEMCQLERPDWQQVMTYVTSIYKHFET----------
C
CCD2
CHD
Probability of microtubule binding
3.0
2.5
2.0
1.5
1.0
0.5
0
0
200
400
600
800
1000
Residue

Figure 5.1

Figure 5.1. Conserved domains within SPECC1L harbor human mutations. (**A**) *SPECC1L* orthologs share a conserved coiled coil domain and Calponin homology domain (**B**) These conserved domains show near perfect conservation at the loci affected by human mutations found in syndromic and atypical facial clefting. (**C**) The second coiled coil domain and Calponin homology domain show high probability of microtubule binding.

acid sequence of conserved peptides ostensibly shared with the last common ancestor of *Strongylocentrotus purpuratus* (gi 115627978 XP) and *Homo sapiens* (gi 300669640 sp Q69Y), circa 500 million years ago, suggesting that the conservation of this region may reflect a critical function (Fig. 5.1B). Similarly, the G1083S mutation (Kruszka et al., 2015) impacts the amino-terminal portion of the CHD in the same proteins, whose conservation is nearly complete at this locus, excepting the most removed species, *Strongylocentrotus purpuratus* (gi 115627978 XP) (Fig. 5.1B).

5.3.2 *SPECC1L* mutation may disrupt conserved regions which likely bind microtubules

Use of the MAPanalyzer algorithm (Zhou et al., 2015) reveals that the conserved region of the second coiled-coil domain affected by human mutations is a predicted high-probability microtubule-binding region (Fig. 5.1C, CCD). The amino-terminal region of the CHD affected by patient mutation G1083S is also a high-probability microtubule binding region (Fig. 5.1C, CCD) (Lupas et al., 1991). This offers a mechanism by which mutations in these domains disrupts SPECC1L colocalization with microtubules, as seen upon expression of these mutant variants (Kruszka et al., 2015).

Human mutations observed throughout the range of clefting severity are likely to impact protein function in two principal ways. Coiled coil domain structure emerges from a heptad repeat of amino acid chemistries, *H*-(hydrophobic)-*C/P* (charged/polar)-*C/P-Leu-C-C/P-C* (Lupas et al., 1991). Both Q415P (Saadi et al., 2011) and T397P (Kruszka et al., 2015) substitute large polar side chain-bearing residues Glutamine or Threonine with the compact residue Proline. These substitutions are likely to disrupt coiled coil dimerization, as shown in solved structures where Proline mutations introduce a peptide kink disrupting the conformation of the entire coiled coil

(Woolfson & Williams, 1990). Y2H protein interaction screens have provided multiple interactors with proteins containing coiled-coil domains (unpublished), suggesting that patient mutations may disrupt these interactions, which should be studied in the future.

Similarly, the I400_H401 deletion (Bhoj et al., 2015), like any deletion, will disrupt the coiled coil heptad repeat, with unpredictable consequences for structure and subsequent function. Interestingly, the other mutation associated with the milder phenotype of Teebi hypertelorism syndrome, E420D (Bhoj et al., 2015) substitutes Glutamic acid with Aspartic acid, both similar and negatively charged residues which may disrupt coiled coil structure and function less severely, as it does not disrupt the basic chemistry of the heptad repeat.

Lastly, the G1083S mutation substituting Glycine with Serine in the highly-conserved region of the CHD also has a plausible disruptive effect, as missense mutations in the CHD have been shown to alter its structure and function, with such mutations suspected in Duchenne muscular dystrophy (Norwood et al., 2000). Additionally, G1083S potentially introduces a phosphorylation site which could also disrupt CHD function. Phosphorylation of similar proteins, such as serine 175 of chick Calponin, are reported to change its conformation (Pin et al., 2000). Also, the already described phosphorylation of Serine 1081 in *SPECC1L* shows that its CHD is interacting with an undescribed protein kinase (Hornbeck et al., 2011).

As mentioned previously, mutations in this coiled coil can introduce a kink in the domain, which could interfere with protein-protein interactions. A recent yeast two-hybrid screen for *SPECC1L* protein interactors yielded 6 protein interactors of direct relevance to microtubule binding, AKT signaling and AJ regulation. Microtubule motor proteins Kinesin 4A (KIF4A) and Kinesin 5C (KIF5C), as well as the microtubule severing protein Spastin (SPAST) interact with *SPECC1L*, offering a possible mechanism for defective microtubule organization seen in patient

mutations (Kruszka et al., 2015). Protein inhibitor of activated STAT 1 (PIAS1) facilitates the stabilizing sumoylation of AKT, discussed below, while Protein inhibitor of activated STAT 2 PIAS2 stabilizes the interactions between Ubiquitin conjugating enzyme E2 I (UBE2I), another SPECC1L interactor, with its substrates (Hillgarth et al., 2004). This suggests a role for SPECC1L in the regulation of protein stability and degradation relevant to the phenotypes seen upon its deficiency. Most important to the regulation of AJ stability, interactor SMARCA4 has been shown to be a corepressor of *ZEB1*, which leads to the dissolution of AJs, seen *in vitro*, as well as the defective EMT shown by the neural crest of *Specc1l*-genetrapped mutant embryos.

Collectively, all patient mutations examined in this study have plausible consequences upon the structure and function of SPECC1L, with severe disruptions correlating with severe clefting (Saadi et al., 2011) and functionally milder mutations unlikely to disrupt the heptad repeat perhaps equating to the less severe disruption seen in Opitz G/BBB and Teebi hypertelorism syndromes (Kruszka et al., 2015, Bhoj et al., 2015). This suggests that the coiled coil interactors of SPECC1L may separate the severe and mild developmental phenotypes observed and should be considered in future studies.

5.4 SPECC1L is a novel regulator of AKT signaling

5.4.1 SPECC1L deficiency results in a reduction in pan-AKT protein levels

Previously, we reported that the severe gene trap *Specc1l* mouse mutant is embryonic lethal at E9.5, showing reduced size compared with WT stage matched littermates, as well as unfused neural folds, with a *Wnt1*-GFP expressing population of cells containing the CNCCs still incorporated into the neural folds (Chapter Three). Protein lysates from these severe *Specc1l* mutants shows reduced pan-AKT levels, compatible with reduced embryonic size. Subsequent

analysis did not reveal a significant difference in *AKT* transcription, leaving the possibility that SPECC1L deficiency disrupts a fundamental process stabilizing AKT protein or preventing its degradation. Further studies indicated that the SPECC1L-kd alteration of cell shape and AJ patterning seen in an *in vitro* model using U2OS cells were prevented by small molecule AKT activation by SC79. WT cells can also show SPECC1L-kd phenotypes by inhibition of upstream PI3K, using Wortmannin. Interestingly, SPECC1L-kd cells show a stark vulnerability to Wortmannin induced apoptosis, when compared with WT U2OS cells which showed no cell death upon the same exposure conditions, indicating that SPECC1L-kd cells already have reduced AKT and downstream resistance to apoptosis.

5.4.2 Possible mechanisms by which SPECC1L reduces pan-AKT protein levels

One of the most intriguing findings of these studies was the discovery that reduction in SPECC1L yields a dramatic reduction in pan-AKT protein level, with subsequent chemical activation of remaining AKT rescuing morphological and cytoskeletal defects in *SPECC1L*-kd U2OS cells. There are several possible mechanisms by which SPECC1L could facilitate AKT protein stability.

5.4.2.1 AKT stabilization through mTOR signaling

Nascent AKT protein is unstable, and its ubiquitination leads to protein degradation by the ubiquitin proteasome system (Facchinetti et al., 2008). Nascent AKT can be stabilized upon association with heat shock protein 90 (HSP90). However, when HSP90 activity is blocked, a subsequent rescue pathway can also stabilize nascent AKT, through the master target of Rapamycin complex 2 (mTORC2) proteins, which phosphorylate AKT at Threonine 450. I

hypothesize that SPECC1L may facilitate one of these rescue pathways. SPECC1L may shield nascent AKT from ubiquitination or encourage the assembly of proteins involved in stabilizing it. However, a search of the literature and Y2H protein interactors with SPECC1L show no interaction among mTOR proteins of either complex 1 or 2, HSP90 or even AKT itself. However, SPECC1L does interact with two ubiquitin-specific peptidases which deubiquitinate proteins (USP10, USP15). Thus, we cannot yet discount the possibility that SPECC1L facilitates the de-ubiquitination of nascent and unstable AKT protein (Fig 5.2, A).

5.4.2.2 AKT stabilization through PIAS1 mediated SUMOylation

Another possible mechanism involves the stabilizing effects of small ubiquitin-related modifier (SUMO) proteins (Li et al., 2013). Recent work has highlighted the importance played by SUMO-induced protein stabilization, including stabilization of AKT itself (Li et al., 2013). Li and colleagues found that AKT lysine 276 is sumoylated by SUMO1, via the Sumo E3 ligase Protein inhibitor of activated STAT1 (PIAS1). Interestingly, mutagenesis of this residue results in dramatic loss of AKT kinase function, yielding reduced proliferation and migration delay in wound assays using H1299 cells derived from non-small cell lung carcinoma (Li et al., 2013). Supporting these findings, increased PIAS1 increases AKT kinase activity, while increased sumo-specific protease (SENP1) decreases AKT kinase activity (Li et al., 2013). Supporting a role for SPECC1L in this interaction, our Y2H screens for SPECC1L protein interactors revealed binding with both PIAS1 and SUMO1, while not associating with its counterpart, SENP1. Perhaps a more robust hypothesis regarding SPECC1L stabilization of AKT involves sumoylation at K276 via conjugation of SUMO1 by PIAS1 (Figure 5.2B, C). SPECC1L interacts with numerous proteins involved in ubiquitination, including PIAS1, SUMO1, E2 ubiquitin ligase UBE2I, E3 ubiquitin

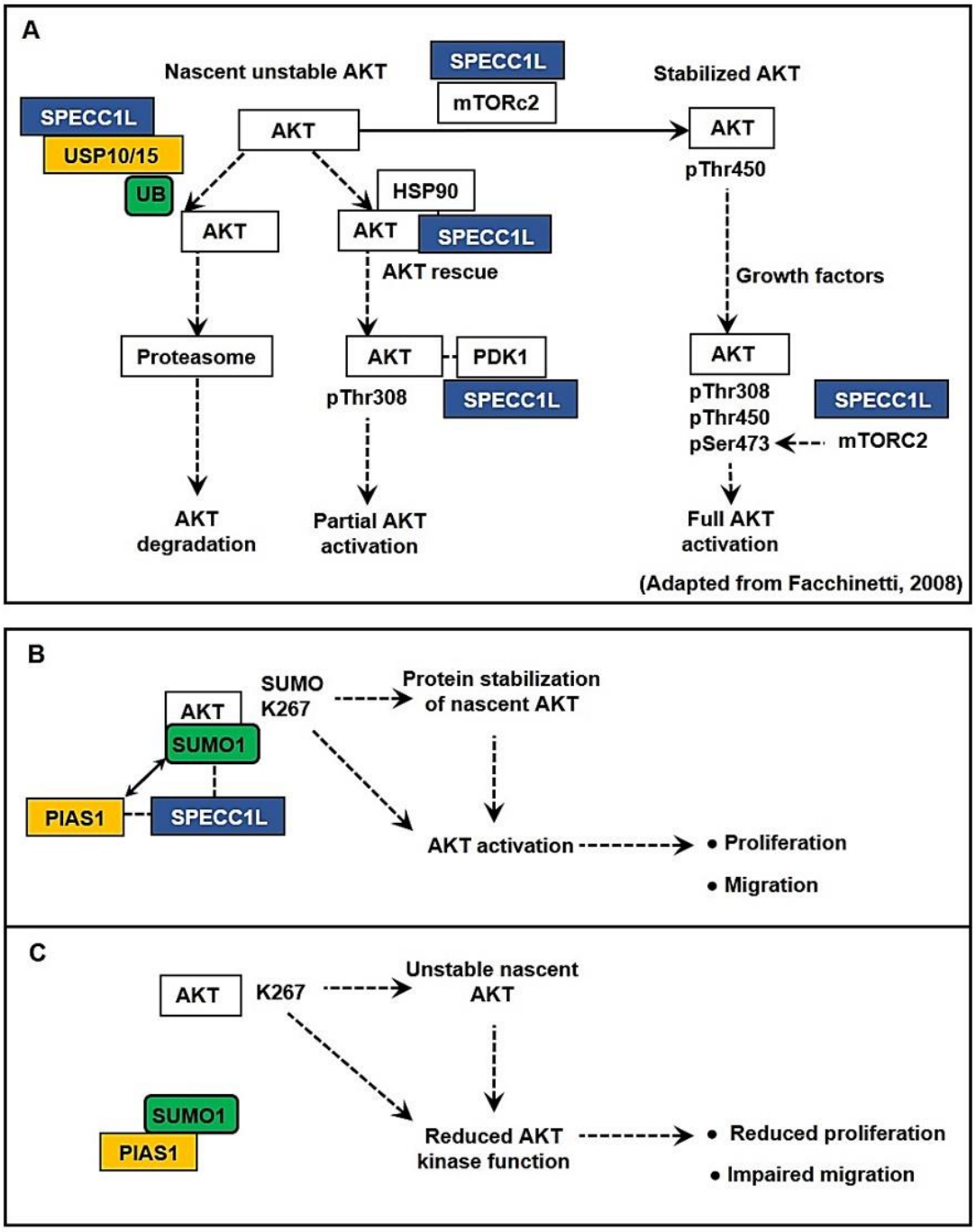

Figure 5.2. Models of SPECC1L stabilization of AKT through mTORc2 or PIAS. (**A**) SPECC1L may rescue nascent AKT from degradation through its interactions with Ubiquitin ligases or interactions with mTORC2. (**B**) SPECC1L may also stabilize nascent AKT prior to ubiquitination, by faciliting PIAS1-mediated stabilization through sumoylation at K276. (**C**) Upon SPECC1L deficiency, the absence of this stabilizing modification may yield AKT vulnerable to degradation.

ligase HERC2 (Wu et al., 2010) as well as ubiquitin specific peptidases 10 (USP10) and 15 (USP15) (Nijman et al., 2005), suggesting a generalized role for *SPECC1L* in facilitating the post-translational modification and subsequent regulation of multiple substrates.

5.5 SPECC1L role in CNCC delamination

5.5.1 SPECC1L deficiency alters AJ patterning *in vitro* and *in vivo*

Chapter Three detailed how SPECC1L-kd U2OS cells, staining of canonical adherens junction (AJ) components, β-Catenin and E-Cadherin, was increased, and electron micrographs revealed an apico-basal diffusion of AJs. To understand the role of SPECC1L in craniofacial morphogenesis, we generated a mouse model of *Specc1l* deficiency. Homozygous mutants were embryonic lethal and showed impaired neural tube closure and CNCC delamination. Staining of AJ proteins was increased in the mutant neural folds. This AJ defect is consistent with impaired CNCC delamination, which requires AJ dissolution. Importantly, AJ changes induced by *SPECC1L*-knockdown were rescued by activating the PI3K-AKT pathway *in vitro*. Together, these data indicate SPECC1L as a novel modulator of PI3K-AKT signaling and AJ stability, required for neural tube closure and CNCC delamination.

5.5.2 Possible mechanisms through which *SPECC1L* modulates AJs.

5.5.2.1 SPECC1L interactor SMARCA4 corepresses *ZEB1* transcription, potentially impacting AJ patterning

There are multiple, plausible mechanisms which can explain how SPECC1L deficiency disrupts AJ patterning. The first involves the role played by SPECC1L interactor SMARCA4 as a corepressor of E-Cadherin transcription (Sanchez-Tillo et al., 2010). This mechanism would

require SPECC1L facilitation of SMARCA4 binding to a regulatory element of this gene, whose repression is an important element of EMT (Duband et al., 2015). Immunostaining using an antibody detecting SPECC1L shows it within the nucleus. Also, some of its interactors are involved in chromatin regulation, so a role for it in the nucleus, in transcriptional regulation cannot be ruled out. Exploration of this potential mechanism could be accomplished by introducing exogenous SPECC1L mutagenized to remove any nuclear localization signal and a subsequent analysis of *Zeb1* expression.

5.5.2.2 Reduced AKT levels upon SPECC1L deficiency lead to increased β-Catenin association with AJs

A mechanism more supported by the findings of this study involves AKT signaling itself, in the altered AJ patterning resulting from SPECC1L deficiency. Previously, deficiency of a catalytic subunit of PI3K, upstream of AKT, was shown to induce a similar disruption of AJ patterning (Cain et al., 2010). AKT has been shown to phosphorylate β-Catenin at serine 552, which promotes its dissociation from AJs, promoting its nuclear localization and subsequent transcription of *Wnt* target genes (Nelson 2004). If, upon SPECC1L-kd, reduced AKT signaling leads to reduced dissociating phosphorylation, this very direct mechanism could be explored with Western blotting of WT and *SPECC1L*-kd cell lysates for phospho-552 β-Catenin and a comprehensive comparison of nuclear versus membrane associated β-Catenin.

5.5.2.3 SPECC1L may facilitate AJ recycling through Clathrin-mediated endocytosis

We reported that SPECC1L interacts with both E-Cadherin and β-Catenin, two canonical AJ components. It has been reported that endocytosis of entire AJs is also a mechanism in

controlling intracellular adhesions, allowing the possibility that this binding may affect junction recycling (Harris & Tepass, 2010).

Clathrin-mediated endocytosis (CME) begins with membrane nucleation around a target cargo destined for internalization through preceding modifications of that target. SPECC1L protein interactors AMOTL2 (Li et al., 2012) and HIPK2 (Kim et al., 2010) are negative regulators of AJ stability, (Fig 5.3A). This targeting process also requires cargo-specific adapter proteins (Sorkin 2004). As SPECC1L interacts with both AJ components and negative regulators of AJ stability, presumably at the plasma membrane, it is possible that SPECC1L is an adapter protein facilitating AJ recycling.

The endocytic organizer Adaptor Protein 2 (AP2) binding is required for clathrin coat assembly to proceed (Henne et al., 2010). SPECC1L interacts with Arrestin β2 (ARRB2), which is involved in internalization of ligand-bound receptors in this process (Chen et al., 2004). Interestingly, disruption of AP2 subunit β1 has been shown to result in cleft palate in mice, suggesting a role for CME in palatogenesis (Li et al., 2012). Indeed, a study of *Drosophila* embryogenesis has shown that E-Cadherin endocytosis is coordinated in an AP2-dependent mechanism which, when defective, causes cell-cell intercalation defects (Levayer et al., 2011).

Additional SPECC1L interactors critical to CME include vesicle scission protein Cortactin (Fig 5.3C) (Cao et al., 2003) and a lipid phosphatase, Synaptojanin, which liberates clathrin from the vesicle coat, enabling the uncoating process (Fig 5.3D) (Verstreken et al., 2003). Finally, SPECC1L interacts with actin-based motor proteins involved in CME, such as Myosin IIIA (MYO3A) and Myosin VC (MYO5C) (Kaksonen et al., 2006). As our protein interactor screen yielded approximately 80 proteins, it seems unlikely that its association with ten proteins involved with AJs or their endocytosis is coincidental.

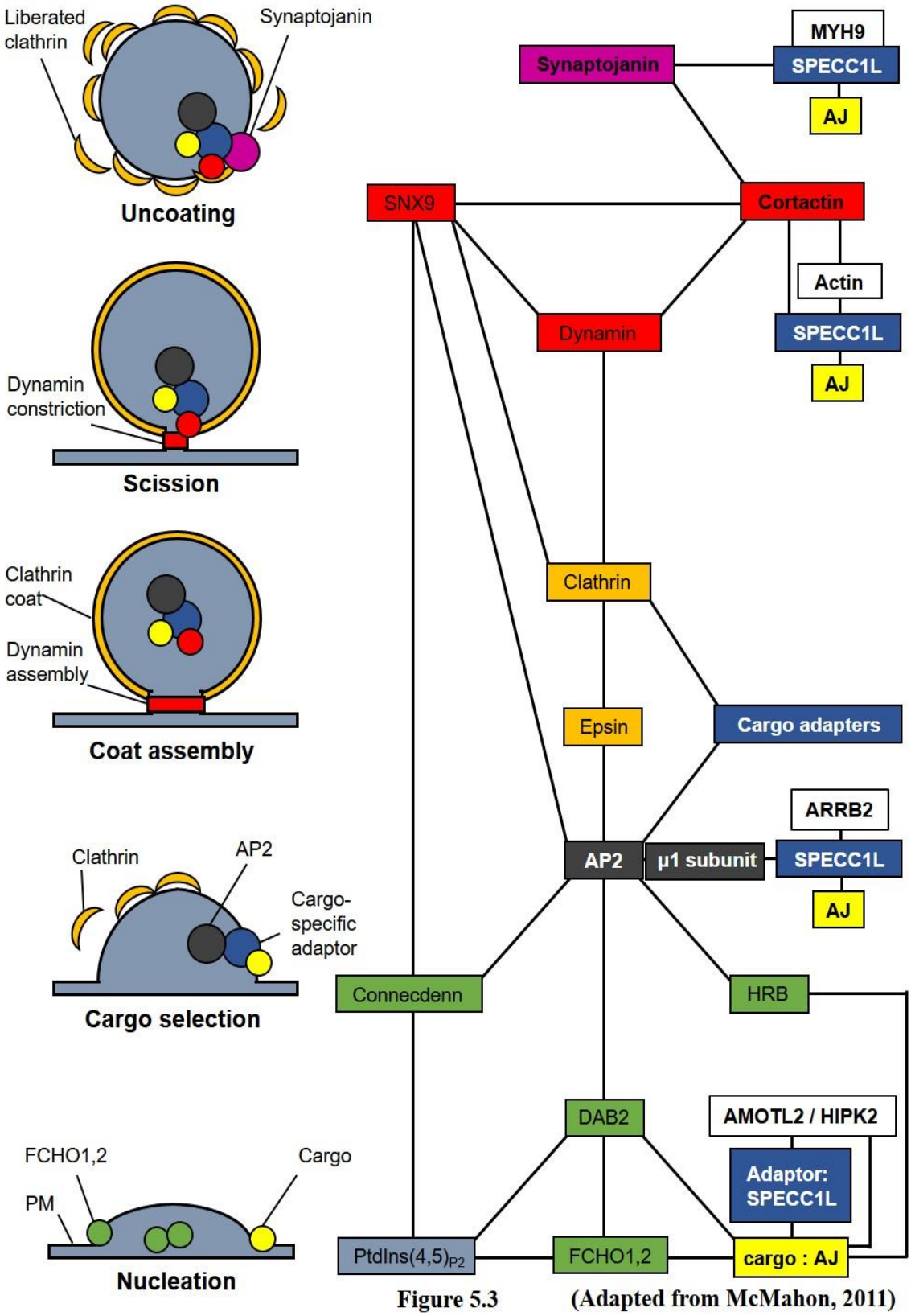

Figure 5.3 **(Adapted from McMahon, 2011)**

Figure 5.3. SPECC1L physically interacts with components of Clathrin-mediated endocytosis. (**A**) During the nucleation stage, SPECC1L binds AJ components and negative regulators of AJs, AMOTL2 and HIPK2. (**B**) In the cargo selection stage of CME, SPECC1L interacts with endocytosis organizer AP2 and Beta Arrestin. (**C**) Upon the scission of dynamin mature vesicles, SPECC1L interacts with Cortactin. (**D**) Upon release and uncoating of Clathrin-coated vesicles, SPECC1L interacts with uncoating protein Synaptojanin and Myosin motors involved in uncoated vesicle recycling.

Previous work has shown that a reduction of the clathrin adapter protein Disabled homolog 2 (DAB2) results in a loss of apical polarization of E-Cadherin (Yang et al., 2007) (Fig 5.3A). This mechanism could be tested by co-immunostaining of AJ and CME proteins, to investigate whether a *SPECC1L*-kd cell line shows a reduction in internalized AJs. Thus, an investigation of any role played by SPECC1L in the CME of AJs should also be included in future efforts.

Interestingly, AKT and GSK3 regulate CME through the regulation of Dynamin, indicating that these two models may be synergistic, rather than mutually exclusive. A synergism between these two models, AKT regulation of AJs directly or through CME, would also explain the partial rescue of the SPECC1L-kd AJ and morphology change seen upon GSK3 inhibition, as compared with the far more robust rescue seen with activation of its upstream negative regulator AKT, in SPECC1L-kd U2OS cells (Chapter Three).

5.6 SPECC1L deficiency affects cell morphology through PI3K-AKT signaling.

5.6.1 AKT regulates cell shape through Rho GTPase-activating protein RHOGAP22

A potential mechanism, which could explain both altered cell shape and migration, involves reduced activation of RHOGAP22 by AKT, upon SPECC1L deficiency. RHOGAP22 phosphorylation by AKT facilitates its binding with the scaffold protein 14-3-3, a prominent mediator in translating AKT substrate phosphorylation into cellular processes (Rowland et al., 2011). Upon AKT-induced association with 14-3-3, RHOGAP22 inhibits RAC1 regulated lamellipodia formation, a critical factor in cell migration, as surplus lamellipodia signal a transition from directional migration to a more amoeboid and less directed motility (Rowland et al., 2011).

However, of direct relevance to cell shape is the effect Ras-related C3 Botulinum Toxin Substrate 1 (RAC1) exercises upon the actin cytoskeleton, encouraging protrusive actin

polymerization and subsequent cell elongation, antagonizing Ras Homolog Family Member A (RHOA) promotion of contractile actin, as observed during lens pit morphogenesis (Chauhan et al., 2011). Indeed, inactivation of RHOGAP22 yields reduced cell circularity *in vitro* (Rowland 2011). This mechanism would also explain altered actin architecture upon *SPECC1L*-kd, given RAC1 function is promoting actin protrusion (Chauhan et al., 2011).

5.6.2 FoxO1 and mTOR regulate cell elongation through PI3K-AKT signaling

An alternative explanation was recently explored. After publication of our report showing that PI3K inhibition is sufficient to induce elongation and AKT activation is sufficient to rescue elongation upon SPECC1L-kd, Tsuji-Tamura and colleagues showed that inhibition of PI3K, AKT or mTORC1 was sufficient to induce elongation in endothelial cells (Tsuji-Tamura & Ogawa, 2016). This suggests that mTORC1 regulation of the actin cytoskeleton may be involved in SPECC1L-kd based elongation, through inhibition of RHOA, which promotes contractile actin, as opposed to RAC1, which promotes protrusive actin (Liu et al., 2011). However, as mTORC1 regulates RHOA and RAC1 regulates mTORC1 (Saci et al., 2011), the two mechanisms proposed may well be interdependent.

5.7 SPECC1L deficiency impairs collective cell migration *in vitro*

5.7.1 Altered actin arrangement upon SPECC1L-kd may affect migration

In Chapter Three, we reported that upon SPECC1L-kd U2OS cells show altered actin architecture, featuring longer actin stress cables associated with Myosin. This most basic feature of SPECC1L deficiency, cytoskeletal alteration has likely consequences upon the mechanical forces which these cells can exert, given the strong Myosin association with these stress cables. Collective cell motions were previously expected to originate with traction forces exerted by so

called ‘leader’ cells at, for example, the edge of a wound assay (Trepat et al., 2009). However, direct measurement of these traction forces show that the mechanical force required for collective cell migration originate in and are mainly generated by cells multiple rows behind the cells of the leading edge, showing that force generation is more of an aggregate property of a cell line, rather than just a traction force at the leading edge (Trepat et al., 2009). Thus, alteration of actin architecture seen upon SPECC1L-kd and the myosin motor forces generated using it are relevant variables in collective cell migration. Indeed, this altered actin architecture can be explained by AKT signaling deficiency, as RAC1 is inactivated by it (Kwon et al., 2000), with more activated RAC1 encourage actin protrusions (Chauhan et al., 2011) and ostensibly subsequent elongation.

Also, activation of depolymerization factor Cofilin 1 (CFL1) promotes the disassembly of actin fibers. Akt activates (SSH1L), which activates Cofilin 1 through removal of an inhibitory phosphorylation (Oh et al., 2007). Thus, it is plausible that reduced Akt upon SPECC1L deficiency reduces the level of active Cofilin 1 available to depolymerize actin filaments, offering a mechanism for altered actin architecture (Nishita et al., 2004).

5.7.2 SPECC1L-kd may impact collective migration through reduced AKT regulation of MERLIN

A frustration to those researching collective cell migration is the relative lack of proteins implicated in its accomplishment. However, one exception offers an alternative mechanism through which SPECC1L deficiency could impair collective migration, in the junctional protein encoded by the Neurofibromatosis type II gene, *MERLIN* (Das et al., 2015). Acting as a mechanochemical transducer, MERLIN spatially organizes collective migration by the dynamic localization of RAC1, with respect to the direction of migration (Das et al., 2015). Thus, MERLIN

is one of the only proteins whose disruption reduces the correlation lengths of migrating streams. While some models place RAC1 upstream of MERLIN, others report the opposite relationship, with the authors concluding the relationship is spatiotemporally dependent (Das et al., 2015). AKT engages in regulatory phosphorylation of both proteins (Kwon et al., 2000, Tang et al., 2007), establishing a plausible model for how SPECC1L disruption or deficiency would cause a reduction in the correlation lengths of migratory streams. While reduced AKT signaling would derepress MERLIN (Tang et al., 2007), its spatiotemporal dynamic with RAC1 strongly suggests that surplus MERLIN could also negatively affect the arrangement of collective migration. The mechanism proposed here would also explain the results of our ongoing work, in which chemical activation of remaining AKT by SC79 rescues closure time in SPECC1L-kd U2OS wound cultures, independently of changes in velocity.

5.8 Conclusion: Severity *of SPECC1L* mutations affects the extent of disruption

5.8.1 Importance of considering the dose dependent effects of *SPECC1L* disruption

The role of SPECC1L in mitosis only requires one functional allele, as a deficiency greater than 50 percent reduction was required to produce the defective spindle rocking phenotype (Mattison et al., 2011). Also, *in vivo* disruption of *SPECC1L* as severe as our gene-trap *Specc1l* mutants will not yield viable organisms for investigation. Effectively, severe SPECC1L deficiency prohibits investigation of craniofacial dysmorphology.

As various embryonic cell lineages have variable needs in terms of their respective rates of proliferation, speed of migration and resistance to apoptosis, it seems reasonable to hypothesize that different lineages either express lineage-specific AKT stabilizing proteins, or show variability in their transcription rates of them, with respect to lineage. It is possible that SPECC1L is the AKT

stabilizing protein of CNCCs, and milder disruptions of SPECC1L function yield defects specific to craniofacial morphogenesis.

5.8.2 A mechanism by which SPECC1L stabilizes AKT at the membrane

I have synthesized the following model based on my work and published findings. As the listing of assumptions is a necessary component in the evaluation of any kind of model, they are below noted by a preceding "*".

*Upon its translation, SPECC1L travels from the Golgi to the plasma membrane along the microtubule cytoskeleton by way of its interactions with microtubule motor proteins KIF4 and KIF5c. It has been shown that AKT is activated at the membrane and deactivated in the cytoplasm. *Therefore, it seems logical to consider that AKT stabilization also occurs at the membrane, as described (Li et al., 2013). Microtubule dynamics regulate this process, suggesting a critical role for microtubule cargos in conveyance of AKT signaling (Jo et al., 2014).

This aspect of SPECC1L transport seems realistic, as SPECC1L has been shown to associate with plus end microtubule regulators such as the interaction between *SPECC1L* ortholog *CG13366* with Clasp, in *Drosophila* (Lowery et al., 2010). More recently, plus end microtubules were shown to be required for gap junction component delivery to the membrane in a mechanism involving β-Catenin and N-Cadherin and the plus end tracking protein Microtubule Associated Protein RP/EB Family Member 1 (MAPRE1), showing a role for plus end microtubule cargo transport in the maintenance and regulation of membrane complexes (Shaw et al., 2006). *Thus, the possibility exists that SPECC1L is such a plus-end microtubule cargo.

SPECC1L localizes to areas of cell-cell contact, physically interacting with β-Catenin and E-Cadherin (Chapter Three), as well as possibly stabilizing AKT so that it can negatively regulate

AJs, through a proposed mechanism involving stabilizing sumoylation of nascent, unstable AKT via the interaction between SPECC1L and PIAS1, which was shown to facilitate this modification (Li et al., 2013)*.

*Upon anchoring the AJ and enabling the stabilization of AKT, SPECC1L then facilitates microtubule severing by its interaction with SPAST (unpublished). Upon stabilization, subsequently activated AKT at the membrane negatively regulates AJs through phosphorylation of β-Catenin at Ser552, inducing its dissociation from AJs (Fang et al., 2007). It has been shown that SPECC1L is an AKT phospho-substrate (Lee et al., 2014, Fantauzzo & Soriano, 2014), but its function has not been explored. *Thus, it is possible that AKT phosphorylation of SPECC1L releases it from AJ components, forming a feedback loop.

*It seems logical that such a feedback loop would exist to tether the processes of AKT stabilization and the negative regulation of AJ stability, as AJs must be recycled to facilitate AKT promoted processes such as migration. Supporting this model, it has been shown that disruption of the microtubule cytoskeleton inhibits AKT signaling and stabilization of microtubules sustains it (Jo et al., 2014).

It has also been shown that SPECC1L interactions with the actin cytoskeleton are best visualized upon treatment with Nocodazole, disrupting its interaction with the MT cytoskeleton and that SPECC1L colocalizes with F-actin throughout the cytoplasm, not just cortical actin (Saadi et al., 2011). *Thus, upon AJ release, SPECC1L leaves the membrane via Myosin interactions with the actin cytoskeleton. This explains its colocalization with both cytoskeletons (Saadi et al., 2011). *As it serves an unknown nuclear role in addition to those described, its trafficking between the two is logical. Protein complexes linking actin filaments with nuclear pore complexes have been observed (Kiseleva et al., 2004).

5.8.3 Hypothesis: *SPECC1L* mutations cause a continuous range of AKT stability

*The ΔCHD deletion is incapable of interacting with either the actin or microtubule cytoskeletons, causing its uniform cytoplasmic pattern, suggesting that actin binding is primary to a secondary yet also functionally important association with the microtubule cytoskeleton, dependent upon it. As such, the Q415P mutant SPECC1L found in severe ObFC, which contains an unaffected CHD, still defectively associates with the MT cytoskeleton.

*The Q415P mutation is more deleterious than the T397P mutation, despite their similar Proline substitution outcomes. *This can be explained as a differential effect shown by Proline mutations in coiled coils, as they are more deleterious when occurring near the center of the coil, introducing a kink, as opposed to its amino or carboxyl ends.

*The Q415P mutation induces a kink in the second coiled coil which disrupts a category of protein-protein interactions with the second coiled coil, perhaps microtubule motor proteins KIF4 or KIF5c. *The T397P mutation does not induce a kink in the second coil domain, or its influence is muted because of its closer proximity to the edge.

*Thus, if a Q415P kink induced in the second coil is sufficiently disruptive, it could prevent SPECC1L transport to the membrane along the microtubule cytoskeleton, assuming that kinesin binding to SPECC1L is severely reduced by that kink. This may explain why the ΔCHD deletion and Q415P were both isolated from severe clefting patients. Severe lack of AKT stabilization specific to CNCCs may be impairing the proliferation and migration of the early facial prominences enough to prevent their having sufficient tissue to ultimately juxtapose. Indeed, reduced neural crest proliferation has been noted in another craniofacial dysmorphology, Treacher Collins syndrome (Trainor, 2010).

*It seems reasonable to propose that mutations in coiled coil domains would generate a range of reduction in loading SPECC1L-bound kinesins with microtubules and a subsequent range of reduced AKT stabilization. Thus, the level of disruption each mutation causes to this domain may directly translate into an equivalent reduction in AKT stabilization, yielding a range of outcome severities. AKT stabilization via SPECC1L-PIAS1-SUMO1, or an unknown equivalent mechanism, is thus a continuous, rather than a discrete range, where, for example, a given mutation might cause a 20% reduction in the rate of the reaction, leading to a 10% reduction is stabilized AKT, after considering zygosity. This would then yield a milder phenotype than a mutation that reduced that reaction rate by 30%.

Intermediate severity syndromic clefting seen upon *SPECC1L* disruption may be caused by an intermediate level of reduced AKT levels, resulting in impaired cross-talk with other pathways involved in facial development. Growth factor signaling upstream of PI3K-AKT signaling, such as EGFRs engage in cross talk with SHH pathway, via Gli1 (Gotschel et al., 2013), where SHH signaling informs midline spatial organization, as seen in its role in the pathogenesis of hypertelorism (Brugmann et al., 2010), which is also a defining symptom of Opitz G/BBB syndromes associated with *SPECC1L* mutations (Kruszka et al., 2015).

The findings of these studies and proposed models of pathogenesis of SPECC1L deficiency in orofacial clefting will serve to enhance our knowledge of the role of this protein in cranial facial morphogenesis.

5.9 Clinical significance

Orofacial clefts including cleft lip and palate are frequent congenital malformations. The CDC estimates that approximately 7,000 U.S. children are born with cleft lip and or palate

annually, making it one of the most frequent malformations. The average cost of cleft lip and palate repair surgery is over 20,000 dollars and frequently exceeds this when multiple surgeries or other treatments are required. While over 400 genes have been linked to rarer syndromic facial clefting disorders, much less is known regarding the underlying pathogenesis of more frequent and typically idiopathic non-syndromic facial clefts and the environmental risk factors which increase occurrence.

One aspect of the clinical significance of this study is its demonstration of the role of PI3K-AKT signaling in facial morphogenesis generally and specifically, the novel role played by SPECC1L in AJ regulation throughout that process. Expanding our knowledge of cell junction biology is clinically important, as recent research findings illustrate human mutations affecting cell junctions are associated with defects in limb formation, epidermal maintenance and other extracutaneous pathologies (Lai-Cheong et al., 2007).

Further, this study demonstrates a fundamental role for SPECC1L-mediated PI3K-AKT signaling in the collective migration of cell populations, during embryonic development. Collective cellular movement is fundamental to embryogenesis, with defects impacting not only craniofacial formation, but cardiac formation and gut innervation. As neonatal cardiac defects are also among the most common and costly malformations (Butler, 2016), furthering our discovery and understanding of the factors facilitating collective migration shows neonatal significance.

Lastly, this study shows the PI3K-AKT signaling pathway as a potential mechanism by which prenatal intervention may reduce facial clefting, in at risk pregnancies. Just as Folic acid supplementation reduces the occurrence of facial clefting and neural tube defects (Tolarova & Harris, 1995), dietary or pharmaceutical treatment modulating downstream effectors of AKT may

show a direct clinical application. Conversely, risk of facial clefting may be reduced by prenatal avoidance of the many drugs and environmental factors which can disrupt PI3K-AKT signaling.

References

Abbas, H. K. & Mirocha, C. J. Isolation and purification of a hemorrhagic factor (wortmannin) from Fusarium oxysporum (N17B). *Appl. Environ. Microbiol.* **54,** 1268–1274 (1988).

Acloque, H., Adams, M. S., Fishwick, K., Bronner-Fraser, M. & Nieto, M. A. Epithelial-mesenchymal transitions: The importance of changing cell state in development and disease. *J. Clin. Invest.* **119,** 1438–1449 (2009).

Adzhubei, I. A. *et al.* A method and server for predicting damaging missense mutations. *Nat. Methods* **7,** 248–249 (2010).

Alexander, C. *et al.* Combinatorial roles for BMPs and Endothelin 1 in patterning the dorsal-ventral axis of the craniofacial skeleton. *Development* **138,** 5135–5146 (2011).

Allanson, J. G syndrome: an unusual family. *Am. J. Med. Genet.* **31**, 637-642 (1988).

Amiel, J. & Lyonnet, S. Hirschsprung disease, associated syndromes, and genetics: a review. *J. Med. Genet.* **38,** 729–39 (2001).

Ashique, A. M., Fu, K. & Richman, J. M. Endogenous bone morphogenetic proteins regulate outgrowth and epithelial survival during avian lip fusion. *Development* **129,** 4647–4660 (2002).

Asselin, E., Mills, G. B. & Tsang, B. K. XIAP Regulates Akt Activity and Caspase-3-dependent Cleavage during Cisplatin-induced Apoptosis in Human Ovarian Epithelial Cancer Cells XIAP Regulates Akt Activity and Caspase-3-dependent Cleavage during Cisplatin-induced Apoptosis in Human Ovarian Epith. 1862–1868 (2001).

Bandyopadhyay, S. *et al.* HHS Public Access. **7,** 801–805 (2011).

Batlle, E. *et al.* The transcription factor snail is a repressor of E-cadherin gene expression in epithelial tumour cells. *Nat. Cell Biol.* **2,** 84–89 (2000).

Baum, B. & Georgiou, M. Dynamics of adherens junctions in epithelial establishment, maintenance, and remodeling. *J. Cell Biol.* **192,** 907–917 (2011).

Belvindrah, R., Hankel, S., Walker, J., Patton, B. L. & Müller, U. β1 Integrins Control the Formation of Cell Chains in the Adult Rostral Migratory Stream. *J. Neurosci.* **27,** 2704–2717 (2007).

Bhoj, E. J. *et al.* Expanding the SPECC1L mutation phenotypic spectrum to include Teebi hypertelorism syndrome. *Am. J. Med. Genet. Part A* **167,** 2497–2502 (2015).

Bolande, R. P. Neurocristopathy: its growth and development in 20 years. Pediatr. Pathol. Lab. Med. 17, 1–25 (1997).

Bonstein, L., Elias, S. & Frank, D. Paraxial-fated mesoderm is required for neural crest induction in Xenopus embryos. *Dev. Biol.* **193,** 156–168 (1998).

Brault, V. *et al.* Inactivation of the beta-catenin gene by Wnt1-Cre-mediated deletion results in dramatic brain malformation and failure of craniofacial development. *Development* **128,** 1253–64 (2001).

Brooks, A. S. *et al.* Congenital diaphragmatic hernia in a female patient with craniofrontonasal syndrome. **11,** 151–153 (2002).

Brugmann, S. A. *et al.* A primary cilia-dependent etiology for midline facial disorders. *Hum. Mol. Genet.* **19,** 1577–1592 (2010).

Bush, J. O. & Jiang, R. Palatogenesis: morphogenetic and molecular mechanisms of secondary palate development. *Development* **139,** 828–828 (2012).

Calderwood, D. A., Shattil, S. J. & Ginsberg, M. H. Integrins and actin filaments: Reciprocal regulation of cell adhesion and signaling. *J. Biol. Chem.* **275,** 22607–22610 (2000).

Calloni, G. W., Glavieux-Pardanaud, C., Le Douarin, N. M. & Dupin, E. Sonic Hedgehog promotes the development of multipotent neural crest progenitors endowed with both mesenchymal and neural potentials. *Proc Natl Acad Sci U S A* **104,** 19879–19884 (2007).

Cano, A. *et al.* The transcription factor Snail controls epithelial – mesenchymal transitions by repressing E-cadherin expression. **2,** (2000).

Cao, H. *et al.* Cortactin is a component of clathrin-coated pits and participates in receptor-mediated endocytosis. *Mol. Cell. Biol.* **23,** 2162–70 (2003).

Cappa, M., Borrelli, P, Marini, Neri, G. The Opitz syndrome: A new designation for the clinically indistinguishable BBB and G syndromes. *American Journal of Medical Genetics* **28**, 303-309 (1987).

Cereijido, M., Valdes, J., Shoshani, L. & Contreras, R. G. Role of tight junctions in establishing and maintaining cell polarity. *Annu Rev Physiol* **60,** 161–177 (1998).

Chai, Y. *et al.* Fate of the mammalian cranial neural crest during tooth and mandibular morphogenesis. *Development* **127,** 1671–1679 (2000).

Chan, C. *et al*. Posttranslational regulation of Akt in human cancer. *Cell & Bioscience* **4**, 59-68 (2014).

Chauhan, B. K., Lou, M., Zheng, Y. & Lang, R. a. Balanced Rac1 and RhoA activities regulate cell shape and drive invagination morphogenesis in epithelia. *Proc. Natl. Acad. Sci.* **108,** 18289–18294 (2011).

Chen, W. *et al.* Activity-dependent internalization of smoothened mediated by beta-arrestin 2 and GRK2. *Sci. (New York, NY)* **306,** 2257–2260 (2004).

Cheung, M. *et al.* The transcriptional control of trunk neural crest induction, survival, and delamination. *Dev. Cell* **8,** 179–192 (2005).

Choe, C. P. *et al.* Wnt-Dependent Epithelial Transitions Drive Pharyngeal Pouch Formation. *Dev. Cell* **24,** 296–309 (2013).

Chung, C. Y., Potikyan, G. & Firtel, R. A. Control of cell polarity and chemotaxis by \protect{Akt/PKB} and \protect{PI3} kinase through the regulation of \protect{PAKa}. *Mol. Cell* **7,** 937–947 (2001).

Cingolani, P. *et al.* A program for annotating and predicting the effects of single nucleotide polymorphisms, SnpEff: SNPs in the genome of Drosophila melanogaster strain w 1118; iso-2; iso-3. *Fly (Austin).* **6,** 80–92 (2012).

Copp, A. J., Greene, N. D. E. & Murdoch, J. N. Dishevelled : linking convergent extension with neural tube closure. **26,** 453–455 (2003).

Copp, A. J. Neurulation in the cranial region--normal and abnormal. *J. Anat.* **207,** 623–635 (2005).

Cordero, D. R. *et al.* Cranial neural crest cells on the move: Their roles in craniofacial development. *Am. J. Med. Genet. Part A* **155,** 270–279 (2011).

Cortés, F. *et al.* Cadherin-mediated differential cell adhesion controls slow muscle cell migration in the developing zebrafish myotome. *Dev. Cell* **5,** 865–76 (2003).

Das, T. *et al.* A molecular mechanotransduction pathway regulates collective migration of epithelial cells. *Nat Cell Biol* **17,** 276–287 (2015).

Davydov, E. V. *et al.* Identifying a high fraction of the human genome to be under selective constraint using GERP++. *PLoS Comput. Biol.* **6,** (2010).

DePristo, M. A. *et al.* A framework for variation discovery and genotyping using next-generation DNA sequencing data. *Nat. Genet.* **43,** 491–8 (2011).

Dixon, M. J., Marazita, M. L., Beaty, T. H. & Murray, J. C. Cleft lip and palate: understanding genetic and environmental influences. *Nat. Rev.* **12,** 167–178 (2011).

D'Souza-Schorey, C. Disassembling adherens junctions: Breaking up is hard to do. *Trends Cell Biol.* **15,** 19–26 (2005).

Engl, W., Arasi, B., Yap, L. L., Thiery, J. P. & Viasnoff, V. Actin dynamics modulate mechanosensitive immobilization of E-cadherin at adherens junctions. *Nat. Cell Biol.* **16,** 587–94 (2014).

Erickson, C. a & Goins, T. L. Avian neural crest cells can migrate in the dorsolateral path only if they are specified as melanocytes. *Development* **121,** 915–24 (1995).

Facchinetti, V. *et al.* The mammalian target of rapamycin complex 2 controls folding and stability of Akt and protein kinase C. *EMBO J.* **27,** 1932–43 (2008).

Fang, D. *et al.* Phosphorylation of β-catenin by AKT promotes β-catenin transcriptional activity. *J. Biol. Chem.* **282,** 11221–11229 (2007).

Fantauzzo, K. a & Soriano, P. PI3K-mediated PDGFRα signaling regulates survival and proliferation in skeletal development through p53-dependent intracellular pathways. *Genes Dev.* **28,** 1005–17 (2014).

Farndon, P., Donnai, D. Male to male transmission of the G syndrome. *Clinical genetics* **24**, 446-448 (1983).

Feng, Y. *et al.* Filamin A (FLNA) is required for cell-cell contact in vascular development and cardiac morphogenesis. *Proc. Natl. Acad. Sci. U. S. A.* **103,** 19836–41 (2006).

Fryburg, J., Lin, K., Golden, W. Chromosome 22q11.2 deletion in a boy with Opitz (G/BBB) syndrome. *American Journal of Medical Genetics* **3**, 274-275 (1996).

Funderburk, S., Stewart, R., Opitz, J. The G and BBB syndromes: Case presentations, genetics, and nosology. *American journal of medical genetics* **2**, 131-144 (1978).

Gendron-Maguire, M., Mallo, M., Zhang, M. & Gridley, T. Hoxa-2 mutant mice exhibit homeotic transformation of skeletal elements derived from cranial neural crest. *Cell* **75,** 1317–1331 (1993).

Gfrerer, L. *et al*. Functional analysis of *SPECC1L* in craniofacial development and oblique facial cleft pathogenesis. *Plast. Reconstr. Surg*. **134**, 748-759 (2014).

Gladdy, R. A. p53-Independent Apoptosis Disrupts Early Organogenesis in Embryos Lacking Both Ataxia-Telangiectasia Mutated and Prkdc. *Mol. Cancer Res.* **4,** 311–318 (2006).

Gorbea, C. *et al.* A protein interaction network for Ecm29 links the 26 S proteasome to molecular motors and endosomal components. *J. Biol. Chem.* **285,** 31616–31633 (2010).

Götschel, F. *et al.* Synergism between Hedgehog-GLI and EGFR Signaling in Hedgehog-Responsive Human Medulloblastoma Cells Induces Downregulation of Canonical Hedgehog-Target Genes and Stabilized Expression of GLI1. *PLoS One* **8,** 1–12 (2013).

Goudy, S., Law, A., Sanchez, G., Baldwin, H. S. & Brown, C. Tbx1 is necessary for palatal elongation and elevation. *Mech. Dev.* **127,** 292–300 (2010).

Guion-Almedia, Richieri-Costa, A. CNS midline anomalies in the Opitz G/BBB syndrome: Report on 12 Brazilian patients. *American journal of medical genetics* **43**, 918-928 (1992).

Gumbiner, B. M. Cell adhesion: The molecular basis of tissue architecture and morphogenesis. *Cell* **84,** 345–357 (1996).

Gurniak, C. B., Perlas, E. & Witke, W. The actin depolymerizing factor n-cofilin is essential for neural tube morphogenesis and neural crest cell migration. *Dev. Biol.* **278,** 231–241 (2005).

Hanson, D., Stevens, A., Murray, P. G., Black, G. C. M. & Clayton, P. E. Identifying biological pathways that underlie primordial short stature using network analysis. *J. Mol. Endocrinol.* **52,** 333–344 (2014).

Harris, M. J. & Juriloff, D. M. Mouse mutants with neural tube closure defects and their role in understanding human neural tube defects. *Birth Defects Res. Part A - Clin. Mol. Teratol.* **79,** 187–210 (2007).

Harris, T. J. C. & Tepass, U. Adherens junctions: from molecules to morphogenesis. *Nat. Rev. Mol. Cell Biol.* **11,** 502–14 (2010).

Harris, A. R., Daeden, A. & Charras, G. T. Formation of adherens junctions leads to the emergence of a tissue-level tension in epithelial monolayers. *J. Cell Sci.* **127,** 2507–17 (2014).

Hartsock, A. & Nelson, W. J. Adherens and tight junctions: Structure, function and connections to the actin cytoskeleton. *Biochim. Biophys. Acta - Biomembr.* **1778,** 660–669 (2008).

Henne, W. M. *et al.* FCHo proteins are nucleators of clathrin-mediated endocytosis. *Science (80-.).* **328,** 1281–1284 (2010).

Hilgarth, R. S. *et al.* Regulation and function of SUMO modification. *J. Biol. Chem.* **279,** 53899–53902 (2004).

Homanics, G. *et al*. Exencephaly and hydrocephaly in mice with targeted modification of the apolipoprotein B (Apob) gene. *Teratology* **51**, 1-10 (1995).

Honoré, S. M., Aybar, M. J. & Mayor, R. Sox10 is required for the early development of the prospective neural crest in Xenopus embryos. *Dev. Biol.* **260,** 79–96 (2003).

Hornbeck, P. V. *et al.* PhosphoSitePlus: A comprehensive resource for investigating the structure and function of experimentally determined post-translational modifications in man and mouse. *Nucleic Acids Res.* **40,** 261–270 (2012).

Hunt, P., Gulisano, M. A distinct Hox code for the branchial region of the vertebrate head. *Nature* **353**, 861 (1991).

Ikeda, A., Ikeda, S., Gridley, T., Nishina, P. M. & Naggert, J. K. Neural tube defects and neuroepithelial cell death in Tulp3 knockout mice. *Hum. Mol. Genet.* **10,** 1325–1334 (2001).

Ingraham, C. R. *et al.* Abnormal skin, limb and craniofacial morphogenesis in mice deficient for interferon regulatory factor 6 (Irf6). *Nat. Genet.* **38,** 1335–40 (2006).

Jeong, J., Mao, J., Tenzen, T., Kottmann, A. H. & Mcmahon, A. P. Hedgehog signaling in the neural crest cells regulates the patterning and growth of facial primordia.pdf. *Genes Dev.* 937–951 (2004). doi:10.1101/gad.1190304

Jin, J. P., Walsh, M. P., Sutherland, C. & Chen, W. A role for serine-175 in modulating the molecular conformation of calponin. *Biochem. J.* **350 Pt 2,** 579–88 (2000).

Jo, H. *et al.* Small molecule-induced cytosolic activation of protein kinase Akt rescues ischemia-elicited neuronal death. *Proc. Natl. Acad. Sci. U. S. A.* **109,** 10581–6 (2012).

Kaida, M., Cao, F., Skumatz, C. M. B., Irving, P. E. & Burke, J. M. Time at confluence for human RPE cells: Effects on the adherens junction and in vitro wound closure. *Investig. Ophthalmol. Vis. Sci.* **41,** 3215–3224 (2000).

Kaksonen, M., Toret, C. P. & Drubin, D. G. Harnessing actin dynamics for clathrin-mediated endocytosis. *Nat. Rev. Mol. Cell Biol.* **7,** 404–414 (2006).

Kennedy, S. G. *et al.* Akt / Protein Kinase B Inhibits Cell Death by Preventing the Release of Cytochrome c from Mitochondria Akt / Protein Kinase B Inhibits Cell Death by Preventing the Release of Cytochrome c from Mitochondria. *Mol. Cell. Biol.* **19,** 5800–5810 (1999).

Khandelwal, K. D. *et al.* Novel IRF6 Mutations Detected in Orofacial Cleft Patients by Targeted Massively Parallel Sequencing. *J. Dent. Res.* (2016). doi:10.1177/0022034516678829

Kim, J., Lo, L., Dormand, E. & Anderson, D. J. SOX10 maintains multipotency and inhibits neuronal differentiation of neural crest stem cells. *Neuron* **38,** 17–31 (2003).

Kim, E.-A. *et al.* Homeodomain-interacting protein kinase 2 (HIPK2) targets beta-catenin for phosphorylation and proteasomal degradation. *Biochem. Biophys. Res. Commun.* **394,** 966–71 (2010).

Kruszka, P. et al. Mutations in SPECC1L, Encoding Sperm Antigen with Calponin Homology and Coiled-Coil Domains 1-like, are Found in Some Cases of Autosomal Dominant Opitz G/BBB Syndrome. *J. Med. Genet.* (2014).

Kulesa, P. M. & McLennan, R. Neural crest migration: trailblazing ahead. *F1000Prime Rep.* **7,** 2 (2015).

Kurima, K. *et al.* A noncoding point mutation of Zeb1 causes multiple developmental malformations and obesity in Twirler mice. *PLoS Genet.* **7,** (2011).

Kwon, T., Chun, J., Kim, J., Kang, S. Akt protein kinase inhibits Rac1-GTP binding through phosphorylation at Serine 71 of Rac1. *Journal of Biological Chemistry* **275**, 423-428 (2000).

Lacassie, Y., Arriaza, M. Opitz G/BBB syndrome and the 22q11.2 deletion. *American Journal of Medical Genetics* **3**, 318 (1996).

Le Douarin, N. The neural crest. (Cambridge University Press, 1982).

Lee, M. Y. *et al.* Endothelial Akt1 mediates angiogenesis by phosphorylating multiple angiogenic substrates. *Proc. Natl. Acad. Sci. U. S. A.* **111,** 1–6 (2014).

Levayer, R., Pelissier-Monier, A. & Lecuit, T. Spatial regulation of Dia and Myosin-II by RhoGEF2 controls initiation of E-cadherin endocytosis during epithelial morphogenesis. *Nat. Cell Biol.* **13,** 529–40 (2011).

Lewis, J. E., Jensen, P. J. & Wheelock, M. J. Cadherin function is required for human keratinocytes to assemble desmosomes and stratify in response to calcium. *J. Invest. Dermatol.* **102,** 870–877 (1994).

Li, H. & Durbin, R. Fast and accurate short read alignment with Burrows-Wheeler transform. *Bioinformatics* **25,** 1754–1760 (2009).

Li, B., Kuriyama, S., Moreno, M. & Mayor, R. The posteriorizing gene Gbx2 is a direct target of Wnt signalling and the earliest factor in neural crest induction. *Development* **136,** 3267–3278 (2009).

Li, Z., *et al.* The Amotl2 gene inhibits Wnt/β-catenin signaling and regulates embryonic development in zebrafish. *J. Biol. Chem.* **287,** 13005–13015 (2012).

Li, V., *et al.* Wnt Signaling through Inhibition of β-Catenin Degradation in an Intact Axin1 Complex. *Cell* **149,** 1245–1256 (2012).

Liu, X., Jian, X., Boerwinkle, E. dbNSFP: A lightweight database of human nonsynonymous SNPs and their functional predictions. *Hum. Mutat.* **32,** 894–899 (2011).

Lowery, L. A. *et al.* Parallel genetic and proteomic screens identify msps as a clasp-abl pathway interactor in Drosophila. *Genetics* **185,** 1311–1325 (2010).

Lupas, A., Van Dyke, M., Stock, J. Predicting coiled coild from protein sequences. *Science* **252**, 1162 (1991).

Mangold, E., Ludwig, K., Nöthen, M. Breakthroughs in the genetics of orofacial clefting. *Trends Mol. Med.* **17,** 725–733 (2011).

Manichaikul, A. *et al.* Robust relationship inference in genome-wide association studies. *Bioinformatics* **26,** 2867–2873 (2010).

Matsuzaki, H. *et al.* Activation of Akt kinase inhibits apoptosis and changes in Bcl-2 and Bax expression induced by nitric oxide in primary hippocampal neurons. *J. Neurochem.* **73,** 2037–46 (1999).

Mattison, C. P., Stumpff, J., Wordeman, L. & Winey, M. Mip1 associates with both the Mps1 kinase and actin, and is required for cell cortex stability and anaphase spindle positioning. *Cell Cycle* **10,** 783–793 (2011).

McKeown, S. J., Wallace, A. S. & Anderson, R. B. Expression and function of cell adhesion molecules during neural crest migration. *Dev. Biol.* **373,** 244–257 (2013).

Migliorini, D. *et al.* Growth Arrest and Neuronal Cell Death during Early Embryonic Mouse Development Mdm4 (Mdmx) Regulates p53-Induced Growth Arrest and Neuronal Cell Death during Early Embryonic Mouse Development. *Society* **4,** 5527–5538 (2002).

Minoux, M. & Rijli, F. M. Molecular mechanisms of cranial neural crest cell migration and patterning in craniofacial development. *Development* **137,** 2605–2621 (2010).

Mueller, G., *et al.* Embryonic lethality caused by apoptosis during gastrulation in mice lacking the gene of the ADP-ribosylation factor-related protein 1. *Mol. Cell. Biol.* **22,** 1488–1494 (2002).

Murdoch, J. N. & Copp, A. J. The relationship between sonic hedgehog signaling, cilia, and neural tube defects. *Birth Defects Res. Part A - Clin. Mol. Teratol.* **88,** 633–652 (2010).

Nanes, B., Kowalczyk, A. Adherens junction turnover: regulating adhesion through cadherin endocytosis, degradation, and recycling. *Subcell. Biochem.* **60**, 197-222 (2012).

Nelson, W. J. & Nusse, R. Convergence of Wnt, beta-catenin, and cadherin pathways. *Science* **303,** 1483–7 (2004).

Nijman, S. M. B. *et al.* A genomic and functional inventory of deubiquitinating enzymes. *Cell* **123,** 773–786 (2005).

Nishimura, T. & Takeichi, M. Remodeling of the adherens junctions during morphogenesis. Curr. Top. Dev. Biol. 89, 33–54, doi:10.1016/S0070-2153(09)89002-9 (2009).

Nishita, M. *et al.* Phosphoinositide 3-Kinase-mediated Activation of Cofilin Phosphatase Slingshot and Its Role for Insulin-induced Membrane Protrusion. *J. Biol. Chem.* **279,** 7193–7198 (2004).

Norwood, F. L. M., Sutherland-Smith, A. J., Keep, N. H. & Kendrick-Jones, J. The structure of the N-terminal actin-binding domain of human dystrophin and how mutations in this domain may cause Duchenne or Becker muscular dystrophy. *Structure* **8,** 481–491 (2000).

Oh, M.-A. *et al.* PKCdelta and cofilin activation affects peripheral actin reorganization and cell-cell contact in cells expressing integrin alpha5 but not its tailless mutant. *J. Cell Sci.* **120,** 2717–2730 (2007).

Ohno, S. Intercellular junctions and cellular polarity: The PAR-aPKC complex, a conserved core cassette playing fundamental roles in cell polarity. *Curr. Opin. Cell Biol.* **13,** 641–648 (2001).

Park, K.-S. & Gumbiner, B. M. Cadherin 6B induces BMP signaling and de-epithelialization during the epithelial mesenchymal transition of the neural crest. *Development* **137,** 2691–701 (2010).

Passos-Bueno, M. R., Ornelas, C. C. & Fanganiello, R. D. Syndromes of the first and second pharyngeal arches: A review. *Am. J. Med. Genet. Part A* **149,** 1853–1859 (2009).

Piotrowski, T. *et al.* Jaw and branchial arch mutants in zebrafish II: anterior arches and cartilage differentiation. *Development* **123,** 345–356 (1996).

Polakowska, R. R., Piacentini, M., Bartlett, R., Goldsmith, L. A. & Haake, A. R. Apoptosis in human skin development: Morphogenesis, periderm, and stem cells. *Dev. Dyn.* **199,** 176–188 (1994).

Pollard, T. D. & Cooper, J. A. Actin, a central player in cell shape and movement. *Science* **326,** 1208–12 (2009).

Quaderi, N. a *et al.* Opitz G/BBB syndrome, a defect of midline development, is due to mutations in a new RING finger gene on Xp22. *Nat. Genet.* **17,** 285–291 (1997).

Reis, C. R. *et al.* Crosstalk between Akt / GSK 3 b signaling and dynamin- 1 regulates clathrin-mediated endocytosis. *EMBO J.* **34,** 1–15 (2015).

Ridley, A. J. *et al.* Cell migration: integrating signals from front to back. *Science* **302,** 1704–9 (2003).

Robin, N., *et al*. Opitz syndrome is genetically heterogeneous, with one locus on Xp22, and a second locus on 22q11.2. *Nature genetics* **11**, 459-461 (1995).

Robin, N., Opitz, J., Muenke, M. Opitz G/BBB syndrome: Clinical comparisons of families linked to Xp22 and 22Q and a review of the literature. *American journal of medical genetics* **62**, 305-317 (1996).

Robinson, R. Link between Cell Junctions and Microtubule Cytoskeleton Is Critical for Epithelial Morphogenesis. *PLoS Biol.* **13,** 1–2 (2015).

Rogers, C. D., Jayasena, C. S., Nie, S. & Bronner, M. E. Neural crest specification: Tissues, signals, and transcription factors. *Wiley Interdiscip. Rev. Dev. Biol.* **1,** 52–68 (2012).

Rørth, P. Collective cell migration. *Annu Rev Cell Dev Biol.* **25,** 407–29 (2009).

Rowland, A. F., Larance, M., Hughes, W. E. & James, D. E. Identification of RhoGAP22 as an Akt-dependent regulator of cell motility in response to insulin. *Mol. Cell. Biol.* **31,** 4789–800 (2011).

Ruland, J. *et al.* Bcl10 is a positive regulator of antigen receptor-induced activation of NF-κB and neural tube closure. *Cell* **104,** 33–42 (2001).

Saadi, I. *et al.* Deficiency of the Cytoskeletal Protein SPECC1L Leads to Oblique Facial Clefting. *Am. J. Hum. Genet.* **89,** 44–55 (2011).

Saadoun, S., Papadopoulos, M. C., Hara-Chikuma, M. & Verkman, A. S. Impairment of angiogenesis and cell migration by targeted aquaporin-1 gene disruption. *Nature* **434,** 786–792 (2005).

Saci, A., Cantley, L. C. & Carpenter, C. L. Rac1 Regulates the Activity of mTORC1 and mTORC2 and Controls Cellular Size. *Mol. Cell* **42,** 50–61 (2011).

Saint-Jeannet, J.-P. *Neural crest induction and differentiation*. *Advances in experimental medicine and biology* (2006). doi:10.1007/978-0-387-46954-6

Sánchez-Tilló, E. *et al.* ZEB1 represses E-cadherin and induces an EMT by recruiting the SWI/SNF chromatin-remodeling protein BRG1. *Oncogene* **29,** 3490–3500 (2010).

Santagati, F. & Rijli, F. M. Cranial neural crest and the building of the vertebrate head. *Nat. Rev. Neurosci.* **4,** 806–18 (2003).

Schorle, H., *et al*. Transcription factor AP-2 essential for cranial closure and craniofacial development. *Nature* **381**, 235 (1996).

Schulze-Bergkamen, H. *et al.* Hepatocyte Growth Factor Induces Mcl-1 in Primary Human Hepatocytes and Inhibits CD95-Mediated Apoptosis via Akt. *Hepatology* **39,** 645–654 (2004).

Schweiger, S. *et al*. The Opitz syndrome gene product , MID1 , associates with microtubules. *Proc. Natl. Acad. Sci.* **96,** 2794–2799 (1999).

Shaw, R. M. *et al.* Microtubule Plus-End-Tracking Proteins Target Gap Junctions Directly from the Cell Interior to Adherens Junctions. *Cell* **128,** 547–560 (2007).

Shaw, T. J. & Martin, P. Wound repair: A showcase for cell plasticity and migration. *Curr. Opin. Cell Biol.* **42,** 29–37 (2016).

Short, K. M. & Cox, T. C. Subclassification of the RBCC/TRIM superfamily reveals a novel motif necessary for microtubule binding. *J. Biol. Chem.* **281,** 8970–8980 (2006).

Shprintzen, R. J., Goldberg, R. B. & Wolford, L. Robert J. Shprintzen, PhD, Rosalie B. Goldberg, Dennison Young, MD, FACC, and Larry Wolford,. **67,** (1981).

Simpson, K. J. *et al.* Identification of genes that regulate epithelial cell migration using an siRNA screening approach. *Nat. Cell Biol.* **10,** 1027–1038 (2008).

Slater, B., Londono, C. & McGuigan, A. P. An algorithm to quantify correlated collective cell migration behavior. *Biotechniques* **54,** 87–92 (2013).

Slavotinek, A. Single gene disorders associated with congenital diaphragmatic hernia. *American Journal of Medical Genetics* **145**, 172-183 (2007).

Smith JL, S. G. Cell cycle and neuroepithelial cell shape during bending of the chick neural plate. *Anat Rec* **218: 196–2,** 196–206 (1987).

So, J. *et al.* Mild phenotypes in a series of patients with opitz GBBB syndrome with MID1 mutations. *Am. J. Med. Genet.* **132 A,** 1–7 (2005).

Sorkin, A. Cargo recognition during clathrin-mediated endocytosis: A team effort. *Curr. Opin. Cell Biol.* **16,** 392–399 (2004).

Stepniak, E., Radice, G. L. & Vasioukhin, V. Adhesive and signaling functions of cadherins and catenins in vertebrate development. *Cold Spring Harb. Perspect. Biol.* **1,** (2009).

Stoll, C. *et al*. Male-to-male transmission of the hypertelorism-hypospadias (BBB) syndrome. *American Journal of Medical Genetics* **20**, 221-225 (1985).

Strobl-Mazzulla, P. H. & Bronner, M. E. Epithelial to mesenchymal transition: New and old insights from the classical neural crest model. *Semin. Cancer Biol.* **22,** 411–416 (2012).

Sun, Y. *et al.* Genome-wide association study identifies a new susceptibility locus for cleft lip with or without a cleft palate. *Nat. Commun.* **6,** 6414 (2015).

Sundaresan, N. R. *et al.* The deacetylase SIRT1 promotes membrane localization and activation of Akt and PDK1 during tumorigenesis and cardiac hypertrophy. *Sci. Signal.* **4,** ra46 (2011).

Szabó, A., Ünnep, R., Méhes, E., Twal, W.O., Argraves, W.S., Cao, Y. and Czirók, A. Collective cell motion in endothelial monolayers. *Physical biology*, ***7***, 4 (2010)..

Takahashi, K. *et al.* Nectin / PRR : An Immunoglobulin-like Cell Adhesion Molecule Recruited PDZ Domain – containing *Protein*. **145,** 539–549 (1999)

Takeichi, M. Cadherin cell adhesion receptors as a morphogenetic regulator. *Science* **251**, 1451 (1991).

Taneyhill, L. a. To adhere or not to adhere. *Cell Adh. Migr.* **2,** 223–230 (2008).

Taneyhill, L. A. & Schiffmacher, A. T. Cadherin dynamics during neural crest cell ontogeny. *Prog. Mol. Biol. Transl. Sci.* **116,** 291–315 (2013).

Tang, X. *et al.* Akt phosphorylation regulates the tumour-suppressor merlin through ubiquitination and degradation. *Nat. Cell Biol.* **9,** 1199–1207 (2007).

Taylor, K. M. & LaBonne, C. SoxE factors function equivalently during neural crest and inner ear development and their activity is regulated by SUMOylation. *Dev. Cell* **9,** 593–603 (2005).

Taylor, J. & Aftimos, S. Congenital diaphragmatic hernia is a feature of Opitz G/BBB syndrome. *Clin. Dysmorphol.* **19,** 225–226 (2010).

Theveneau, E. & Mayor, R. Can mesenchymal cells undergo collective cell migration? The case of the neural crest. *Cell Adhes. Migr.* **5,** 490–498 (2011).

Theveneau, E. & Mayor, R. Cadherins in collective cell migration of mesenchymal cells. *Curr. Opin. Cell Biol.* **24,** 677–684 (2012).

Theveneau, E. & Mayor, R. Neural crest migration: Interplay between chemorepellents, chemoattractants, contact inhibition, epithelial-mesenchymal transition, and collective cell migration. *Wiley Interdiscip. Rev. Dev. Biol.* **1,** 435–445 (2012).

Thiery, J. P. & Sleeman, J. P. Complex networks orchestrate epithelial-mesenchymal transitions. *Nat. Rev. Mol. Cell Biol.* **7,** 131–42 (2006).

Thomas-Tikhonenko, A. Cancer genome and tumor microenvironment. (Springer, 2010).

Tobin, J. L. *et al.* Inhibition of neural crest migration underlies craniofacial dysmorphology and Hirschsprung's disease in Bardet-Biedl syndrome. *Proc. Natl. Acad. Sci. U. S. A.* **105,** 6714–6719 (2008).

Trainor, P. A. Neural crest cells: evolution, development and disease. (Elsevier/AP, 2014).

Trainor, P., Krumlauf, R., Ridgeway, T. & Hill, M. Patterning the Cranial Neural Crest : Hindbrain Segmentation and Hox Gene Plasticity. **1,** 116–124 (2000).

Trainor, P. Craniofacial birth defects: The role of neural crest cells in the etiology and pathogenesis of Treacher Collins syndrome and the potential for prevention. *American Journal of Medical Genetics* **152**, 2984-2994 (2010).

Tsuji-Tamura, K. & Ogawa, M. Inhibition of the PI3K/Akt and mTORC1 signaling pathways promotes the elongation of vascular endothelial cells. *J Cell Sci* **1,** jcs–178434 (2016).

Tudela, C. *et al.* TGF-β3 is required for the adhesion and intercalation of medial edge epithelial cells during palate fusion. *Int. J. Dev. Biol.* **46,** 333–336 (2002).

Urnov, F. D., Rebar, E. J., Holmes, M. C., Zhang, H. S. & Gregory, P. D. (13) Genome editing with engineered zinc finger nucleases. *Nat. Rev. Genet.* **11,** 636–46 (2010).

Verstreken, P. *et al.* Synaptojanin is recruited by endophilin to promote synaptic vesicle uncoating. *Neuron* **40,** 733–748 (2003).

Waardenburg, P. J. A new syndrome combining developmental anomalies of the eyelids, eyebrows and nose root with pigmentary defects of the iris and head hair and with congenital deafness. *Am. J. Hum. Genet.* **3,** 195–253 (1951).

Wang, K., Li, M. & Hakonarson, H. ANNOVAR: functional annotation of genetic variants from high-throughput sequencing data. *Nucleic Acids Res.* **38,** e164 (2010).

Webb, D. J., Brown, C. M. & Horwitz, A. F. Illuminating adhesion complexes in migrating cells: Moving toward a bright future. *Curr. Opin. Cell Biol.* **15,** 614–620 (2003).

Willnow, T. E., Christ, A. & Hammes, A. Endocytic receptor-mediated control of morphogen signaling. *Development* **139,** 4311–9 (2012).

Wilson, G., Oliver, W. Further delineation of the G syndrome: A manageable genetic cause of infantile dysphagia. *Journal of medical genetics* **25**, 157-163 (1988).

Wilson, N. R. *et al.* SPECC1L deficiency results in increased adherens junction stability and reduced cranial neural crest cell delamination. *Nat. Publ. Gr.* 1–15 (2016). doi:10.1038/srep17735

Witze, E. *et. al*. Wnt5a control of cell polarity and directional movement by polarized redistribution of adhesion receptors. *Science* **320**, 365-369 (2008).

Woolfson, D. N. & Williams, D. H. The influence of proline residues on α-helical structure. *FEBS Lett.* **277,** 185–188 (1990).

Wu, D., Pan, W. GSK3: A multifaceted kinase in Wnt signaling. *Trends in biochemical sciences* **35**, 161-168 (2010).

Wu, W. *et al.* HERC2 is an E3 ligase that targets BRCA1 for degradation. *Cancer Res.* **70,** 6384–6392 (2010).

Xu, X. *et al.* Modulation of mouse neural crest cell motility by N-cadherin and connexin 43 gap junctions. *J. Cell Biol.* **154,** 217–229 (2001).

Yamaguchi, N., Mizutani, T., Kawabata, K. & Haga, H. Leader cells regulate collective cell migration via Rac activation in the downstream signaling of integrin β1 and PI3K. *Sci. Rep.* **5,** 7656 (2015).

Yang, D. H., Cai, K. Q., Roland, I. H., Smith, E. R. & Xu, X. X. Disabled-2 is an epithelial surface positioning gene. *J. Biol. Chem.* **282,** 13114–13122 (2007).

Yang, W., *et. al*. The E3 ligase TRAF6 regulates Akt ubiquitination and activation. *Science* **325**, 1134-1138 (2009).

Yap, A. S., Brieher, W. M. & Gumbiner, B. M. Molecular and Functional Analysis of Cadherin-Based Adherens Junctions. *Annu. Rev. Cell Dev. Biol* **13,** 119–46 (1997).

Yoshida, M. *et al.* Periderm cells covering palatal shelves have tight junctions and their desquamation reduces the polarity of palatal shelf epithelial cells in palatogenesis. *Genes to Cells* **17,** 455–472 (2012).

Yu, Z. *et al.* Induction of cell-cycle arrest by all-trans retinoic acid in mouse embryonic palatal mesenchymal (MEPM) cells. *Toxicol. Sci.* **83,** 349–354 (2005).

Zaghloul, N. A. & Brugmann, S. A. The emerging face of primary cilia. *Genesis* **49,** 231–246 (2011).

Zamir, E. a., Czirók, A., Rongish, B. J. & Little, C. D. A Digital Image-Based Method for Computational Tissue Fate Mapping During Early Avian Morphogenesis. *Ann. Biomed. Eng.* **33,** 854–865 (2005).

Zeitlin, S., Liu, J. P., Chapman, D. L., Papaioannou, V. E. & Efstratiadis, A. Increased apoptosis and early embryonic lethality in mice nullizygous for the Huntington's disease gene homologue. *Nat. Genet.* **11,** 155–163 (1995).

Zhou, Y., Yang, S., Mao, T. & Zhang, Z. MAPanalyzer: A novel online tool for analyzing microtubule-associated proteins. *Database* **2015,** 1–12 (2015).

APPENDIX A:

SPECC1L PROTEIN INTERACTORS

Table A.1. SPECC1L protein interactors from literature search and Yeast-two hybrid screens used in Ingenuity pathway analyses and subsequent hierarchical edge bundling

Symbol	Protein interactor	PMID
ACTB	Beta actin	26496610
AMOTL2	Angiomotin-like protein 2	†
ANKRD26	Ankyrin repeat domain 26	26496610
ANLN	Anillin	26496610
AP2M1	Adaptor-related protein complex 2, mu 1 subunit	26186194, †
APC	Adenomatous polyposis coli	20936779
ARRB2	Beta arrestin-2	†
ATAD2	ATPase family AAA domain-containing protein 2	†
ATBF1	Zinc finger homeobox protein 3	†
ATMIN	ATM interactor	‡
BEGAIN	Brain-enriched guanylate kinase-associated protein	†
C10ORF2	Chromosome 10 open reading frame 2	26496610
CABIN1	Calcineurin-binding protein cabin-1	†
CALML3	Calmodulin-like 3	26496610
CAPZA2	Capping protein muscle Z-line, alpha 2	26496610
CCDC8	Coiled-coil domain containing 8	24711643
CCNJ	Cyclin J	‡
CDK2	Cyclin-dependent kinase 2	26496610
CFAP97	Cilia and flagella associated protein 97	†
CHRNA9	Cholinergic receptor, nicotinic, alpha 9 (neuronal)	26186194
DBN1	Drebrin 1	26496610
DDX23	Probable ATP-dependent RNA helicase DDX23	†
DUSP22	Dual specificity phosphatase 22	‡
ECM29	Proteasome-associated protein ECM29 homolog	20682791
EDC4	Enhancer of mRNA-decapping protein 4	†
EDRF1	Putative transcription activator BRLF1 homolog	†
EEF2	Elongation factor 2	†
FBXO25	F-box protein 25	20473970
FEZ1	Fasciculation and elongation protein zeta 1 (zygin I)	‡
FSCN2	Fascin actin-bundling protein 2, retinal	‡
FSD1	Fibronectin type III and SPRY domain containing 1	26186194
G2E3	G2/M-phase specific E3 ubiquitin protein ligase	‡
GLIS2	GLIS family zinc finger 2	17289029
HERC2	HECT and RLD domain containing E3 ub. ligase 2	25476789
HIPK1	Homeodomain-interacting protein kinase 1	†

Symbol	Protein interactor	PMID
HIPK2	Homeodomain-interacting protein kinase 2	†
HMMR	Hyaluronan mediated motility receptor	†
IGSF9	Protein turtle homolog A	†
IQGAP1	IQ motif containing GTPase activating protein 1	26496610
ITGA5	Integrin alpha 5 (fibronectin receptor alpha)	26496610
KCTD17	Potassium channel tetramerization containing 17	26186194
KIF4	Chromosome-associated kinesin KIF4A	†
KIF5C	Kinesin heavy chain isoform 5C	†
LIMA1	LIM domain and actin binding 1	26496610
LPXN	Leupaxin	‡
LRFN4	Leucine rich repeat and FN type III domain 4	26186194
LUZP4	Leucine zipper protein 4	25662211
MYH10	Myosin, heavy polypeptide 10, non-muscle	26496610
MYH9	Myosin, heavy chain 9, non-muscle	26496610, †
MYO18A	Myosin 18A	26496610
MYO19	Myosin 19	26496610
MYO1C	Myosin 1C	26496610
MYO5C	Myosin 5C	26496610
MYT1	Myelin transcription factor 1	†
NCOR1	Nuclear receptor corepressor 1	†
NFKBIA	Nuclear factor of kappa light polypeptide enhancer α	26186194
NOP14	Nucleolar protein 14	†
OBFC1	Oligonucleotide-binding fold containing 1	26186194
PAN2	PAN2 poly(A) specific ribonuclease subunit	23398456
PDLIM7	PDZ and LIM domain 7 (enigma)	26496610
PIAS1	E3 SUMO-protein ligase PIAS1	†
PIAS2	E3 SUMO-protein ligase PIAS2	†
PPP1CB	Protein phosphatase 1, catalytic subunit, β isozyme	26496610
PPP1R12A	Protein phosphatase 1 regulatory subunit 12A	†
PPP1R12C	Protein phosphatase 1 regulatory subunit 12C	†
PRDM15	PR domain zinc finger protein 15	†
RBAK	RB-associated KRAB zinc finger protein	†
RCN1	Reticulocalbin 1, EF-hand calcium binding domain	26186194
RPL15	Ribosomal protein L15	‡
SAFB	Scaffold attachment factor B1	†
SAMM50	Sorting and assembly machinery component 50	26496610
SETX	Probable helicase sentaxin	†
SLC25A41	Solute carrier family 25, member 41	26186194
SLC30A6	Solute carrier family 30 (zinc transporter), member 6	26186194
SMARCA4	Transcription activator BRG1	†
SMARCAD1	SWI/SNF-related regulator of chromatin AD1	†

Symbol	Protein interactor	PMID
SMARCC1	SWI/SNF complex subunit SMARCC1	†
SMARCE1	SWI/SNF-related regulator of chromatin E1	†
SNW1	SNW domain-containing protein 1	†
SPAST	Spastin	†
SPC25	SPC25, NDC80 kinetochore complex component	26186194
SPECC1	Sperm antigen with CHD and coiled-coil domains 1	†
SRGAP3	SLIT-ROBO Rho GTPase-activating protein 3	†
SYNPO	Synaptopodin	26496610
TDG	G/T mismatch-specific thymine DNA glycosylase	†
TNFRSF22	TNF receptor superfamily member 22	†
TOX3	TOX high mobility group box family member 3	†
UBC	Ubiquitin C	23314748
UBE2I	SUMO-conjugating enzyme UBC9	20936779, †
USO1	USO1 vesicle docking factor	26496610
USP15	Ubiquitin carboxyl-terminal hydrolase 15	†
VAV1	Vav 1 guanine nucleotide exchange factor	‡
ZBTB16	Zn finger and BTB domain-containing protein 16	†
ZBTB41	Zn finger and BTB domain-containing protein 41	†
ZCCHC7	Zn finger CCHC domain-containing protein 7	†
ZKSCAN1	Zn finger protein with KRAB and SCAN domains 1	†
ZSCAN2	Zn finger and SCAN domain-containing protein 2	†
ZSCAN21	Zn finger and SCAN domain-containing protein 21	†

† Unpublished data from Saadi, I (2016)

‡ Unpublished data from Huttlin, EL (2014):

https://thebiogrid.org/166968/publication/the-bioplex-network-of-human-protein-interactions-additional-unpublished-ap-ms-results.html

(Courtesy of Lina Yu, University of Nebraska)

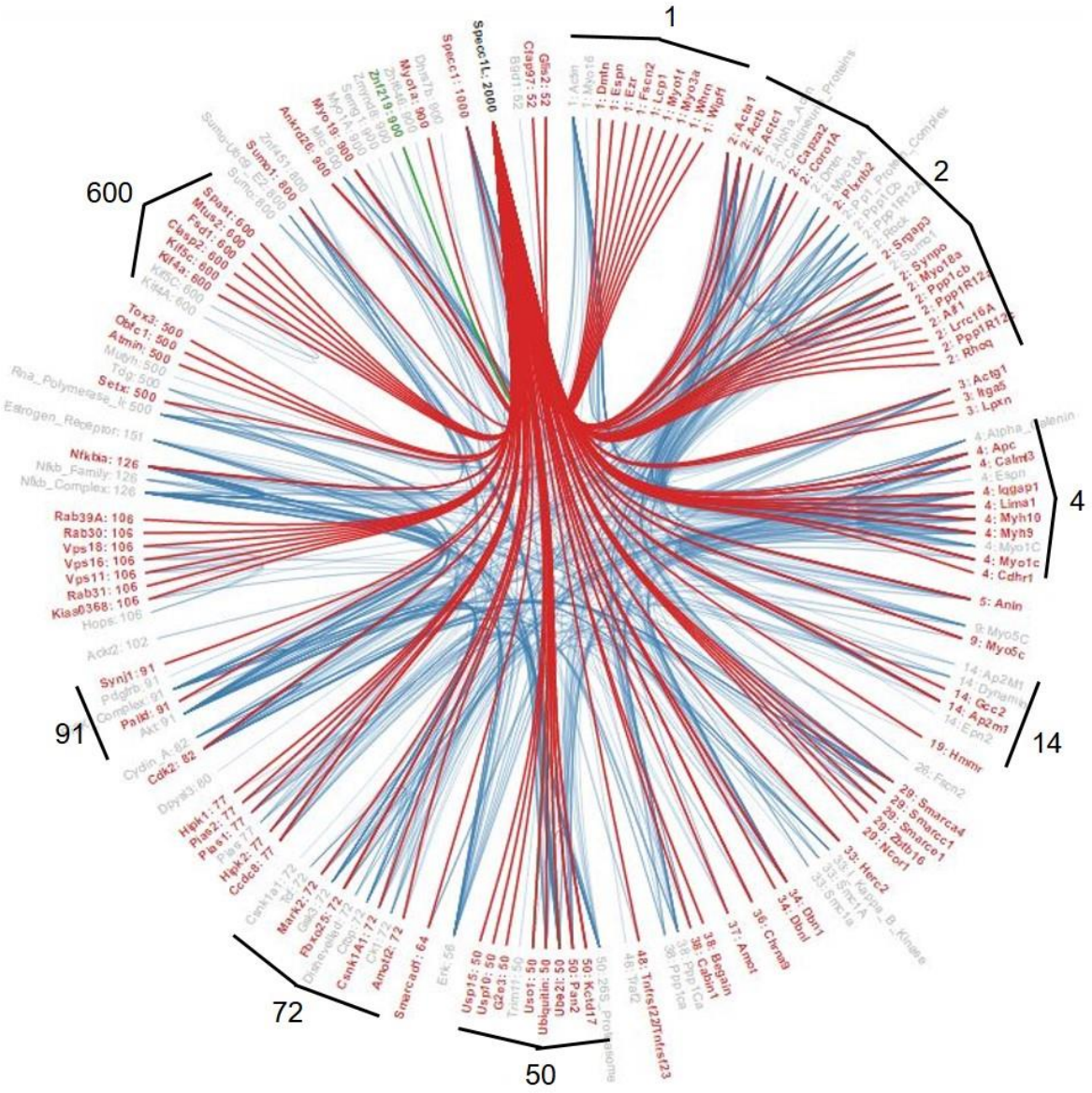

Figure A.1. SPECC1L protein interactors show phenotypically-relevant clusters. Heirarchical edge bundling of the interactions between SPECC1L and its protein interactors. Edge bundling shows interactions between SPECC1L **(top)** and its interactors **(red),** as well as interactions between interactors only **(blue)**. Edge bundling highlights that approximately half of all SPECC1L protein interactors cluster into a small number of phenotypically-relevant cellular functions, including actin cytoskeletal signaling **(1),** actin-based motility **(2)** and microtubule cytoskeleton **(600)**. Signaling involving Adherens junctions **(4),** β-Catenin **(72)** and PI3K/AKT signaling **(91)** also involve many SPECC1L interactors. Other potentially relevant functions include clathrin-mediated endocytosis **(14)** and protein ubiquitination **(50)**. The interactive model is hosted at: http://lyvis.x10host.com/index_minus.html